# Molecular Sensing and Signaling in Leukocyte-Endothelial Adhesion: From Integrin Activation to Orai Gating

By

Zainab Haydari

A dissertation submitted in partial satisfaction of the

requirement for the degree of

Joint Doctor of Philosophy
with the University of California, San Francisco

in

Bioengineering

in the

Graduate Division

of the

University of California, Berkeley

Committee in charge:

Professor Mohammad R.K. Mofrad, Chair
Professor Ahmet Yildiz
Professor Hana El-Samad

Summer 2020

# Abstract

## Molecular Sensing and Signaling in Leukocyte-Endothelial Adhesion: From Integrin Activation to Orai Gating

By

Zainab Haydari

Joint Doctor of Philosophy
with University of California, San Francisco
in Bioengineering
University of California, Berkeley
Professor Mohammad R.K. Mofrad, Chair

Leukocyte-endothelial adhesion and firm adhesion are chief steps in leukocyte recruitment cascade and immune system response to inflammation. Irregularities in these processes have been related to several human diseases including arthritis, cancer, and atherosclerosis. Given the fundamental importance of integrin activation and $Ca^{2+}$ signaling in adhesion assembly and strengthening, understanding the molecular mechanisms of kindlin-mediated integrin activation and STIM-mediated Orai gating have potentially important implications in designing new therapeutic interventions. This study employs molecular dynamics and bioinformatic techniques to unravel detailed molecular interactions in these two activation processes.

First, we analyzed the effect of kindlin cooperation with talin for integrin activation. Integrins are transmembrane proteins that mediate the signaling between the cytoplasm and extracellular matrix to promote cell adhesion. In order to initiate signaling, integrins must be activated from a low-affinity state to a high-affinity conformation for binding to extracellular molecules. Talin and kindlin are two cytoplasmic proteins that bind to integrin and modulate its affinity for extracellular ligands. Although the molecular details of talin-mediated integrin activation are known, the mechanism of kindlin involvement in this process remains elusive. Here, we carried out, for the first time, a comprehensive molecular

dynamics study of integrin activation mediated through simultaneous interaction of talin and kindlin with its β subdomain. We showed that kindlin modifies the molecular mechanisms of inside-out activation by enhancing talin interaction with the membrane proximal region of integrin and decreasing the crossing angle between transmembrane helices of integrin, which eventually results in parallelization of integrin dimer.

Second, we investigated the molecular details of STIM-Orai interaction and its downstream consequences on the Orai channel gating. The immune response is triggered by a decline in $Ca^{2+}$ concentration within the endoplasmic reticulum (ER) that is followed by the opening of the calcium release-activated channels (CRAC), thus increasing the intracellular $Ca^{2+}$ concentration. Stromal interaction molecule (STIM) has been identified as a $Ca^{+2}$ sensor in the ER activating the CRAC channel via physical interaction with Orai, the pore unit of the CRAC channel. In this study, we showed that the forces from STIM binding allosterically propagate through Orai helices, which lead to opening of the basic region of the pore. Moreover, we demonstrated important interactions that maintain the open structure of the Orai channel.

Overall, this study provides valuable insights into the molecular mechanisms that contribute to the activation of mechanosensitive proteins involved in leukocyte adhesion and firm adhesion.

Dedicated to

**Maysam**, for all his love, support, and encouragement.

**Rayhaneh**, my lovely daughter, for her patience.

**My parents**, for their true love and kindness.

# Acknowledgement

I would like to first thank my research advisor and dissertation chair Prof. Mohammad Mofrad for his mentorship, guidance, support, and encouragement throughout my PhD and for providing me with the freedom to explore my ideas and research interests. It was a great experience and a great pleasure to work with him and I have learned a lot from his expertise. I am very grateful to my PhD committee, Prof. Ahmet Yildiz and Prof. Hana El-Samad for their dedication and all the invaluable things that I have learned from them. I would also like to thank my qualification exam committee, Prof. Song Li and Prof. Gerald Marriott for their great advice and feedback.

I am very grateful of Dr. Hengameh Shams, my friend and lab mate who patiently helped me learn molecular dynamics simulations and jump start my project. We continued to work together on some interesting joint projects. During my research at UC Berkeley, I also had the opportunity to work with my friend and lab mate, Dr. Zeinab Jahed. I am very grateful for this collaboration opportunity through which I learned a lot. Zeinab was always available to discuss research and we had a great time working together.

I would like to acknowledge all fruitful discussions, suggestions, and help offered by former and current members of the Molecular Cell Biomechanics Laboratory, especially Mehrdad, Kiavash, Mohammad, Ehsan, Mohaddeseh, and Atsushi.

I would like to express my sincere gratitude to my husband, Maysam for all his love and support. His patience, help, and wisdom have made this long journey very pleasant for me and he has supported me in every aspect of my life. I am also very grateful of my beautiful daughter Rayhaneh for all her smiles and the happiness that she brought to our life.

Last but not certainly least, I would like to thank my parents for their sincere unconditional love and emotional support, and my brothers, Alireza and Mahdi, for all their support and encouragement, despite the long physical distance.

Hereby, I would like to dedicate this dissertation to my husband, to my daughter, and to my parents.

# Table of Contents

# List of Figures

# Chapter 1

# Background and Significance

## 1.1. Immune System Response to Infection

Many people suffer from different types of immune system disorders across the world. In the United States alone, autoimmune system disorders such as inflammatory bowel diseases, rheumatoid arthritis, and multiple sclerosis disease affect more than 23.5 million people [2]. Understanding the mechanisms of immune system response in these conditions is key to control these disease states and can potentially revolutionize the design of targeted medications by improving the efficacy and response time as well as reducing the side effects.

### Leukocyte Recruitment Cascade

The immune system function involves a series of events that constitute signaling pathways. Leukocyte recruitment is a critical step in these signaling pathways and has a central involvement in different autoimmune and inflammatory diseases [3]. The recruitment of circulating leukocytes, known as white blood cells, to the site of infection mediates the immune system response to inflammation. The migration of leukocytes from blood stream into the inflamed tissue happens via a series of complex adhesive events between endothelial and the leukocyte cells, through which various endothelial markers must be expressed. These markers promote leukocyte tethering and arrest on blood vessels, and trigger leukocyte migration through the endothelial lining. Leukocyte recruitment process is tightly mediated by adhesion molecules and molecular signaling at the vascular endothelium [4]. Deciphering the molecular mechanisms of leukocyte recruitment cascade sheds light to the function of immune system response to inflammation and can also inform the design of new therapeutics [5]. A multi-step cascade of events is involved in the process of leukocyte recruitment, including rolling, capture or slow rolling, arrest or adhesion, firm adhesion or adhesion strengthening, crawling or spreading, and transmigration (Figure 1.1).

At the cellular scale, the process begins with the capture of rolling leukocytes in the blood and subsequent rolling along the surface of endothelial cells. E-, P-, and L-selectins mediate the rolling process. Basically, association and dissociation of endothelial E- and P-selectins with leukocyte L-selectin initiate the rolling process of leukocytes that are under blood flow conditions [6]. These selectin-ligand interactions reduce the rolling speed of leukocytes; therefore, leukocytes can receive signals from chemokines on the surface of endothelial cells. The chemokine signals activate integrins, thereby initiating the adhesion step [3], [7], [8].

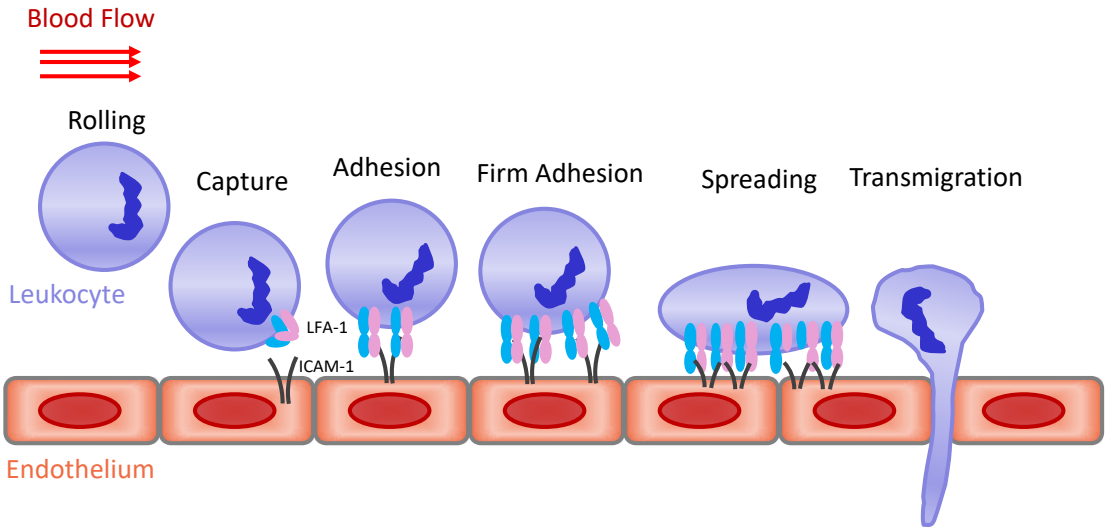


Figure 1.1: Schematics of leukocyte recruitment cascade during immune system response to inflammation. In an inflammatory response, circulating leukocytes engage with the luminal surface of endothelial cells through integrin-ligand interaction forming nascent adhesions. Integrins then assemble in two stages, micro- and macro-clustering, via a positive feedback mechanism, which eventually leads to leukocyte adhesion and firm adhesion. Then, leukocytes spread on the endothelial cell surface through the locomotion process to find an appropriate location to transmigrate into the tissue of insult.

Integrin activation mediates leukocyte adhesion and firm adhesion by binding to their endothelial ligands. Integrins αLβ2 (LFA-1) are one of the most important integrins that participate in leukocyte adhesion by interacting with ICAM-1 ligand on the endothelial cell surface (Figure 1.1). After firm adhesion, through the locomotion process, leukocytes crawl on the surface of endothelial cells to find an appropriate location to migrate to the tissue [9], [10]. Trans-endothelial migration is the final step in the leukocyte recruitment process which leukocytes emigrate into inflamed tissue through venular walls [3], [11] (Figure 1.1).

**Leukocyte Adhesion**

Integrin-mediated leukocyte adhesion and firm adhesion are very important steps in the leukocyte recruitment cascade (Figures 1.2 and 1.3). Circulating leukocytes target and adhere to the endothelial wall to mediate the recruitment process. The importance is highlighted by leukocyte adhesion deficiency syndromes (LAD I), the rare genetic diseases showing immunodeficiency in people lacking β2 integrin [12]. Therefore, it is important to understand the molecular mechanisms by which leukocytes adhere to the endothelial cells.

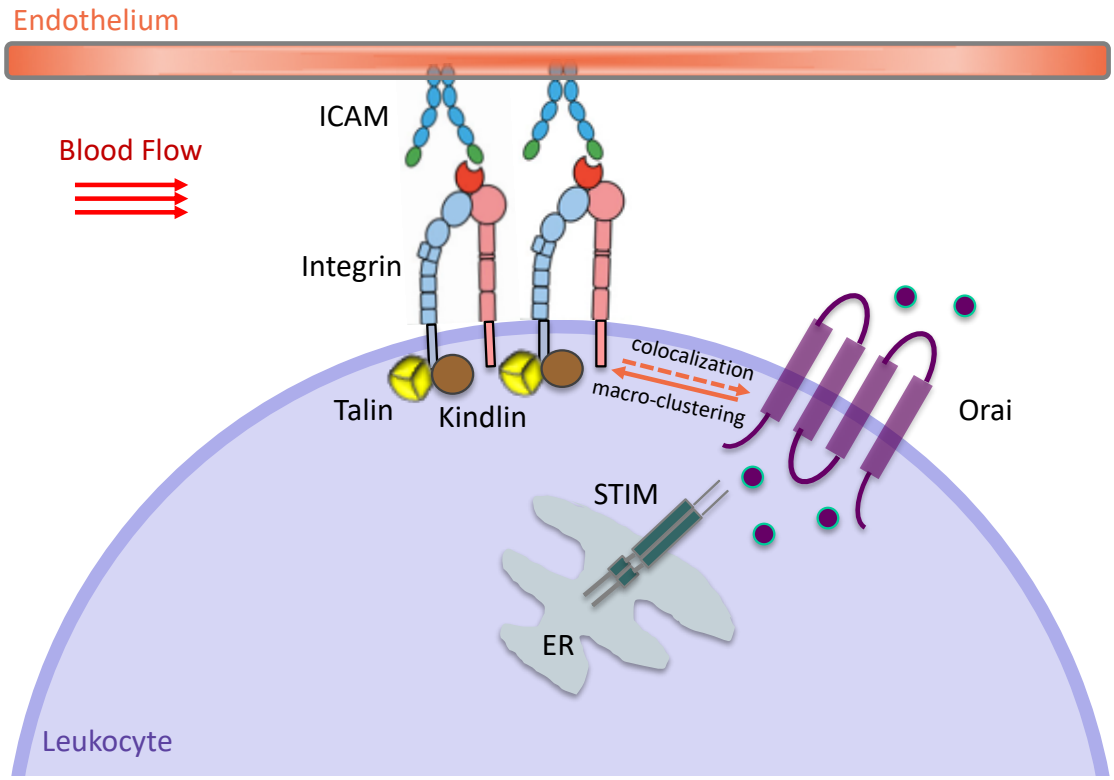


Figure 1.2: An illustration of leukocyte adhesion to the endothelial wall. In order to initiate leukocyte adhesion, integrins must be activated from a low-affinity state to a high-affinity state for binding to the endothelium ligand ICAM. After integrin extension, integrin-ICAM bonds sense the shear force from blood stream. It has been shown that as integrin-ICAM bonds take up tensile forces, they recruit kindlin and facilitate $Ca^{2+}$ flux through colocalization with Orai protein. However, the underlying mechanism remains unknown. On the other hand, $Ca^{2+}$ flux through Orai channel enhances integrin clustering resulting in adhesion strengthening. STIM protein clusters and reaches the plasma membrane to physically bind and activate Orai protein. For clarity, only one monomer of Orai hexamer is shown.

Integrin is a key membrane receptor in leukocyte adhesion that senses and transduces signals from environment and its proper activation is the first step for anchoring leukocytes to the endothelial ligand. Chemokine and selectin signaling initiate talin binding to the proximal NxxY motif that leads to a weak integrin-ligand affinity. Then, integrin-ICAM bond senses the shear forces from blood flow. When integrin-ICAM bonds take up tensile forces, they recruit kindlin to the site of adhesion. Binding of kindlin to the distal NxxY motif of integrin elevates transition to a high-affinity extended open conformation and stabilizes micro-clustering of integrin dimers [13], [14]. Micro-clusters are referred to as

the non-covalent oligomer of integrins that are formed on the cell surface over an area with a diameter less than 100 nm [15]–[19].

Kindlin recruitment and micro-clustering of integrins result in an increased inward $Ca^{2+}$ flux through calcium release activated channel (CRAC) channels. It has been shown that high-affinity integrin clusters and shear force are critical to initiate $Ca^{2+}$ flux in leukocyte adhesion process [4], [20]. Based on recent experimental studies it has been postulated that tensile forces acting on integrin-ICAM bonds recruit kindlin and then colocalization of integrin, kindlin, and Orai proteins activates CRAC channel and induces $Ca^{2+}$ flux [4], [5]. The precise molecular mechanisms of how this colocalization leads to the activation of CRAC channel is, however, yet to be determined. It is believed that $Ca^{2+}$ flux further enhances integrin clustering resulting in macro-clusters and adhesion strengthening (Figure 1.2 and 1.3) [5], [21]. Macro-cluster of integrins refer to integrins clustered together over an area with a dimeter greater than 200 nm [20], [21]. This mechanism reinforces leukocyte attachment to the endothelial wall (Figures 1.2 and 1.3).

Orai channel protein is the pore subunit of the CRAC channel that plays a central role in $Ca^{2+}$ signaling and leukocyte adhesion. Recent studies have shown that $Ca^{2+}$ flux through Orai protein is necessary for integrin macro-clustering and adhesion maturation [9], [54], [55]. Stromal interaction molecule (STIM) is a $Ca^{2+}$ sensor in the endoplasmic reticulum (ER) that can also activate Orai channel in response to the lower intracellular calcium contents [56]. STIM clusters upon depletion of ER calcium storage and reaches the plasma membrane to physically bind and activate Orai protein (Figure 1.2 and 1.3) [57]-[59].

Overall, integrin and Orai proteins are two important membrane molecules in the leukocyte adhesion cascade, the activation of which play a vital role in this process. My dissertation is focused on studying the molecular mechanisms of the activation of integrin and Orai proteins in the context of leukocyte adhesion. Precisely, I aim to understand how kindlin association with integrin promotes integrin activation and clustering and also, how STIM protein activates Orai protein. In the rest of this chapter, I will further explain the biology of integrin activation and $Ca^{2+}$ signaling through Orai channel.

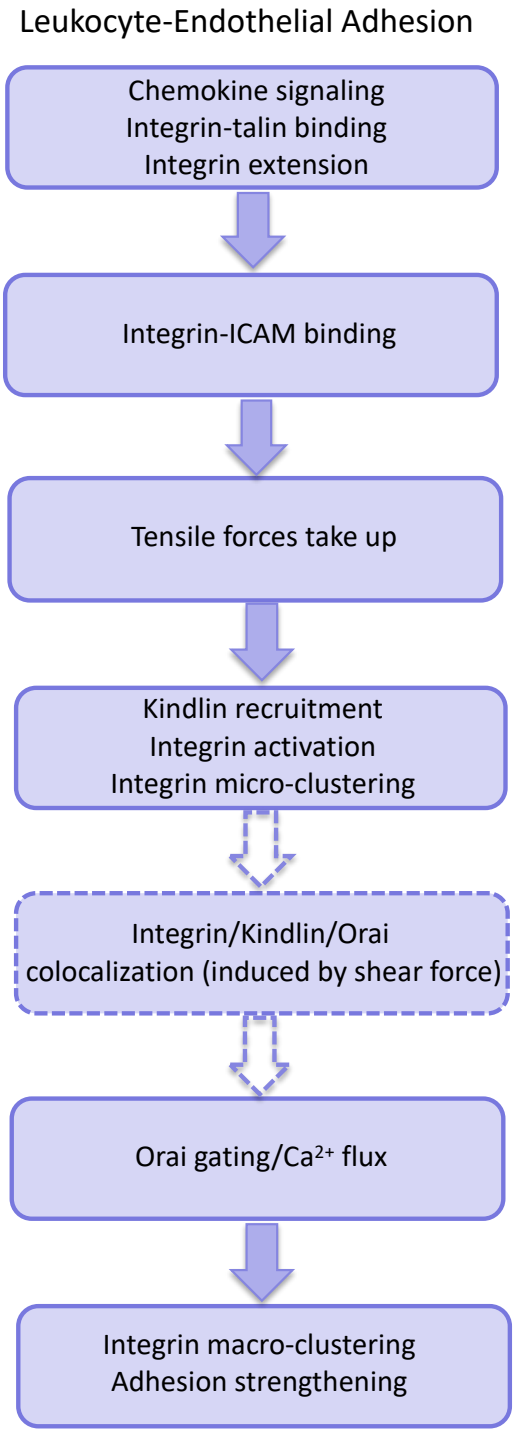


Figure 1.3: The sequence of events in leukocyte-endothelial adhesion and adhesion strengthening. Chemokine signaling induces talin binding to the integrin β cytoplasmic tail, which then changes the conformation of integrin to extended state. Then, integrin can bind to endothelial ligand ICAM

and take up tensile forces from blood flow. The tensile force acting on high-affinity integrin-ICAM bonds recruits kindlin protein to the adhesion site. Kindlin recruitment to the integrin β cytoplasmic tail fully activates integrin and initiates integrin micro-clustering. High-affinity integrin clusters and kindlin recruitment result in an increased inward $Ca^{2+}$ flux through Orai protein. It has been shown that the colocalization of integrin, kindlin, and Orai activates CRAC channel and enhances $Ca^{2+}$ flux, however, the detailed mechanism is not completely known. On the other hand, $Ca^{2+}$ flux further enhances integrin clustering, resulting in macro-clusters and adhesion strengthening.

## 1.2. Integrin Activation

As discussed in the previous section, leukocyte-endothelial adhesion is a critical step in immune system response to inflammation. Among all adhesion proteins that are involved in this process, integrin is of utmost importance, since its activation prompts focal adhesion formation and therefore, plays a pivotal role in leukocyte adhesion. More broadly, integrin activation can lead to other cell-cell adhesion processes that are important for a variety of physiological and pathological conditions [24], [25]. Undoubtedly, a more comprehensive understanding of the underlying molecular mechanisms of integrin-mediated cell-cell adhesion is highly demanded.

### Integrin Biology

Integrin receptors are α-β heterodimeric transmembrane proteins that transfer signals bidirectionally between the extracellular matrix (EMC) and cytoskeleton or between cells. Integrin may be activated by mechanical or biochemical signals within the cell (‘‘inside-out signaling’’) or by mechanical stresses generated in the extracellular domain (‘‘outside-in signaling’’) [26]–[29]. Inside-out signaling involves the interaction of intracellular proteins with the integrin cytoplasmic tail, which modulates integrin’s affinity for extracellular ligands [26], [30], [31].

There are 18 α and 8 β integrin subunits in mammals, which form 24 different combinations of non-covalently associated α and β subunits (Figure 1.4). Different integrin subtypes have different affinities for ligands and can be divided into four different categories according to their ligands: arginine-glycine-aspartate (RGD) receptors, collagen receptors, leukocyte specific (LDV) receptors, and laminin receptors (Figure 1.4).

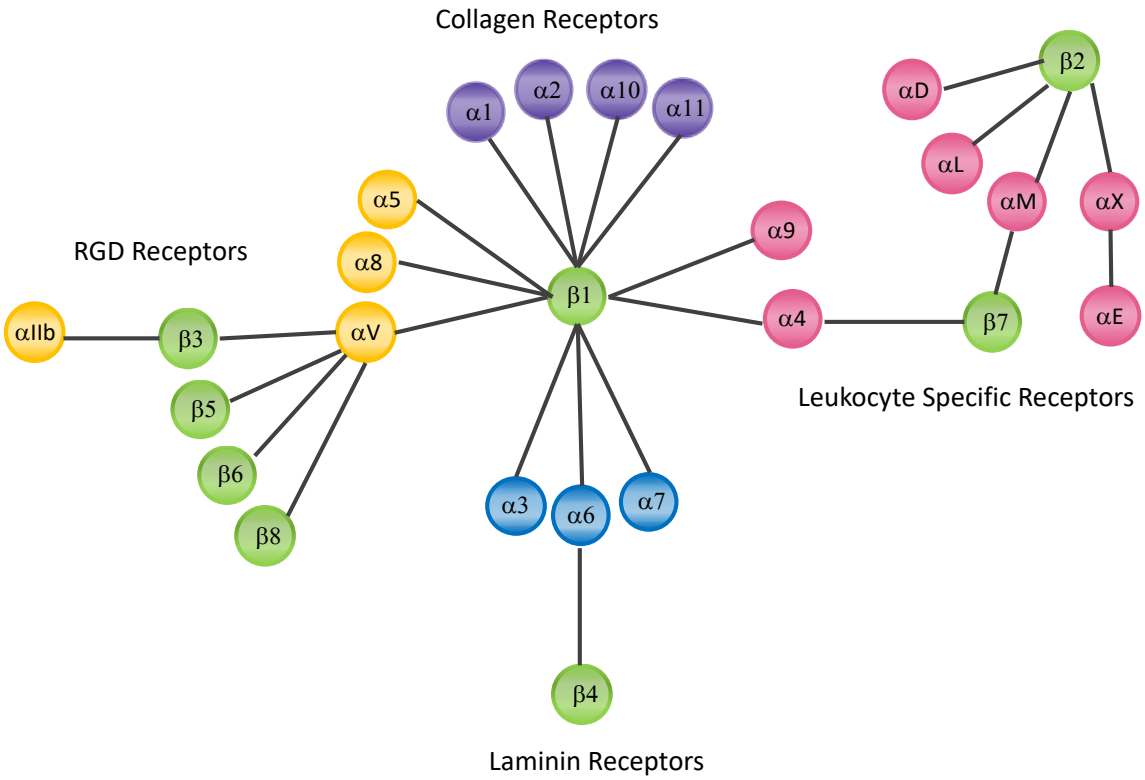


Figure 1.4: Different integrin subtypes categorized based on their ligand binding motifs. 18 α and 8 β subunits form 24 distinct combinations of integrin heterodimers. Various integrin subtypes are shown according to their ligand binding, i.e., RGD, laminin, collagen, and leukocyte specific receptors. The figure is adapted from Kapp et al. 2013 [1] with modifications.

Integrin αLβ2 (LFA-1) is the most abundant type in leukocytes. ICAM-1 is an integrin ligand at the plasma membrane that binds to integrin αLβ2 to promote leukocyte-endothelial adhesion (Figures 1.2). Integrin αIIbβ3 is also one of the well-known integrin subtypes that is only expressed in platelets and is necessary for the hemostatic function of platelets [1], [25], [32]. The full dimer structure of integrin αIIbβ3 is experimentally solved and has more than 60% similarities in the transmembrane and cytoplasmic domains to integrin β2. Therefore, it can be employed for molecular dynamics analyses.

### Integrin Structure

Three distinct conformational states of integrin have been determined: bent-closed or resting state, extended-closed or intermediate state, and extended-open state (Figure 1.5) [25]. Integrin activation entails a conformational transition of integrin from bent-closed (low-affinity) to extended-open (high affinity) state [33], [34]. Each integrin subunit

consists of a large extracellular ectodomain (ECD), a single pass transmembrane helix (TM), and a short cytoplasmic tail (CT) (Figure 1.5) [35], [36].

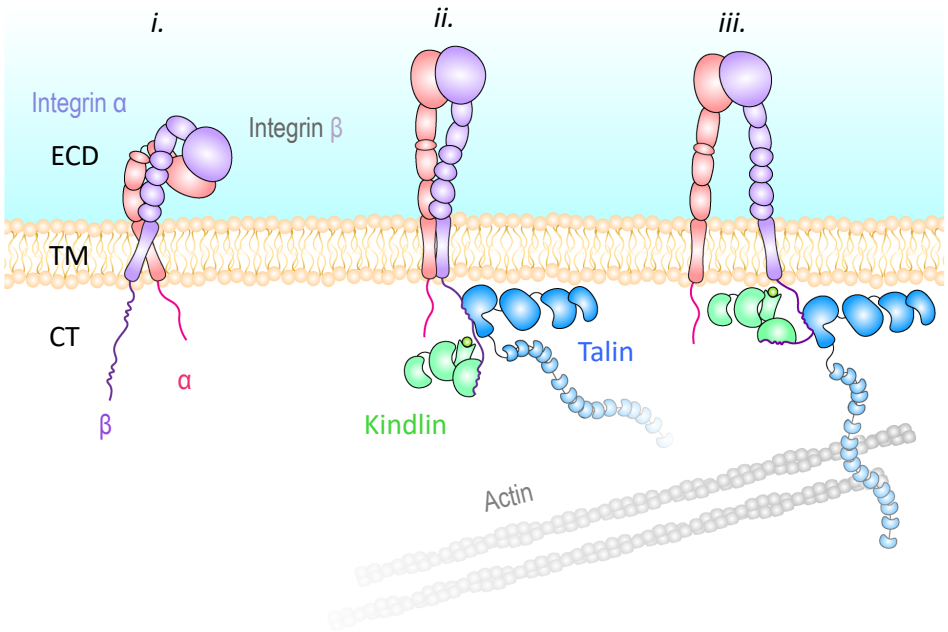


Figure 1.5. Schematic representations of the three conformational states of integrin: i) bent-closed (inactive) ii) extended-closed (intermediate) iii) extended-open (active). Talin and kindlin are both involved in integrin activation by binding to the distinct motifs of β cytoplasmic domain. Talin association to the actin cytoskeleton provides a linkage between the extracellular environment and the cytoskeleton. Only the FERM domain of talin is shown for clarity.

Extracellular domain of integrin α and β subunits consist of about 1100 and 800 residues, respectively. The N-terminus of integrin extracellular domain, headpiece, is an interface for different ligands through non-covalent association of α and β subunits. The integrin headpiece has a closed or bent conformation in inactive state, which makes its affinity low for binding to ligands. Conformational changes in integrin headpiece (from bent-closed to extended-open) induced by cytoplasmic interactions of β, increase its ligand affinity and activate integrin [1].

The helical integrin transmembrane domain (TM) of α and β consist of about 24 and 29 residues, respectively. In the resting or inactive state, α and β are non-covalently associated and β is tilted inside the lipid. There are two interaction networks between integrin α and β transmembrane domains in the inactive state: the inner membrane clasp (IMC) and the outer membrane clasp (OMC) (Figure 1.6).

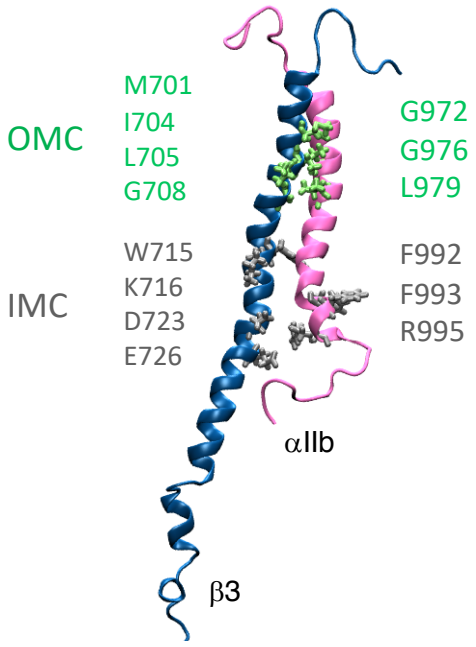


Figure 1.6. IMC and OMC interactions between αIIb and β3 heterodimer. Structures of integrin αIIb and β3 helices are shown in pink and blue, respectively. Interacting residues in the IMC region are shown in silver and in the OMC region in green, respectively. αIIb R995-β3 D723/D726 form salt bridges in inactive state of integrin. IMC and OMC interactions are the dominant factors for maintaining the closed state of integrin dimer. Mutations in these residues disrupt α-β interactions, initiating integrin activation.

In integrin αIIbβ3, IMC is formed by the hydrophobic interactions between highly conserved $^{991}$GFFKR$^{995}$ motif of αIIb and W715, K716, and I719 residues of β3, as well as salt bridges between residue R995 on αIIb and D723/E726 on β3 (Figure 1.6). OMC is composed of associations between $^{972}$GXXXG$^{976}$ motif on αIIb and V700, M701, and I704 residues on β3, as well as interactions between αIIb $^{979}$LL$^{980}$ and β3 $^{705}$LXXG$^{708}$ residues (Figure 1.6). The IMC and OMC are the most important interactions that hold integrins in the resting state and unclasping of these interactions causes integrin conformational changes and opening of integrin extracellular headpiece. Experimental observations showed that mutations of residues involved in IMC or OMC cause disruption of interactions between α and β helices, and hence initiating integrin activation [25], [27], [37]–[39].

Cytoplasmic domain of integrins α and β are less than 20 and 75 residues in length, respectively. There is a significant homology between different types of integrin α and β cytoplasmic tails with the conserved active sites. In resting state, the membrane proximal region of cytoplasmic tail of integrin α and β interact with each other [25]. The cytoplasmic domain of integrin β subunit contains two NxxY motifs, the interactions of which with focal adhesion proteins lead to integrin conformational changes and initiate inside-out activation. A significant number of cytoskeletal proteins interacting with cytoplasmic tail of α and β has been reported, i.e., talin, kindlin, filamin, and α-actinin. However, among

all proteins that interact with the cytoplasmic domain of α and β, talin and kindlin proteins are known to directly bind and activate integrin, the details of which will be discussed in the Section "mechanisms of integrin activation through talin and kindlin". In addition to integrin activation, integrin clustering is also an important step for the firm adhesion of circulating leukocytes.

**Integrin Clustering**

Reinforcement of integrin-mediated adhesions or adhesion strengthening is possible through integrin clustering, which is essential for focal adhesion formation. Although it has been known that integrin activation is required for clustering and a strong correlation exists between them, their interplay has remained elusive and it is not yet known how the former triggers the latter [26], [40]–[45]. Two models have been proposed for integrin clustering: homo-oligomerization and multivalent ligand. In the first model, homo-oligomerization of activated α and β subunits through their transmembrane interactions mediate integrin clustering. In the second model, researchers believe that integrin clustering is independent of homo-oligomerization and binding of several integrins to multivalent ligands (instead of monovalent ligands) triggers integrin clustering [18], [26], [44], [46].

Cytoplasmic proteins that directly interact with integrin cytoplasmic domain may also play an important role in clustering, i.e, talin, kindlin, α-actinin, and filamin. There has been a long-standing hypothesis that kindlin may also be involved in the clustering of activated integrins. Recent crystallography data on kindlin in complex with integrin provided valuable insights into molecular mechanisms of kindlin's involvement in integrin activation and clustering [47]. It was suggested that kindlin could form dimers that can bind to two integrins simultaneously. This observation provided a mechanistic explanation of how kindlin may promote integrin clustering. The initiation of clustering could potentially be mediated either through the dimerization of kindlin after binding to integrins or via the simultaneous binding of two integrins to a kindlin dimer [29].

**Mechanisms of Integrin Activation through Talin and Kindlin**

Prior experimental and computational studies had shown that talin was necessary and sufficient for integrin activation [15], [48]. However, there is now ample evidence suggesting that talin cannot activate integrin without the help of kindlin family of proteins [49], [50]. Therefore, kindlin is now believed to be required for integrin activation and serves as a co-activator of integrin with talin [51]. Additionally, kindlin-associated diseases such as Leukocyte Adhesion Disease III (LADIII) have been linked to deficiencies in

integrin function, further corroborating the contribution of kindlin in integrin activation [39].

Talin is a FERM (protein4.1, ezrin, radixin, and moesin) domain containing protein that has two isoforms: talin-1 and talin-2. Kindlin belongs to a family of evolutionarily conserved proteins, including kindlin-1, -2, and -3. Kindlin also is a FERM domain containing protein. FERM domain is composed of four structural subdomains, i.e., F0-F3. Compared to typical FERM domain proteins, kindlin FERM features a pleckstrin homology (PH) domain inserted into the F2 subdomain (Figure 1.7A and B). Although different talin and kindlin isoforms exhibit sequence similarities, they often present tissue-specific distributions [15], [29]. Both talin and kindlin interact with the β cytoplasmic domain of integrin through their F3 subdomains. Specifically, talin binds to the membrane proximal NxxY motif and kindlin interacts with the membrane distal NxxY motif of β cytoplasmic tail. These distinct talin and kindlin binding sites on integrin suggests that they can simultaneously interact with β cytoplasmic tail and trigger activation [52]. However, the molecular mechanisms of the interplay between talin and kindlin for inducing integrin activation are not yet well understood.

Experimental and computational studies have shown important molecular details of integrin inside-out activation. These studies suggest that the interactions between α and β helices of integrin dimer maintain its closed conformation and unclasping induced by talin or other activators triggers activation [53]–[55] They also showed that the disruption of α-β interactions results in an increase in the integrin dimer crossing angle [24], [56], [57]. Despite these important experimental observations, a comprehensive theoretical analysis of molecular mechanisms of kindlin's role in integrin activation and its interplay with talin has been hindered because the crystal structure of kindlin was not solved until recently [16]. Therefore, all previous computational studies published to date, have overlooked the role of kindlin in their models [27], [58], [59].

In this dissertation, I discuss the molecular mechanism of kindlin-mediated integrin activation through simultaneous binding of talin and kindlin using a rigorous molecular dynamics simulation method. Specifically, I show how forces of talin and kindlin binding to the cytoplasmic domain of integrin transfer to its transmembrane region to initiate integrin activation. To the best of our knowledge, this is the first computational analysis of the integrin activation process when considering both talin and kindlin simultaneously.

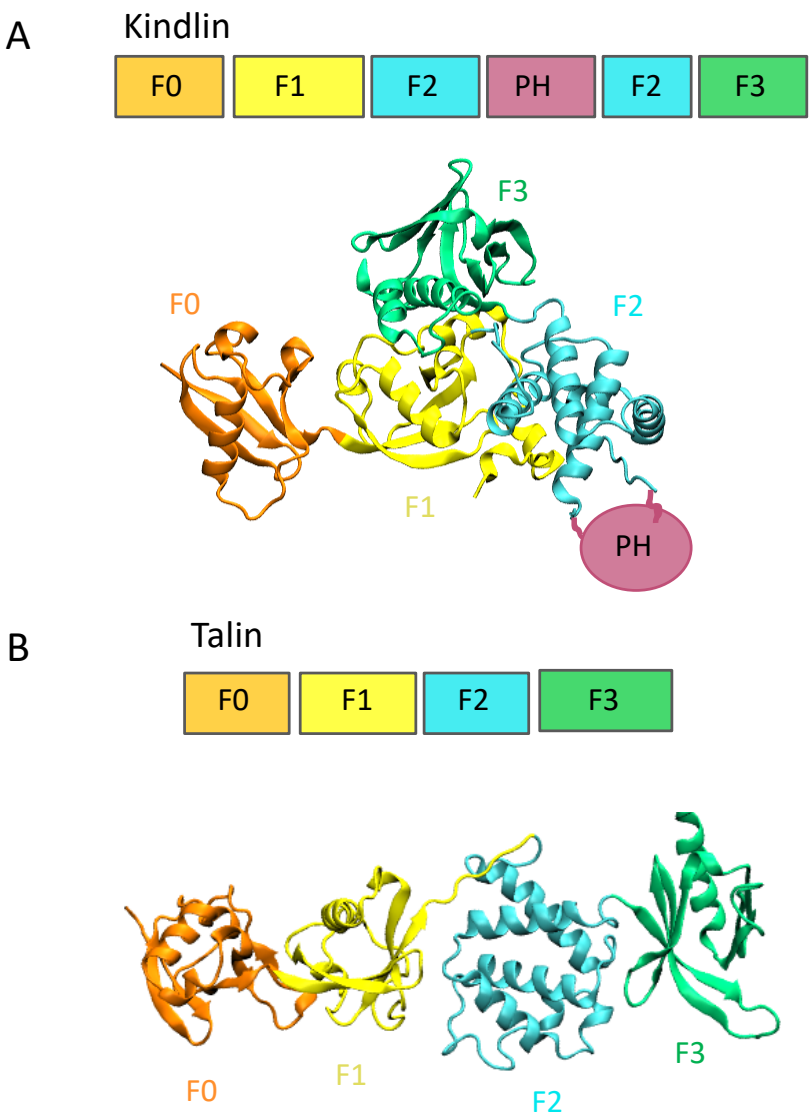


Figure 1.7: Structural domains of kindlin and talin molecules. (A) The sequence location of different domains of kindlin2 is shown on the top. Also, the structure of kindlin2 monomer (PDB: 5XPY) is shown in the bottom. A complete structure of kindlin2 including PH domain doesn't exit. Here, the PH domain is indicated by a circle. (B) Domain organization (top) and structure (bottom) of talin1 FERM domain (PDB: 6MFS) are shown.

## 1.3. $Ca^{2+}$ Signaling

As we discussed in Section 1.1, $Ca^{2+}$ signaling plays a vital role in leukocyte-endothelial integrin-mediated adhesion strengthening. $Ca^{2+}$ signaling is also essential for many other functions such as blood clotting by platelets, regeneration of skin, and tooth development [60]. CRAC channel is the best characterized store operated calcium channel, which was first described in immune cells. Orai is a plasma membrane protein that forms the pore subunit of the CRAC channel. There are three highly conserved homologs of Orai proteins, i.e., Orai 1, Orai2, and Orai3. These highly selective calcium channels are necessary for integrin macro-clustering and adhesion strengthening [4], [61], [62]. STIM family of ER calcium sensors (STIM1 and STIM2) constitute the functional component of CRAC channel. The decreased calcium concentration in endoplasmic reticulum (ER) is sensed by STIM protein. Orai channels are usually activated upon depletion of internal calcium stores. STIM clusters upon depletion of calcium stores and moves near the plasma membrane and activates Orai channel via protein-protein interactions. Although there are some experimental studies on the activation mechanism of Orai channel using STIM protein, many details are not yet known and there is a need for comprehensive computational studies to unravel the molecular details of channel activation.

### Orai Structure

The crystal structure of drosophila melanogaster Orai (dOrai) in closed conformation showed a hexameric structure of this protein (Figure 1.8A and B). The dOrai channel shows more than 70% sequence similarity (in transmembrane regions) to human Orai1. Each Orai monomer is composed of four transmembrane helices, i.e., TM1-TM4 and a cytoplasmic extension of TM4 (TM4e). The closed conformation of Orai is formed by coiled-coil interactions of TM4-extensions of adjacent Orai subunits. The inner surface of the pore comprises of six TM1 helices around the center axis. Orai pore can be divided into four regions: selectivity filter (a ring of glutamate residues on the extracellular region), hydrophobic region (three helical turns within transmembrane region), basic region (three helical turns close to intracellular region), and cytosolic region (wider region that extends into cytoplasm) (Figure 1.8C).

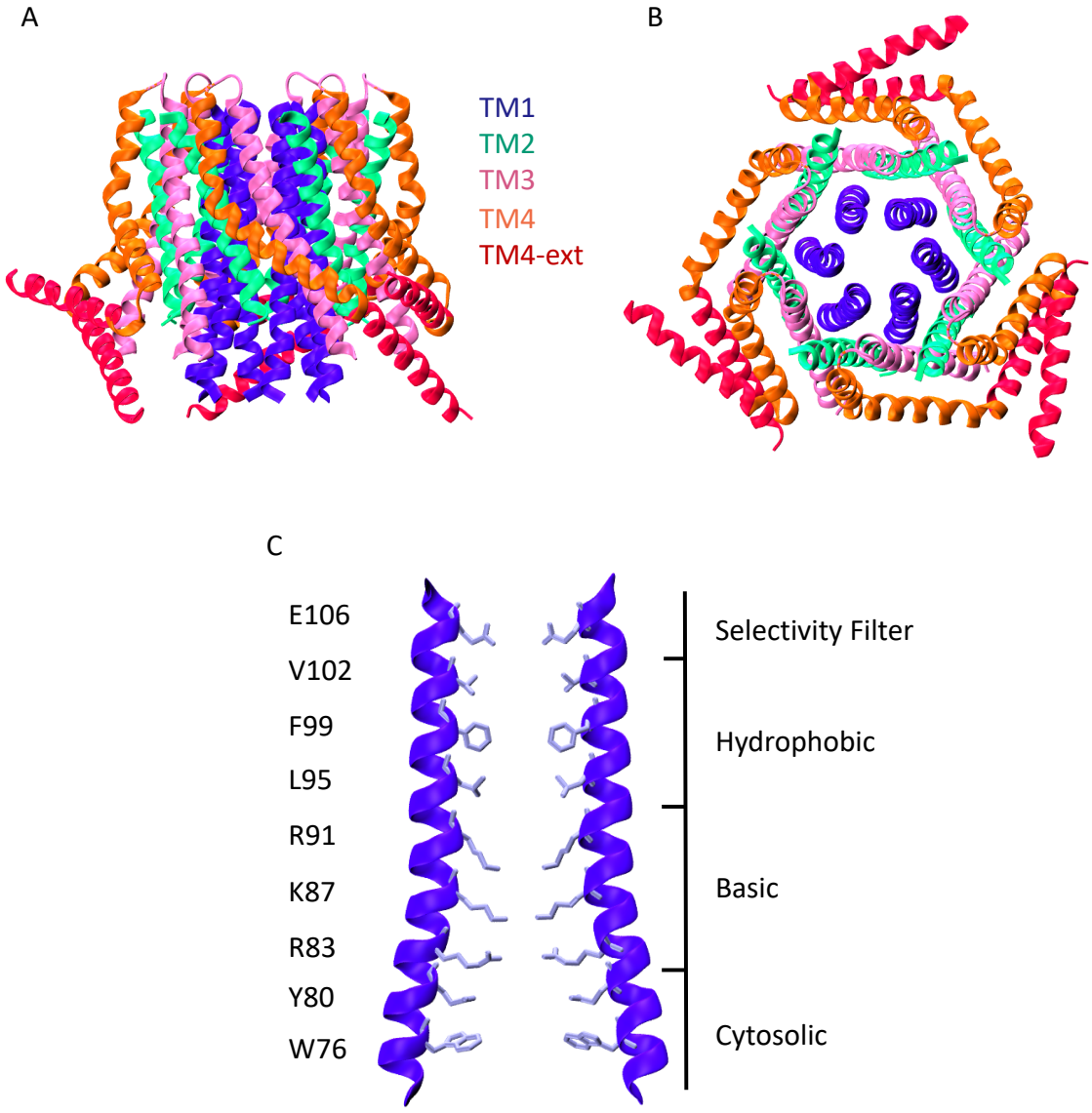


Figure 1.8: Crystal structure of drosophila Orai hexamer in closed conformation. (A) A side view of hexameric dOrai crystal structure (PDB ID: 4HKR). (B) Top-down view of dOrai crystal structure. The channel shows six TM1 helices around a center axis. (C) A side view of TM1 helices lining the dOrai pore showing distinct pore functional regions: selectivity filter, hydrophobic gate, basic gate, and cytosolic region. The labels on the left side show the counterpart residues of Orai1. For clarity, only two TM1 helices from spatially opposite subunits are represented.

### Orai-STIM binding

The cytoplasmic domain of STIM contains three coiled-coil CC domains (CC1, CC2, and CC3) (Figure 1.9A). It has been shown that the CRAC-activation domain (CAD or SOAR domain) of STIM is essential for activating Orai channel [63]–[65] (Figure 1.9A). There are two known STIM binding sites on Orai: C-terminus (TM4-extension) and N-terminus (cytoplasmic extension of TM1) (Figure 1.9B). It is widely accepted that the C-terminus binding site is required for channel gating and STIM strongly binds to this region and activates the channel [66], [67]. However, the necessity of association of STIM with TM1 helices of Orai for channel gating is unknown. It has been shown that the cytosolic extension of TM1 is essential for STIM-mediated Orai activation [68]; however, the physical interaction of STIM with this region is still unclear [65], [69], [70].

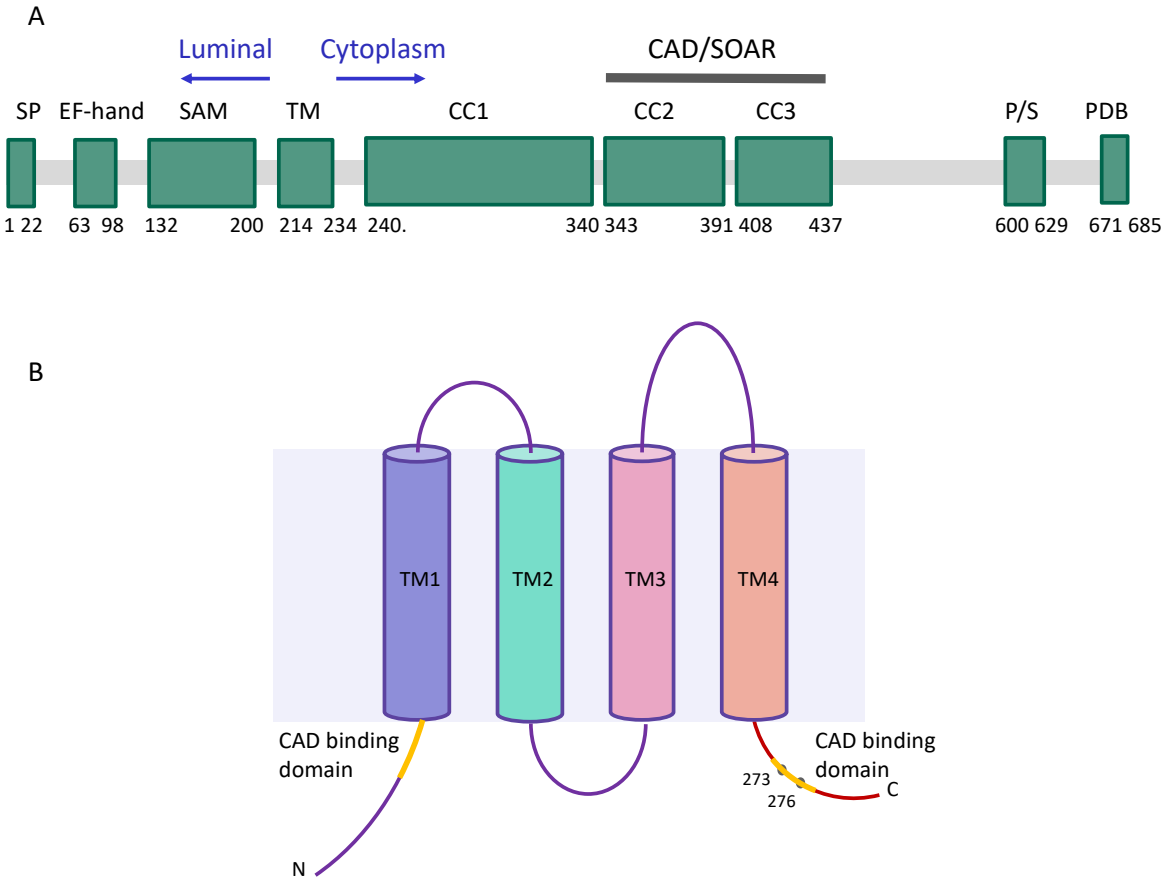


Figure 1.9: Schematics of domain organization of STIM and Orai proteins (A) Domain organization of STIM1 showing different structural domains is shown. CC2 and CC3 domains of STIM form the CAD or SOAR binding domain responsible for Orai activation. (B) A schematic representation of one Orai1 monomer with highlighted CAD binding domains in N and C terminus is shown. Also, the location of residues L273 and L276 in the C-terminus of Orai1 is shown.

Two different models have been proposed to explain STIM interaction with the C-terminus of Orai channel: dimeric and monomeric. In the dimeric model, a dimer of STIM interacts with a dimer of Orai, a pair of adjacent TM4-extensions. This model is based on NMR solution of STIM1 CC1-CC2 domains in complex with Orai1 C-terminus [67], [71]. The monomeric model postulates binding of a dimer of STIM with only one monomer of Orai. This model can explain how STIM dimer can independently bind to Orai monomers and crosslink two subunits, an essential step for Orai clustering. These two binding models may represent different steps in Orai channel gating and each one can separately contribute to Orai activation [67], [72].

**Orai gating by STIM**

One of the important questions in Orai activation is how forces from STIM binding can transmit to the pore and activate the channel. Crystal structure and mutational studies of Orai channel provide some insight about how STIM binding is allosterically propagated through the pore [73]. It has been shown that the resting state of Orai is stabilized by interactions between different TM helices and conformational changes in the pore regions are required for channel gating and $Ca^{2+}$ influx. Two different pore regions have been suggested for Orai channel gating. The first gating region is assumed to be at the extracellular side of the hydrophobic section of the pore, near residue V102 of Orai1, while the second gating region is suggested to be in the basic section of the pore (Figure 1.8C) [74], [75].

Some gating models have recently been proposed to show the open state of Orai channel based on conformational changes in gating regions discussed earlier. First gating model, pore rotation, is based on the assumption that the hydrophobic side chains of residues V102 and F99 of Orai1 (Figure 1.8C) create a barrier for calcium permeation in the Orai closed state. In this model, it was proposed that STIM binding to Orai makes about 20 degrees rotation of TM1 helices, resulting in outward moving of the side chains of hydrophobic region residues [74], [75]. Second gating model suggests a widening in the basic region of the pore. This model, which is based on the crystal structure of open dOrai mutant, showed about 10Å dilation in the inner pore of the channel [76]. The third gating model assumed two gates in both hydrophobic and basic regions of the pore. This model, based on the molecular dynamic simulations of the constitutively active Orai mutant, showed a small local dilation of these regions of the pore (1-2 Å). The dilation of both basic and hydrophobic regions allows water to fill the pore and therefore, facilitating the permeation of $Ca^{2+}$ by reducing the energy barrier [77].

In this dissertation, I examine the molecular mechanism of STIM-mediated Orai activation using all-atom molecular dynamics simulations. Specifically, I will discuss the conformational changes of Orai helices upon STIM interaction with the C-terminus of Orai.

## 1.4. Dissertation Objectives

The goal of my dissertation is to uncover the molecular mechanisms behind critical activation processes in the leukocyte-endothelial adhesion cascade (Figure 1.3), using computational approaches of molecular dynamics (MD) simulations and bioinformatics techniques based on the following specific objectives:

1. Uncovering the molecular mechanisms of kindlin-mediated integrin activation and clustering.
2. Investigating the mechanisms of Orai channel gating mediated by STIM protein.

## 1.5. Structure of Thesis Document

The above objectives will be discussed and demonstrated in the following structure:

- Chapter 2 focuses on understanding the molecular mechanisms of integrin inside-out activation via interaction with talin and kindlin both individually and simultaneously. Our results show the cooperative role of kindlin in integrin activation.
- In Chapter 3, we provide a more comprehensive analyses of integrin α-β crossing angle change during talin-mediated integrin activation process. Our results highlight the importance of kindlin binding to integrin β subunit for α-β crossing angel change.
- In Chapter 4, we employ all-atomic molecular dynamics simulations to study allosteric regulation of Orai channel activation upon interaction with STIM protein. Our results provide mechanistic insights into residues involved in the Orai channel gating.
- Chapter 5 will present conclusions and future directions for this research.

# Chapter 2

# A Cooperative Role for Kindlin in Integrin Activation

The contents of this chapter have been published as:

Z. Haydari, H. Shams, Z. Jahed, and M. R. K. Mofrad, "Kindlin Assists Talin to Promote Integrin Activation," *Biophys. J.*, vol. 118, no. 8, pp. 1977–1991, Apr. 2020.

Z. Jahed*, Z. Haydari*, A. Rathish, and M. R. K. Mofrad, "Kindlin Is Mechanosensitive: Force-Induced Conformational Switch Mediates Cross-Talk among Integrins," *Biophys. J.*, vol. 116, no. 6, pp. 1011–1024, Mar. 2019.

## 2.1. Introduction

Integrin plays a central role in regulating cell-matrix and cell-cell adhesion and is crucial for various signaling pathways involved in cell migration, proliferation, and differentiation [78], [79]. Integrins are heterodimeric proteins composed of α and β subunits that associate noncovalently. Each subunit consists of a large extracellular ectodomain (ECD), a single pass transmembrane helix (TM), and a short cytoplasmic tail (CT) (Figure 2.1A) [35], [36]. There are 24 different combinations of integrin α and β subunits. Integrin αIIbβ3 is one of the well-known types that is only expressed in platelets and is necessary for the hemostatic function of platelets [25], [32]. Integrins mediate bidirectional, inside-out and outside-in signaling across the membrane. Inside-out signaling involves the interaction of intracellular proteins with the integrin CT, which modulates integrin's affinity for extracellular ligands [26], [30], [31].

Three distinct conformational states of integrin have been determined: bent-closed or resting state, extended-closed, and extended-open (Figure 2.1A) [25]. Integrin activation entails a conformational transition of integrin from a low-affinity to a high affinity state (Figure 2.1A) [33], [34]. It was previously believed that talin was both necessary and sufficient for inducing integrin activation [28], [48], whereas recent studies contradict this notion [49], [51], [80] and suggest that kindlin is also needed as a co-activator of integrin [50], [51], [81] . For example, Moser et al. showed that the knockout of kindlin3 results in inactivated integrins despite the presence of talin [82]. Moreover, kindlin-associated diseases like Leukocyte Adhesion Disease III (LADIII), reflecting deficiencies of integrin function, show the necessity of kindlin in integrin activation [32].

Both talin (talin-1 and -2) and kindlin (kindlin-1, -2, and -3) isoforms include a FERM (4.1 protein, ezrin, radixin, moesin) domain, which is composed of four structural subdomains F0-F3 [39]. Kindlin also features a pleckstrin homology (PH) domain inserted into its F2 subdomain, which has been shown to directly interact with the lipid membrane (Figure 2.1B) [83]. Talin and kindlin both bind to the CT domain of integrin β through their F3 subdomains. Specifically, talin binds to the NxxY motif at the membrane proximal region, whereas kindlin associates with this motif at the membrane distal part of CT suggesting that kindlin and talin can simultaneously bind to integrin tail and trigger activation [52]. The molecular mechanisms of the interplay among talin and kindlin for inducing integrin activation are not yet well understood. Recently solved crystal structure of kindlin provided the opportunity to study the molecular mechanisms of kindlin involvement in mechanotransduction and integrin activation [47].

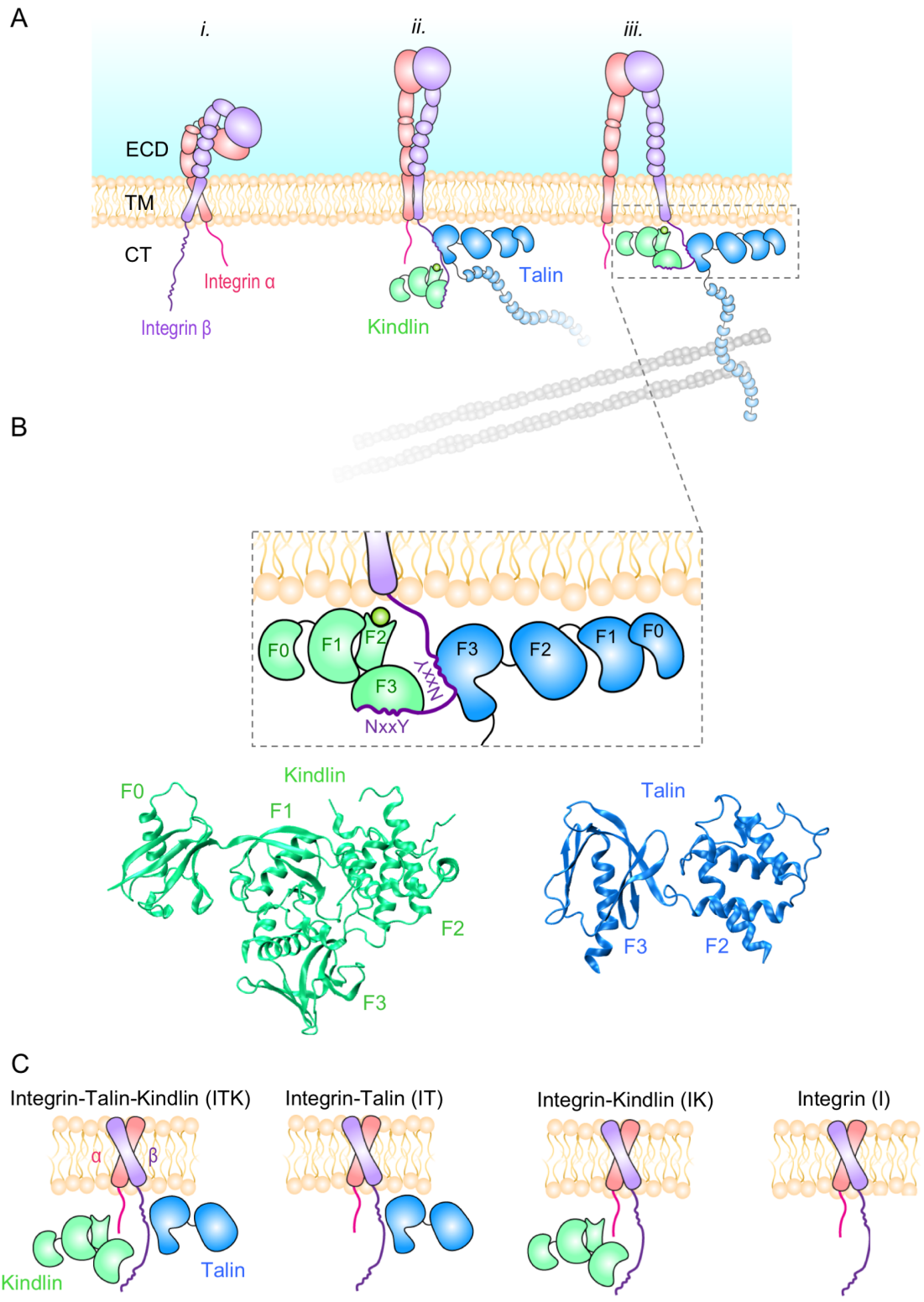
A
i.
ii.
iii.
ECD
TM
CT
Integrin α
Integrin β
Kindlin
Talin
B
F0
F1
F2
F3
NxxY
F0
F1
F2
F3
NxxY
Kindlin
F0
F1
F2
F3
Talin
F3
F2
C
Integrin-Talin-Kindlin (ITK)
Integrin-Talin (IT)
Integrin-Kindlin (IK)
Integrin (I)
α
β
Kindlin
Talin

Figure 2.1: Cytoplasmic interactions with the integrin β tail mediate inside-out signaling. (A) Schematic representations of the three conformational states of integrin: i) bent-closed (inactive) ii) extended-closed iii) extended-open (activated). Talin and kindlin are both involved in integrin activation by binding to the cytoplasmic domain of β. Talin association to the actin cytoskeleton provides a linkage between the extracellular environment and the cytoskeleton. (B) The F3 subdomain of talin and kindlin bind to the membrane proximal and membrane distal regions of β–integrin, respectively (top). The crystal structure of kindlin2 (F0-F3 subdomains) and talin1 (F2-F3 domains) (bottom). (C) Schematic representations of the four molecular models used in our simulations: integrin in complex with talin and kindlin (ITK), integrin in complex with talin (IT), integrin in complex with kindlin (IK), and integrin only (I).

**Kindlin is mechanosensitive**

Numerous studies have shown that kindlin's main partner and co-activator of integrin, namely talin, is mechanosensitive [84]–[86]. Ever since our first molecular dynamics models proposing the mechanisms of talin's mechanosensitivity [85], the molecular responses of talin to force have been experimentally validated and extensively studied [84], [86], [87]. On the other hand, kindlin's involvement in mechanotransduction has only recently been proposed [88], [89] and the molecular mechanisms remain completely unknown.

The crystal structure of kindlin2dimer/integrinβ1 structure complex providing invaluable insights into molecular mechanisms of kindlin's involvement in integrin activation and clustering [90]. One important observation was that kindlin could surprisingly form dimers that bind to two integrins, which provided a mechanistic explanation of how kindlins may promote integrin clustering. Using the newly identified molecular structure, we modeled the response of kindlin2-intergin dimer complex to mechanical cytoskeletal forces. Using molecular dynamics simulations, we show, in a highly reproducible manner, that forces on integrin are transmitted to the kindlin2 protomer-protomer interface and results in a shift in the interactions at this interface, which further stabilizes the complex. This residue network consists of highly conserved residues R577, S550 and E553 on each protomer. Under force, R577 on one protomer switches from interacting with S550, to forming new h-bonds with E553 on the neighboring protomer. This conformational switching is directly correlated with the end-to-end distance of integrins. This force-induced strengthening is similar to the catch bond mechanisms that have previously been observed in other adhesion molecules [91], [92].

Several studies have shown that the size of focal adhesions is proportional to adhesion strength, especially during the initial stages of myosin-mediated adhesion maturation [93]–[95]. Based on our results we propose that the kindlin dimer can play strengthen integrin mediated focal adhesion under force by taking the load off of integrin and strengthening its interactions under tensile forces [29].

**Kindlin involvement in integrin activation**

Recent experimental and computational studies have revealed important molecular details of integrin inside-out activation. These studies have suggested that the inner membrane clasp (IMC) between the CT domains of integrin subunits is critical for maintaining the closed state of integrin. In addition, these studies have shown that unclasping of the IMC induced by talin or other activators triggers integrin activation [53]–[55], and ultimately results in an increase in the crossing angle between α and β monomers [24], [56], [57]. However, all computational studies on integrin-mediated inside-out signaling to date have overlooked the role of kindlin due largely to lack of sufficient structural information [26], [27], [96], [97]. In the present study we use the recently solved crystal structure of kindlin [90] to investigate the molecular mechanisms of integrin activation through simultaneous binding of talin and kindlin.

Previous studies from our group have also looked at the molecular interactions between focal adhesion proteins using MD simulations [98]–[101]. For example, Golji et al. investigated the interaction of talin with two different states of vinculin, i.e. autoinhibited and activated. This study showed that talin could completely bind to activated vinculin. MD is a powerful technique to shed light into molecular details of interactions between proteins, especially when the resolved protein structures are available. To identify these critical interactions, different simulation scenarios can be designed in which the effect of different molecules can be exclusively and/or simultaneously be studied. We use all-atomic microsecond-scale molecular dynamics simulations of integrin αIIbβ3 TM/CT structure in an explicit lipid-water environment (I) and under the following three conditions: in complex with talin1 F2-F3 subdomains (IT), with kindlin2 (IK), and with both talin1 and kindlin2 (ITK) to uncover the role of kindlin in integrin activation (Figure 2.1C). Specifically, we explore how talin and kindlin binding affect allosteric transition of forces across the integrin molecule, i.e. from CT to TM, and eventually to the ectodomain. Our results show that kindlin2 cooperates with talin1 to facilitate integrin αIIbβ3 activation by enhancing talin1 interaction with the membrane proximal (MP) region of β3-integrin [102].

## 2.2. Computational Procedures

### System Setups

The crystal structure of TM/CT domains of integrin αIIbβ3 (PDB: 2KNC [103]), talin1 (PDB: 3IVF [83]), and kindlin2 FERM domain (PDB: 5XPY [47]) were taken from the Protein Data Bank. Since the talin FERM domain is both necessary and sufficient for integrin activation [104], [105], the talin rod domain was excluded from our models to reduce the system size and minimize the computational overhead. Two regions of kindlin2 FERM domain in F1 and F2 subdomains are missing in the current resolved crystal structure. These regions are connected to the current crystal structure via flexible linkers and the motions of these missing regions are independent of other parts of the molecule [106]. Also, since there are no known interactions between the kindlin missing residues and talin or integrin molecules, no homology modeling techniques were used as they would introduce uncertainties.

Four different models were built using VMD: integrin αIIbβ3 (I), integrin αIIbβ3 in complex with either talin1 (IT) or kindlin2 (IK), or both talin1 and kindlin2 (ITK). First, the TM domains of integrin were embedded in a patch of POPC lipid bilayer with dimensions of 200×250 $Å^2$ using VMD. Also, the lipid chains overlapping with the integrin were removed. Then, the structures of integrin in complex with talin (PDB: 3G9W [107]) and kindlin (PDB: 5XQ1 [106]) were used as templates for finding the best orientation of talin and kindlin molecules with respect to integrin and the membrane. Two different orientations were tested for IT and ITK scenarios (IT, IT_o, ITK, and ITK_o). Additionally, two different trial runs were conducted for ITK (ITK and ITK_2).

All systems were solvated using TIP3P explicit water model in NAMD [108] and water molecules inside the lipid membrane were removed. Then all systems were neutralized and ionized with 150 mM of KCl. The number of atoms reached 744946 in ITK and ITK_2, 556876 in IT, 625742 in IK, 425820 in I, 745559 in ITK_o, and 556511 in IT_o.

### MD simulations

We performed all-atom molecular dynamics (MD) simulations to investigate the conformational changes of integrin αIIbβ3 upon simultaneous interaction with talin1 and kindlin2 (ITK, ITK_2, and ITK_o) and compared them to the control simulations (I, IT, IT_o, and IK). Molecular dynamics simulations were carried out using NAMD and CHARMM36 force field [109]. Molecular visualization and analysis were performed using

Visual Molecular Dynamics (VMD) package [110]. Periodic boundary conditions were used in all three dimensions and a 2 fs time step was used in all simulations. The Langevin piston Nose-Hoover pressure control algorithm, and the Langevin damping thermostat for temperature control were used [109]. Pressure was maintained at 1 bar and temperature at 310 K with a damping coefficient of 5/ps. Each trial was initially minimized for 100,000 timesteps using the conjugate gradient and line search algorithm to relax the structures and remove all bad contacts. Following the minimization process, each configuration was equilibrated for 25 ns or longer until equilibrium was reached. Fully equilibrated structures were then used in the final production simulations that ran for 1000 ns for ITK and IT, 760 ns for IK, 625 ns for I, and 400 ns for ITK_o, IT_o, and ITK_2.

To provide a side by side comparison between different simulation scenarios, we presented density plots that show the distribution of combined data obtained from various orientations and repetitions for each ITK and IT conditions. The density plots of the talin-integrin analyses for ITK_a (i.e., ITK, ITK_2, and ITK_o) and IT_a (i.e., IT and IT_o) data are overlaid to facilitate the comparison.

**H-bond calculations**

VMD hbonds plug-in (version 1.2) [110] was used to calculate the number of hydrogen bonds (hbonds) between regions of interest. The cutoff distance and angle were set to 4 Å and 20 Å, respectively. The density- and time-dependent plots were all prepared in R matrixStats and gplot [111], [112].

**Principal component analysis**

Principal component analysis (PCA) was used to examine the time evolution of the integrin structure along all trajectories and understand the conformational differences induced by cytoplasmic interactions. The principal components were defined as the orthogonal axes of maximal variance and identified by superpositioning the structures on the invariant core and calculating the variance using the tools introduced by the Bio3D package [113].

**Residue cross correlation**

To examine how atomic fluctuations and displacements within the integrin heterodimer are correlated throughout our simulations, we performed pairwise residue cross-correlation analysis using cross-correlation function (*dccm.xyz*) in the Bio3D package [113]. The matrix of all pairwise cross-correlations between residues was visualized using a dynamical cross-correlation heatmap.

### Cross correlation function

The cross correlation function (CCF) in R was used to understand the relationship between two time series representing different features along the trajectories. The first argument was treated as the predictor (cause) of the second argument. The lag period indicates when the effect of a change in one feature is reflected in the other feature [113].

### Solvent accessible surface area

The solvent-accessible surface area (SASA) of each molecule was calculated using the measure *SASA* command in VMD [110].

### Force distribution analysis

To monitor changes in the internal forces of the integrin heterodimer upon cytoplasmic interactions, we performed Time-resolved Force Distribution Analysis (TRFDA) implemented in the GROMACS software package [114]. Atomic pairwise forces were calculated for all residues of both integrin subunits and included only the non-bonded electrostatic interactions acting on each residue. The comparison between force propagation along the transmembrane domains of integrins indicated the allosteric signal propagation across the membrane. The punctual stress measured for α- and β-subunits is the sum of absolute values of scalar pairwise forces exerted on each atom.

### Structural alignment

To determine the changes in the conformation of kindlin and talin upon interactions with integrin, we compared the initial structures of these molecules with the final structures after ~1000 ns of simulation. The final structures of talin in the ITK or IT simulations were aligned to the initial structure of talin using the *struct.aln* function in the bio3D package in R [113]. Similarly, the final structures of kindlin in the ITK or IK simulations were aligned to the initial kindlin structure. To quantify the distances between residues in the two aligned structures, a difference vector was calculated between the two structures using the *dist.xyz*function in R [113].

## 2.3. Results

To explore the role of kindlin in the activation of integrin as part of the integrin-mediated inside-out signaling, we developed all-atomic microsecond-scale molecular dynamics simulations of αIIbβ3 using an explicit lipid-water environment under four distinct scenarios, namely integrin alone (I) and in complex with talin1 F2-F3 subdomains (IT), with kindlin2 (IK), and with both talin1 and kindlin2 (ITK).

### The interactions of talin1 and kindlin2 with the cytoplasmic domain of integrin β3 regulate its conformation

The mechanism of interactions of talin1 and kindlin2 with integrin β3 can be characterized based on the conformational transitions of the integrin heterodimer. These conformational changes were determined by comparing the first and last frames of our microsecond molecular dynamics simulations, featuring identical starting conformation of integrin for all scenarios (Figure 2.2A). The crossing angle between the transmembrane regions of integrin monomers was notably increased in IT simulation changing the shape to open scissors (see below for further details). Unexpectedly, the final shape of integrin in the ITK simulation was changed to closed scissors (Figure 2.2A). No significant change was observed in the crossing angle in IK simulation, and only a small decrease in this angle was seen in I simulation.

Conformational transitions of the integrin dimer in response to cytoplasmic interactions with talin1 and/or kindlin2 were quantified via principal component analysis (PCA). For PCA calculations, the invariant core of the structure in each simulation was identified. The distribution of structures was extracted from each trajectory and conformational differences were quantified for equivalent residues. The first two principal components accounted for over 45% of the variance in all simulations. Since the contribution of all other principal components was relatively minimal, the structural distribution was projected in PC1-PC2 space as shown in Figure 2.2B and Figure 2.3A. The color gradient from red to black represents the time evolution of simulation trajectories in the PCA plots. For IT, ITK, IT_o, ITK_o, and ITK_2, the final state of the system falls far from the initial state in the principal component (PC) space indicating remarkable conformational transition; however, this is not notable in neither IK nor I.

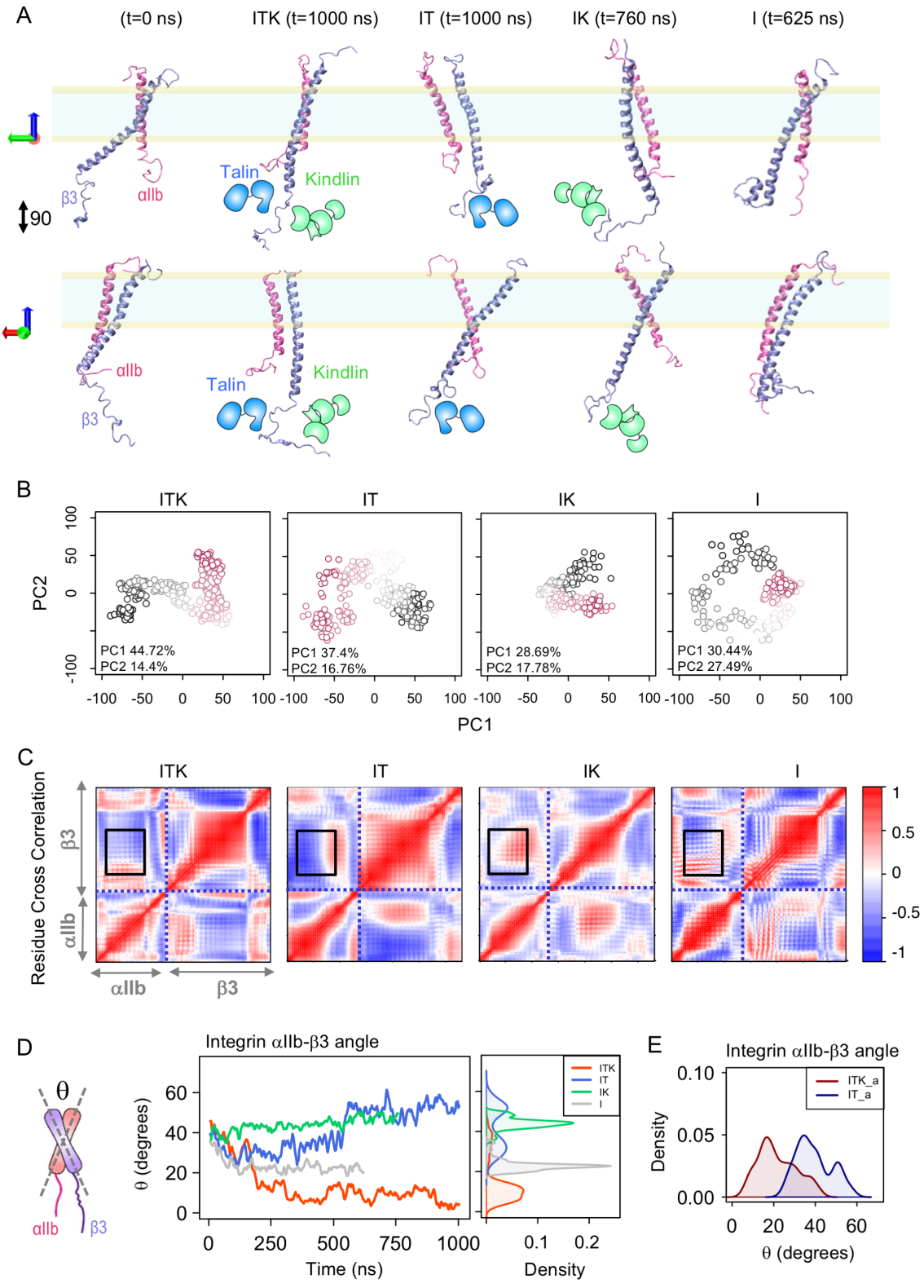
A
(t=0 ns)
ITK (t=1000 ns)
IT (t=1000 ns)
IK (t=760 ns)
I (t=625 ns)
Talin
Kindlin
αIIb
β3
90
B
ITK
IT
IK
I
PC2
PC1
PC1 44.72%
PC2 14.4%
PC1 37.4%
PC2 16.76%
PC1 28.69%
PC2 17.78%
PC1 30.44%
PC2 27.49%
C
Residue Cross Correlation
ITK
IT
IK
I
β3
αIIb
αIIb
β3
D
θ
αIIb
β3
Integrin αIIb-β3 angle
θ (degrees)
Time (ns)
Density
ITK
IT
IK
I
E
Integrin αIIb-β3 angle
Density
θ (degrees)
ITK_a
IT_a

Figure 2.2: Conformational changes of integrin αIIbβ3. (A) Schematics of talin and kindlin overlaid with the cartoon representations of the integrin αIIb (mauve) β3 (iceblue) heterodimer in two different views (90 degrees). Snapshots of the trajectories of the integrin αIIbβ3 dimer for the last simulation frame of the ITK (t=1000ns), IT (t=1000ns), IK (t=760ns), and I (t = 625ns) simulations are shown. (B) The principal component analysis (PCA) of all trajectories. Each point is a structural state in the PC1-PC2 space. Points corresponding to the beginning of all trajectories are shown in red, middle frames are represented by smooth color change to white and end frames are illustrated in black. (C) Residue cross correlation heatmaps of the integrin αIIb and β3 helices averaged over simulation time. The αIIb and β3 regions are indicated on the heatmaps. Black boxes indicate the TM regions of integrin dimer. A representative heatmap is shown for each of the four ITK, IT, IK, and I simulations. (D) A schematic representation of the integrin dimer showing angle θ between the αIIb and β3 helices (right). The time and density plots of angle θ for the ITK, IT, IK, and I simulations are shown in red, blue, green, and grey respectively. (E) The density plots of the θ angle are shown for the combined ITK simulations (ITK_a) and combined IT simulations (IT_a) in dark red and dark blue, respectively.

Residue cross correlation analyses between all residue pairs of the integrin αIIb and β3 in ITK, ITK_2, ITK_o IT, IT_o, IK, and I were performed to examine how the fluctuations within the integrin dimer are correlated (Figure 2.2C and Figure 2.3B). Interestingly, we observed a correlation and hence a coupling between the transmembrane regions of integrin αIIb and β3 (black boxes in Figure 2.2C and Figure 2.3B). This coupling was dominantly observed in ITK and IT scenarios. The level of residue correlations was notably lower in IK and I simulations (Figure 2.2C).

In addition, we calculated the crossing angle between αIIb and β3 helices (θ) as a function of time (Figure 2.2D) to quantify the conformational changes of integrins. Specifically, we calculated the angle between the line crossing residues 967 to 979 in αIIb and the line crossing residues 697 to 709 in β3. As expected, an increase in crossing angle of β3 in IT simulations was observed. Interestingly, in ITK, the θ angle starts from 40 degrees and then approaches zero after 250 ns of simulation and αIIb and β3 helices become almost parallel to each other. In the case of binding of kindlin2 without talin1 (IK), our results showed a small angle change (10 degrees) in θ, which is clearly in contrast with the cases of binding of talin1 that resulted in a noticeable change of θ (i.e., 30 degrees change in IT and 40 degrees change in ITK). Also, the crossing angle immediately drops in the first 150 ns of the simulation in which we only considered integrin (I) and stabilizes to approximately 20 degrees after 150 ns.

Moreover, we added an overlaid density plots that shows the distribution of the combined data obtained from various orientations and repetitions for ITK and IT scenarios. Basically, the density plots of the angle between integrin monomers for all the ITK (i.e., ITK, ITK_o, ITK_2) and IT (i.e., IT and IT_o) data are overlaid (Figure 2.2E). The distinction between the peak of the combined ITK density plots (i.e., ITK_a) and the peak of the combined IT density plots (i.e., IT_a) clearly shows higher angle values for IT compared to ITK in each orientation and each repetition.

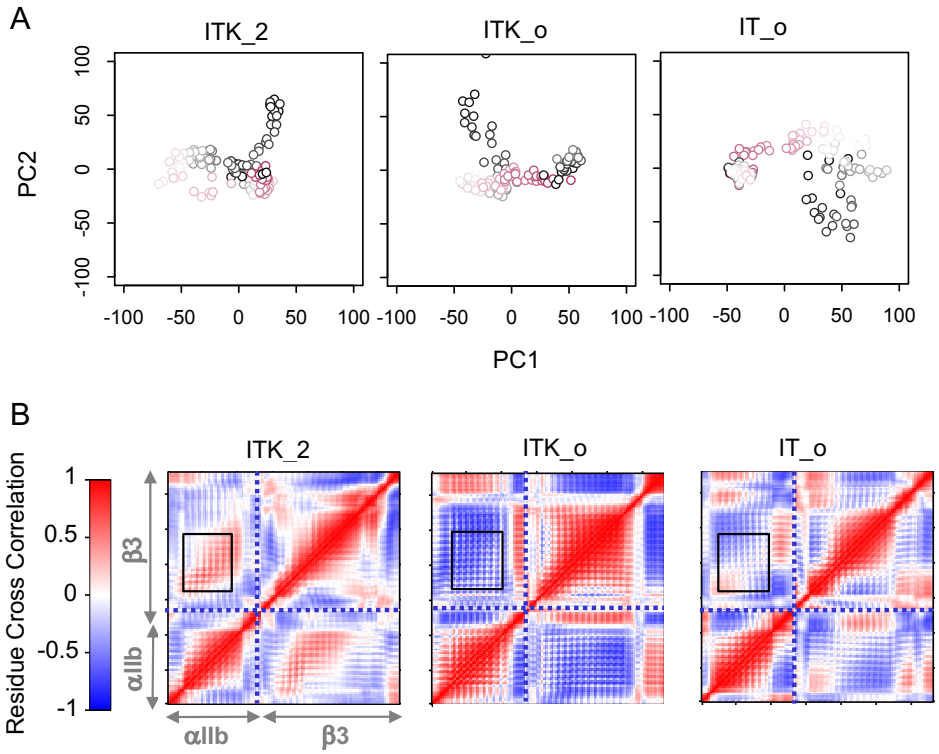


Figure 2.3: PCA and dynamic cross correlation of integrin αIIbβ3. (A) The principal component analysis (PCA) of ITK_2, ITK_o, and IT_o trajectories. Each point is a structural state in the PC1-PC2 space. Points corresponding to the beginning of all trajectories are shown in red, middle frames are represented by smooth color change to white, and end frames are illustrated in black. (B) Residue cross correlation heatmaps of the integrin αIIb and β3 helices averaged over the entire simulation time. The αIIb and β3 regions are identified on the heatmaps. Black boxes indicate the TM regions of integrin dimer. A representative heatmap is shown for each of the three ITK_2, ITK_o, and IT_o simulations.

**Interactions between integrin αIIb and β3 upon binding of talin1 and kindlin2**

In order to determine the conformational transition in integrin β3 upon binding of talin1 and kindlin2, we next analyzed the interaction energy between αIIb and β3 helices. Two interaction interfaces on the integrin αIIbβ3 TM/CT domains are known to stabilize the resting conformation of the dimer: the inner membrane clasp (IMC) and the outer membrane clasp (OMC). IMC is characterized by the interactions between the highly conserved $^{991}$GFFKR$^{995}$ motif of αIIb and W715, K716, and I719 residues of β3, and a salt bridge between residue R995 on αIIb and D723 on β3 (Figure 2.4A). The R995-E726 salt bridge is also known to be involved in maintaining integrin in an inactive conformation. OMC is defined as an interaction network between $^{972}$GXXXG$^{976}$ on αIIb and V700, M701, and I704 residues on β3, as well as associations between αIIb $^{979}$LL$^{980}$ and β3 $^{705}$LXXG$^{708}$ residues (Figure 2.4A). Mutations in the residues involved in IMC or OMC result in disruption of interactions between αIIb and β3 helices leading to integrin activation [25], [27], [37]–[39].

To examine whether the binding of kindlin2 or talin1 could disrupt the IMC and OMC interactions in our simulations, we calculated the non-bonded interaction energies between IMC and OMC regions over the course of simulation time (Figure 2.4B). Our results showed that the interaction energies of IMC and OMC decrease upon simultaneous binding of talin1 and kindlin2 (ITK simulation), and stabilize after 250ns to approximately zero in IMC, and -4 kcal/mol in OMC. In IT simulation, the non-bonded interaction energy in OMC approaches zero and remains zero after 500ns. On the other hand, IMC interactions in IT simulations switch between zero and -100 kcal/mol. In IK and I simulations, there is no change in the OMC interactions and a stable nonbonded interaction energy of ~-7 kcal/mol is maintained throughout the simulation. The IMC level is also stable but slightly higher in I (~-150 kcal/mol) compared to IK (~ -120 kcal/mol), due to an initial increase in the IMC level in I. This initial IMC increase in I simulation can possibly result in the initial decrease in the θ angle as shown in Figure 2.2D.

These results indicate that the cooperation of kindlin2 and talin1 can destabilize integrin αIIbβ3 dimer at IMC region and weaken their association in OMC region. Our results also suggest that kindlin2 alone is not sufficient to disrupt the IMC or OMC interactions. Also, the stable interactions (IMC and OMC) in I simulation confirm that the disruption of these interactions in IT and ITK are not random and are a result of the binding of kindlin2 and talin1 to the cytoplasmic regions of integrin.

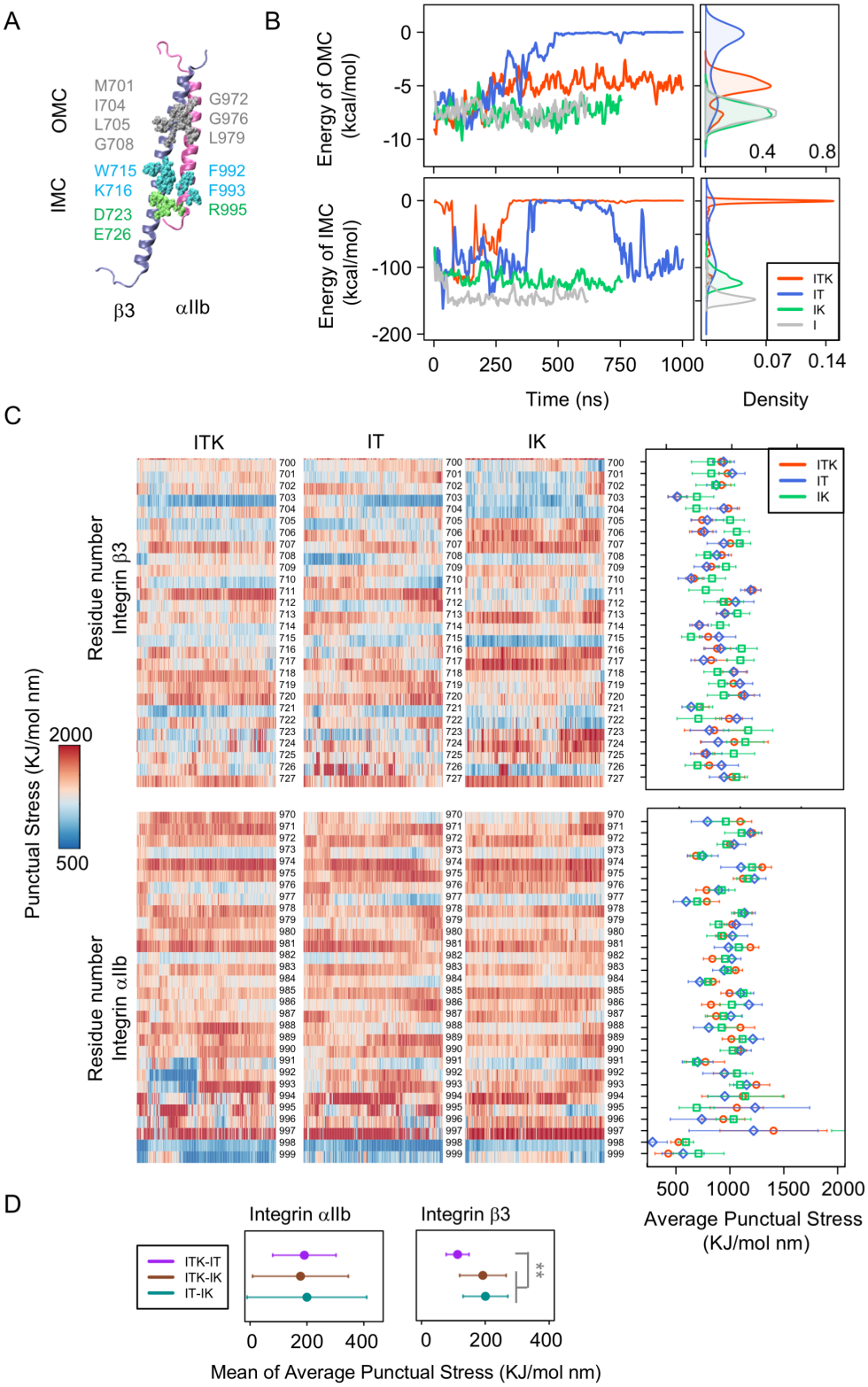
A
OMC
IMC
M701
I704
L705
G708
W715
K716
D723
E726
G972
G976
L979
F992
F993
R995
β3
αIIb
B
Energy of OMC (kcal/mol)
Energy of IMC (kcal/mol)
Time (ns)
Density
ITK
IT
IK
I
C
ITK
IT
IK
Residue number Integrin β3
Residue number Integrin αIIb
Punctual Stress (KJ/mol nm)
2000
500
Average Punctual Stress (KJ/mol nm)
D
Integrin αIIb
Integrin β3
ITK-IT
ITK-IK
IT-IK
**
Mean of Average Punctual Stress (KJ/mol nm)

Figure 2.4: Interactions between αIIb and β3 dimer. (A) Structure of the αIIb (mauve) β3 (iceblue) heterodimer. Interacting residues in the OMC region are shown in silver, in the IMC region in blue, and the αIIb R995 - β3 D723/D726 salt bridges in green. (B) The time and density plots of energy of interactions between OMC (top) and IMC (bottom) residues are shown for the ITK, IT, IK, and I simulations in red, blue, green, and gray respectively. (C) Time-resolved force distribution analysis (TRFDA) and time-averaged punctual stresses (for the last 300 ns of the simulations) within the integrin αIIb and β3 dimer were calculated. Representative heat maps of per-residue punctual stress values over simulation time for the integrin β3 residues 700 to 727 and αIIb residues 971 to 996 are shown. A representative heatmap is shown for each of the three ITK, IT, and IK simulations. (D) The average values and SDs are shown for the mean of the time-average of punctual stresses of ITK-IT, ITK-IK, and IT-IK. Mean of time-average of ITK-IT is significantly lower than ITK-IT, and IT-IK; p-value <1e-8.

Moreover, significant conformational changes in the TM of integrin in ITK and IT compared to IK and I (Figure 2.2) show a correlation between OMC disruption and the open/close structure of integrin. Basically, the disruption of interactions in OMC region cause separation of αIIb and β3 helices leading to the conformational changes in the TM region of integrin as discussed in more detail in the following section.

Mechanical signal transmission entails dynamic force redistribution across the integrin αIIbβ3 molecule. To investigate how cytoplasmic interaction(s) with talin1 and/or kindlin2 allosterically impact the stress distribution within the TM, especially near the IMC and OMC, we performed time-resolved force distribution analysis (TRFDA) for the binding simulations as shown in Figure 2.4C. For this purpose, we calculated punctual stresses for residues of integrin αIIb and β3 helices (see Computational Procedures) and showed the results over time or time-averaged of the last 300 ns of the simulations. The time-average of punctual stress of all integrin residues was used as a measure to compare force distribution patterns between simulations as shown in Figure 2.4C right side, bars indicate standard deviation. Moreover, in order to see the differences between punctual stresses of the simulations, the time-average of the punctual stresses was calculated for the differences between any pair of two out of the three states of ITK, IT, and IK simulations for each residue (ITK-IT, ITK-IK, and IT-IK) (Figure 2.5).

Significant differences in the punctual stresses of integrin β3 were almost exclusively observed in IK compared to ITK and IT simulations. Basically, more similarities in the time averaged punctual stresses can be seen between ITK and IT simulations (Figure 2.4C, 2.4D and Figure 2.5). Specifically, time-averaged punctual stresses experienced in residues

704 and 705 (part of IMC), 706, 711, 715 (part of OMC), 717, 722, 723 and 724 were remarkably different in IK, while they were almost the same in IT and ITK simulations. Notably, residue 711 showed a most significantly different punctual stress within the IK simulation.

Force distribution analysis (FDA) results show the punctual stress changes within the transmembrane helices and cytoplasmic regions of integrin αIIbβ3 are imposed by talin1 and/or kindlin2 binding to the integrin cytoplasmic region resulting in IMC and OMC disruption and separation of αIIb and β3 helices in ITK and IT.

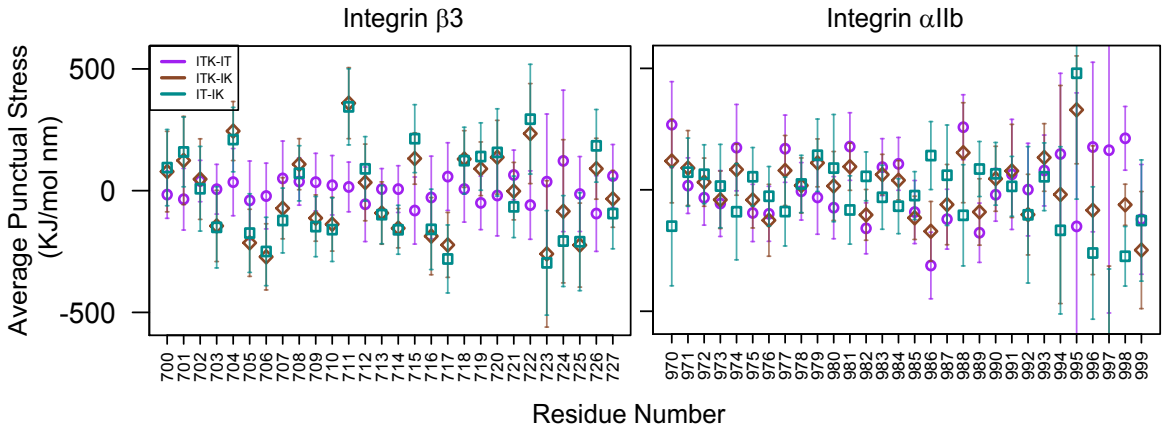


Figure 2.5: Time-averaged force distribution analysis (FDA) of integrin αIIbβ3. The difference time-averaged punctual stresses between any pair of two out of three simulation states of ITK, IT, and IK are shown for each residue of integrin β3 (residues 700 to 727) and αIIb (residues 971 to 996). The averages were taken for the last 300 ns of the simulations.

### αIIb-β3 angle change (θ) is correlated with OMC

To understand whether changes in the angle (θ) between αIIb and β3 (Figure 2.2D, 2.2E) were correlated with the interaction energies of IMC and OMC (Figure 2.4B), we performed a cross correlation analysis using the cross correlation function for time series in R, as described in Materials and Methods (Figure 2.6 and Figure 2.7). This function computes the covariance between two time series up to a defined lag. Based on the results shown in Figure 2.6 and Figure 2.7 (top), the angle θ was not a significant predictor of IMC, most likely because IMC was either abruptly disrupted or remained stable throughout the simulation. This suggests that IMC dissociation is directly regulated by cytoplasmic interactions and not through angle change. In other words, interaction at the cytoplasmic

region exerts tension that is transmitted by both bonded and non-bonded interactions across integrin residues towards the membrane, which eventually breaks IMC and allows angle change.

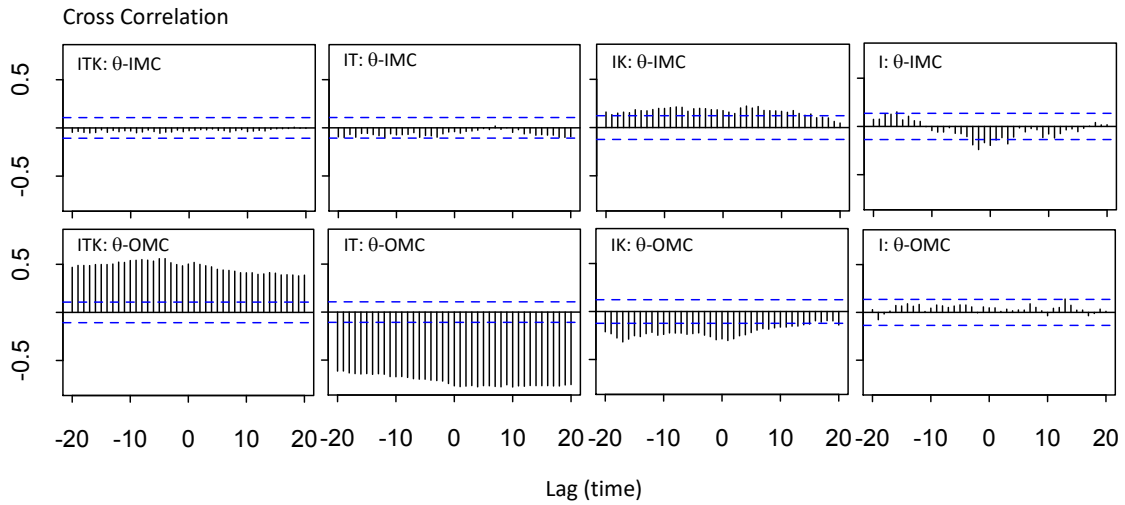


Figure 2.6: Integrin αIIb-β3 crossing angle correlation with IMC and OMC. Cross correlation of IMC and angle changes of αIIb and β3 (top); and OMC and angle changes of αIIb and β3 (bottom) are shown. The horizontal blue lines are the approximate 95% confidence interval. Cross correlation plot is shown for each of the four ITK, IT, IK, and I simulations. High correlations exist between θ and OMC in ITK and IT, while the other correlations are negligible.

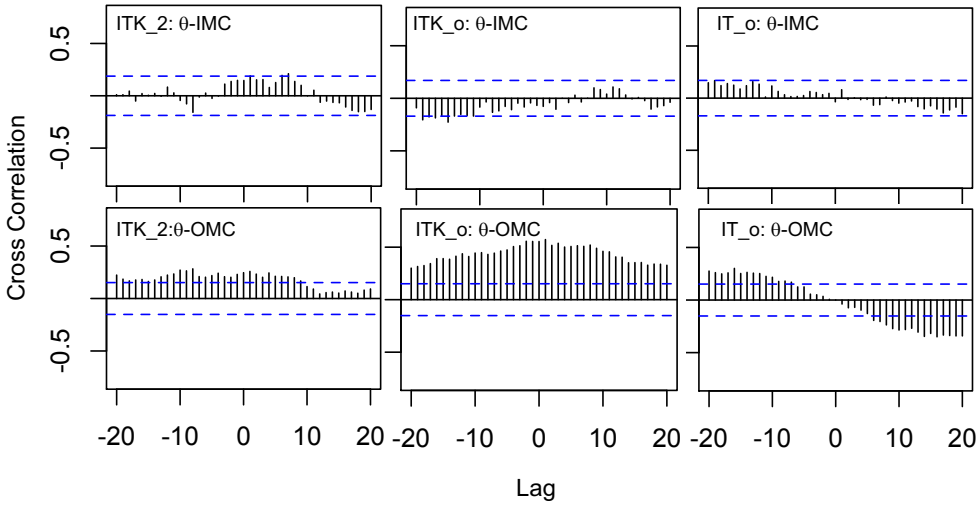


Figure 2.7: Cross correlation of angle θ and interaction energy of IMC and OMC. Cross correlation of IMC and angle changes of αIIb and β3 (top); and OMC and angle changes of αIIb and β3

(bottom) are shown. The horizontal blue lines are the approximate 95% confidence interval. Cross correlation plot is shown for each of the three ITK_2, ITK_o, and IT_o simulations. There is a correlation between θ and OMC, while no correlation was observed between θ and IMC in any of the cases.

Conversely, dynamics of OMC interactions were highly correlated with θ in ITK and IT simulations (Figure 2.6 bottom). The reverse correlations of ITK and IT reflects opposite directions of angle change. OMC interactions were also correlated with θ in ITK_2, ITK_o, and IT_o simulations (Figure 2.7 bottom). Since there is no significant change in angle (θ) in the IK, and only a small rapid decrease in θ in I simulations, we see a minimal θ-OMC correlation in IK and I compared to ITK and IT simulations (Figure 2.6 bottom).

**Talin1 binds more effectively/strongly to integrin αIIbβ3 in the presence of kindlin2**

Integrin β3 tail contains 47 residues and two NxxY motifs. The first NPLY motif (membrane proximal) is the binding site for talin1 and the second NITY motif (membrane distal) is the kindlin2 binding site. Talin1 and kindlin2 can simultaneously bind to β3 through their F3 domains and initiate inside-out signaling [35]. In order to understand how this inside-out signaling may be initiated by the cooperation between kindlin2 and talin1, we investigated the molecular mechanisms of simultaneous binding of talin1 and kindlin2 to the short CT of β3 and compared them with individual binding of integrin with talin1 and kindlin2 in our simulations. Specifically, we calculated non-bonded interaction energies between integrin β3 and kindlin2 or talin1, as well as solvent accessible surface areas of integrin β3 CT, talin1 and kindlin2.

We first calculated the non-bonded interaction energies between the CT of integrin β3 and talin1 or kindlin2 F3 domains (Figure 2.8A, 2.8B). Specifically, we calculated the interaction between residues 720 to 762 of β3 and residues 569 to 680 of talin1 or residues 560 to 680 of kindlin2. In the IT simulation, talin1 and β3 maintain an average interaction energy of 105 kcal/mol (Figure 2.8A top). However, talin1 is able to bind much more strongly to integrin β3 over time in ITK simulation. In this simulation, the non-bonded interaction energy between talin1 and β3 increases from 100 to 400 kcal/mol with an average energy of 222±94 kcal/mol. Similarly, the overlaid density plots of the talin-integrin interaction for the combined ITK (ITK_a) and combined IT (IT_a) data show higher energies in ITK_a compared to IT_a (Figure 2.8B top), confirming the stronger talin-integrin interaction in the presence of kindlin. Kindlin2, on the other hand (Figure

2.8A bottom) binds more strongly to integrin β3 in IK simulation with an interaction energy of 258±61 kcal/mol, compared to 124±57 kcal/mol in ITK simulation. The overlaid density plots of kindlin-integrin interactions for ITK_a and IK data show lower peak value in ITK_a compared with IK (Figure 2.8B bottom).

The crystal structures of the kindlin2-integrinβ3 and talin1-integrinβ3 complexes revealed the hbond network between the molecules [47]. To determine the stability of kindlin2 or talin1-integrin complex, we calculated the number of hbonds between integrin CT - kindlin F3 and integrin CT - talin F3 (Figure 2.8C). Our results show that talin1 forms a slightly higher number of hbonds with integrin β3 tail in the presence of kindlin2. However, kindlin2 can form a larger number of hbonds with integrin β3 tail in the absence of talin1.

Next, we calculated the solvent accessible surface area (SASA) of the integrin-binding-F3 subdomains of talin1 and kindlin2, and integrin β3 CT (see Materials and Methods, Figure 2.8D). Our results show that the SASA of talin1 is lower in ITK simulations (5929±210 $Å^2$) compared with IT simulation (6034±163 $Å^2$) (Figure 2.8A top). The SASA of kindlin2 immediately drops in the first 250ns of simulation in IK simulations. However, when talin1 is present, the SASA of kindlin2 fluctuates much more slowly and is much higher in value as shown in the density plots (Figure 2.8D middle). The SASA of integrin CT is the lowest in ITK simulations compared to IT or IK simulations. The average values of 2575±189 for ITK, 2698±221 for IT, and 2805±158 for IK suggest that both can bind to various regions on integrin and reduce its SASA (Figure 2.8D bottom). Also, in IT simulation, the SASA of integrin CT peaks at a slightly lower value than IK simulation, indicating a closer contact between integrin and talin1, compared to integrin and kindlin2 in conditions where only one of them is present. Based on the interaction energies and SASA results, it is evident that talin1 binds more effectively in the presence of kindlin2, and kindlin2 can bind to integrin much more strongly in the absence of talin1.

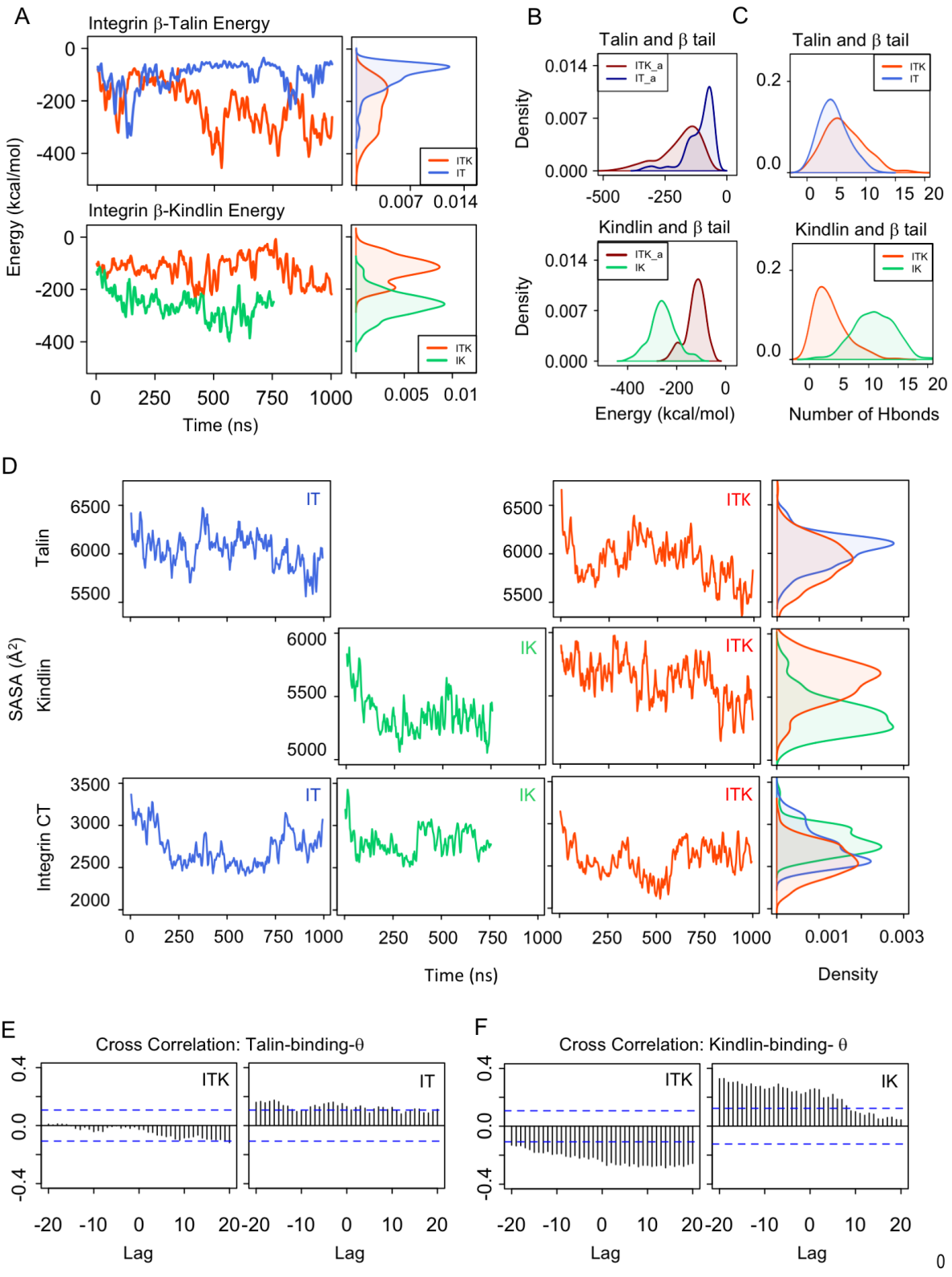
A
Integrin β-Talin Energy
Integrin β-Kindlin Energy
Energy (kcal/mol)
Time (ns)
ITK
IT
IK
B
Talin and β tail
Kindlin and β tail
Density
ITK_a
IT_a
IK
Energy (kcal/mol)
C
Talin and β tail
Kindlin and β tail
Number of Hbonds
D
Talin
Kindlin
Integrin CT
SASA (Å²)
Time (ns)
Density
E
Cross Correlation: Talin-binding-θ
Lag
F
Cross Correlation: Kindlin-binding- θ
Lag

Figure 2.8: Integrin β3-talin1 or kindlin2 binding. (A) The time and density plots of interaction energies between integrin β3 CT and talin1 F3 domain (top) and integrin β3 CT and kindlin2 F3 domain (bottom) are shown in three simulations of ITK, IT, and IK. (B) The density plots of interaction energies are shown for the ITK_a and IT_a in dark red and dark blue (top); also, for ITK_a and IK in dark red and green, respectively (bottom). (C) Density plot representations of the number of hbonds between integrin β3 CT and talin1 F3 domain (top) is shown for each of the ITK and IT simulations. The same plot is shown for kindlin2 (bottom) for each of the ITK and IK simulations. (D) Solvent accessible surface area (SASA) of talin1 (subdomain that binds integrin), in IT or ITK simulations (top), SASA of kindlin2 (subdomain that binds integrin), in IK or ITK simulations (middle), and SASA of the CT of integrin in IT, IK, or ITK simulations (bottom) are shown. (E) Cross correlation function between binding energy of talin1- integrin β3 and θ in ITK and IT simulations are shown. (F) Cross correlation between binding energy of kindlin2 - integrin β3 and θ in ITK and IK are shown (bottom).

Finally, to determine whether the interaction energies between integrin αIIbβ3 CT and talin1 or kindlin2 were directly correlated with the changes observed in the crossing angle between αIIb-β3 (θ), we also calculated the cross correlation between these parameters (Figure 2.8E and 2.8F). The interaction between talin1 and integrin β3 was promptly formed in both IT and ITK, while kindlin2 binding was relatively gradual. In both IT and ITK, talin1 binding did not show a major correlation with the angle change (Figure 2.8E) mainly because talin1 interaction was stable throughout the simulations. This suggests that a stable binding with talin1 is necessary for the subsequent changes in the integrin conformation. However, kindlin2 binding lagged the angle change in both IK and ITK (Figure 2.8F). This shows that role of kindlin2 is more complex as it may both directly and indirectly modulate integrin activation.

**Force distribution analysis of integrin β3 cytoplasmic tail**

We performed time-resolved force distribution analysis to monitor the dynamics of stress redistribution within the β3 cytoplasmic region upon simultaneous binding to talin1 and kindlin2. We have calculated the punctual stresses, scalar pairwise forces exerted on each atom, for the residues 728 to 762 of integrin β3 cytoplasmic domain over time for both IT and ITK simulations (Figure 2.9A). It can be seen from the heat map that the punctual stress fluctuates in most of the residues, except in residues 729 and 736, where the punctual stress remains high all the time both in IT and ITK.

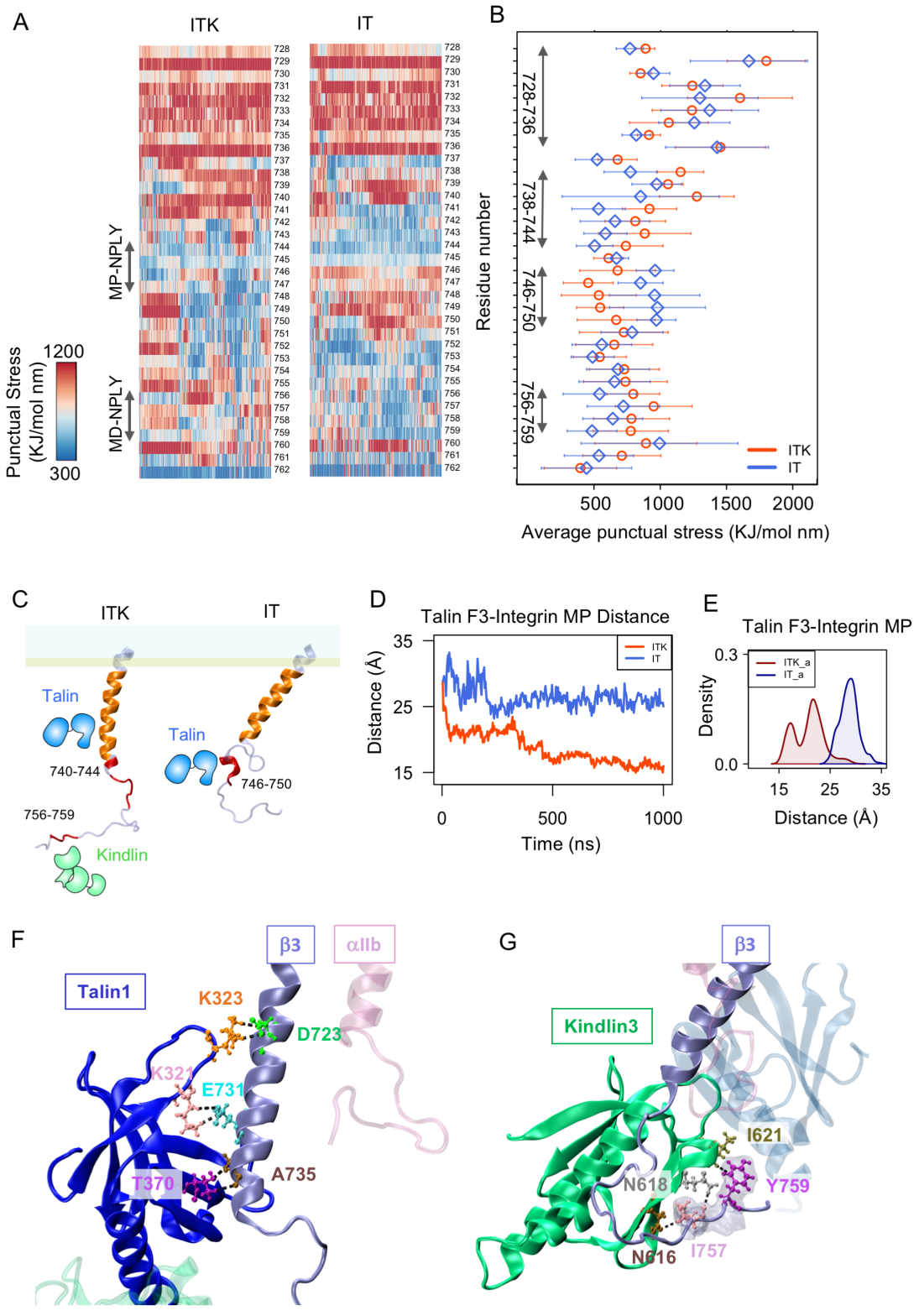
A
ITK
IT
MP-NPLY
MD-NPLY
Punctual Stress (KJ/mol nm)
1200
300
B
Residue number
728-736
738-744
746-750
756-759
ITK
IT
500
1000
1500
2000
Average punctual stress (KJ/mol nm)
C
ITK
IT
Talin
740-744
756-759
Talin
746-750
Kindlin
D
Talin F3-Integrin MP Distance
Distance (Å)
35
25
15
ITK
IT
0
500
1000
Time (ns)
E
Talin F3-Integrin MP
Density
0.3
0.0
ITK_a
IT_a
15
25
35
Distance (Å)
F
β3
αIIb
Talin1
K323
D723
K321
E731
T370
A735
G
β3
Kindlin3
I621
N618
Y759
N616
I757

Figure 2.9: Force distribution analysis of integrin αIIbβ3 cytoplasmic domain. (A) TRFDA of integrin αIIb and β3 subunits. Representative heat maps of per-residue punctual stress values over simulation time for the integrin β3 cytoplasmic regions are shown. A representative plot is shown for each of the three ITK, IT, and IK simulations. (B) Time-averaged punctual stress for the last 300 ns of the IT and ITK simulations for integrin β3 CT residues are shown. Different distinct regions can be identified based on whether the punctual stress of IT or ITK dominates. (C) Schematic representations of the final structure of the integrin β3 CT in ITK and IT simulations. Regions with high punctual stress values are shown in red and orange on β3 CT. (D) The time plot of distance between the center of mass of residues 720 to 736 in integrin β3 and talin1 F3 subdomain are shown for the ITK and IT simulations in red and blue, respectively. (E) The density plots of the distance between the center of mass of residues 720 to 736 in integrin β3 and talin1 F3 subdomain are shown for the combined ITK simulations (ITK_a) and combined IT simulations (IT_a) in dark red and dark blue, respectively. (F) Strong interactions between talin1 F3 subdomain and integrin β3 membrane proximal region in ITK simulation, mainly between residues K321, K323, and T370 on talin1, and residues D723, E731, and A735 on β3. Hydrogen bonds are shown with dashed black lines. (G) Interactions between kindlin2 F3 subdomain and integrin β3 NITY motif in ITK simulation, mainly between residues N616, N618, and TI621 on kindlin2, and residues I757 and Y759 on β3. Hbonds are shown with dashed black lines.

Also, we have calculated the time-averaged punctual stresses over the last 300 ns of the simulations (Figure 2.9B). Different distinct regions can be identified on Figure 2.9B and 6C based on whether the punctual stress of IT or ITK dominates. Time-averaged punctual stress is higher in residues 746 to 750, which overlaps with the talin1 binding site (NPLY), in IT compared to ITK. Conversely, the kindlin2 binding site (NITY) consisting of residues 756 to 759 shows higher time-averaged punctual stress values in ITK compared to IT. This most likely indicates that direct binding of integrin with kindlin can locally increase stress levels. However, the region consisting of residues 738 to 744 exhibits higher average stress values in ITK compared to IT. We should note that in ITK, the stress value suddenly declines in residues 748 and 749, while at the same time it increases in residues 737 and 739.

Moreover, we see similar high stress values in the region consisting of residues 728 to 736 in both IT and ITK. Our analysis of binding interactions in this region revealed that these residues interact strongly with the membrane in both IT and ITK. On the other hand, the distance between talin1 F3 subdomain and integrin β3 residues 728 to 736 decreases more significantly when kindlin2 is present (Figure 2.9D). Interestingly, the SASA of the MP (membrane proximal; residues 720 to 736) region of integrin CT and the SASA of talin1

F3 S1-S2 loop (residues 320 to 327) also decrease dramatically after 400 ns in ITK while it only slightly fluctuates in IT (Figure 2.10). Also, the distinct peak of the combined ITK density plot (i.e., ITK_a) from the peak of the combined IT density plot (i.e., IT_a) in talin-MP distance and SASA of the MP, clearly show the enhancement of talin-integrin binding, mediated by kindlin in all various orientations and repetitions of ITK simulations (Figure 2.9E and Figure 2.10B). Therefore, the presence of kindlin2 resulted in significantly stronger interaction of talin1 with integrin β3 membrane proximal region in ITK simulations compared to IT simulations. This is most probably an important factor in integrin activation as it can disrupt IMC.

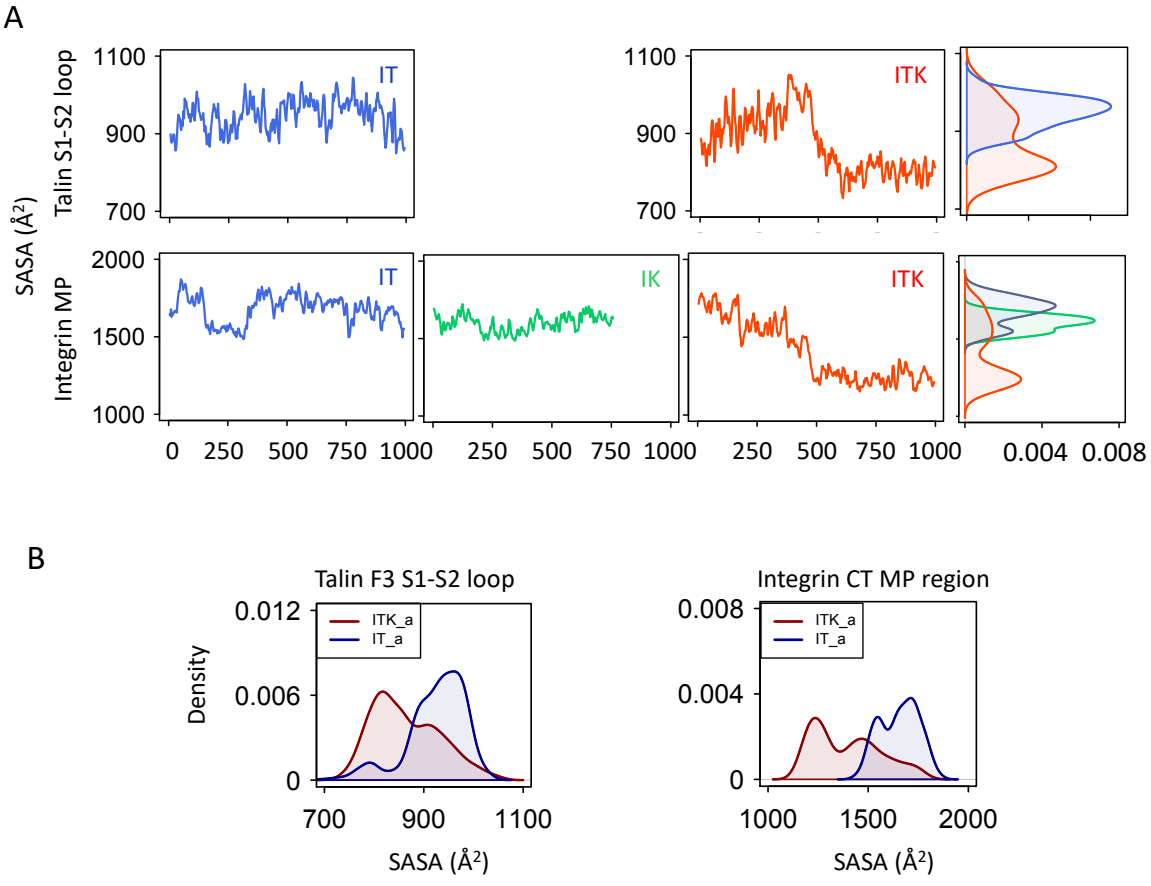


Figure 2.10: SASA of talin1 and integrin β3. (A) Solvent accessible surface area (SASA) of talin1 F3 S1-S2 loop (residues 320 to 327) for IT or ITK simulations are shown (top). Also, SASA of the membrane proximal region of integrin CT (residues 720 to 736) for IT, IK, and ITK simulations are shown (bottom). (B) The density plots of SASA of talin1 F3 S1-S2 loop (left) and SASA of integrin MP region (right) are shown for the ITK_a and IT_a in dark red and dark blue, respectively.

Furthermore, we studied the interactions of talin1 and kindlin2 with high-stress regions of integrin β3 over the course of the ITK simulation. We observed three important interactions between the F3 subdomain of talin1 and the MP region of integrin β3 (residues 723 to 736), namely, 1) talin1 K323- β3 D723, 2) talin1 K321- β3 E731, and 3) talin1 T370- β3 A735 (Figure 2.9F). In addition, interactions formed between the F3 subdomain of kindlin2 and the NITY motif of integrin β3 (residues 756 to 759). Specifically, residues N616/N618 and I621 of kindlin2 interacted with I757 and Y759 of integrin β3, respectively, which remained stable for the last 50ns of the ITK simulation (Figure 2.9G).

**Distinct conformational changes of kindlin2 and talin1 in presence of each other**

To determine whether any conformational changes were induced in kindlin2 or talin1 by their mutual interactions with integrin αIIbβ3, we performed structural alignments between the final structures of kindlin2 (at t=760ns) and talin1 (at t=1000ns) in each simulation, and their initial crystal structures. The structural alignments were performed using all subdomains that were simulated (i.e. F2-F3 for talin1 and F0-F3 for kindlin2). However, for clarity, the alignments are shown separately for each subdomain (Figure 2.11). In order to quantify the deviation of each residue from its original position, the distance between residues of the initial and final structures were calculated after structural alignment was performed (Figure 2.11).

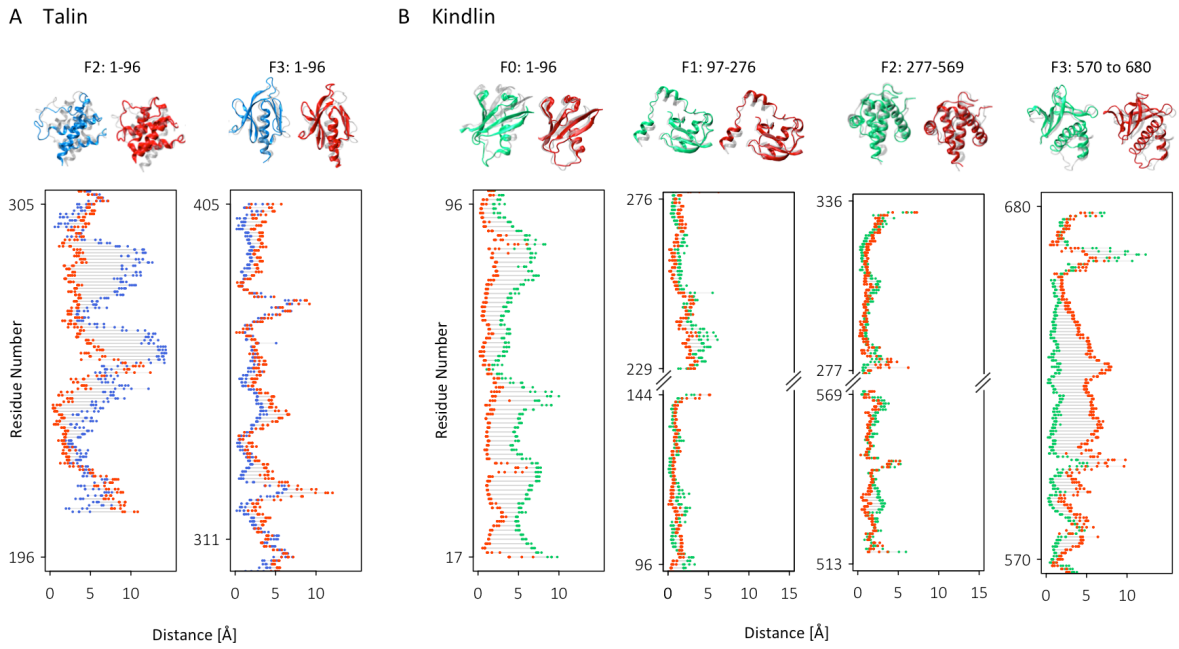

Figure 2.11: Kindlin2 and talin1 structural alignment. (A) Final frames of talin1 in IT (blue) and ITK (red) were aligned to initial PDB of talin1 (transparent). The distance shows the 3D distance between each residue in the two structures after alignment. (B) Final frames of kindlin2 in IK (green) and ITK (red) were aligned to the initial PDB of kindlin2 (transparent) (by RMSD minimization methods). The distance shows the 3D distance between each residue in the two structures after structural alignment.

Our results show that the conformational changes observed in the F2 subdomain (residues 196 to 305) of talin1 are much higher in IT simulation compared with ITK simulation (Figure 2.11A). These conformational changes are mainly observed in two α helices (~ residues 224 to 294) in the four helix bundle of the F2 subdomain in IT simulation. The conformational changes observed in the F3 subdomain of talin1 were similar between IT and ITK conditions and mostly limited to the loop regions as expected. The movement limitation imposed by simultaneous binding of talin1 F3 domain with integrin CT and the membrane (Figure 2.12A, 2.12C left) can account for lower conformational changes of F3 compared to F2 in IT and ITK.

The structural alignment of kindlin2 showed significant conformational changes in the F0 subdomain in IK simulations, and F3 in ITK simulations, whereas the F1 and F2 subdomains showed very small changes in both simulations. Previous work showed that the F0 subdomain of kindlin2 is highly dynamic and moves independently of F1-F3 subdomains. Also, kindlin F0 subdomain is interacting with the membrane during our simulations and has stronger and more stable interaction in ITK compared to IT in the last 200 ns of the simulations (Figure 2.12B bottom, 2.12C right). This stronger lipid interaction can account for lower conformational changes of F0 in ITK compared to IK. On the other hand, the conformational changes in F3 were seen in integrin binding regions (i.e. residues 590 to 656) and are likely attributed to the distinct interactions of kindlin2 with integrin β3 in IK vs ITK simulations. These results suggest that conformational changes are induced in talin1 and kindlin2 upon interactions with integrin β3, and that these changes are distinct when both molecules are present.

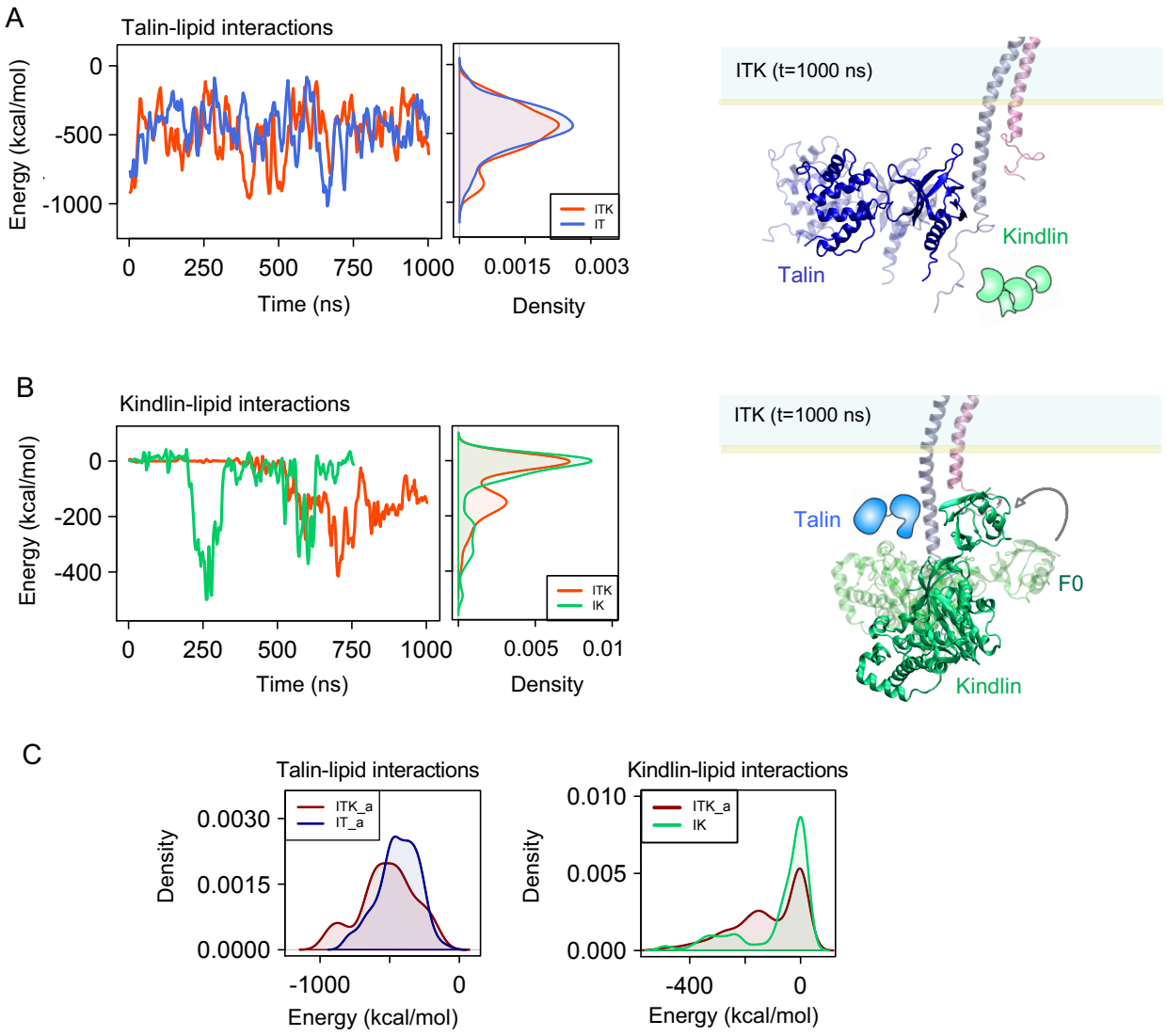


Figure 2.12: Kindlin/Talin-membrane interactions. (A) The time and density plots of interaction energies between talin1 and membrane are shown for ITK and IT simulations (left). Cartoon representations of integrin αIIbβ3 and talin1 overlaid with schematic of kindlin are shown for the last frame of the ITK simulation (1000 ns). The initial orientation of talin is shown transparent. (B) The time and density plots of interaction energies between kindlin2 and membrane are shown for ITK and IK simulations (left). Cartoon representations of integrin αIIbβ3 and kindlin2 overlaid with schematic of talin are shown for the last frame of the ITK simulation (1000 ns). Also, the initial orientation of kindlin is shown transparent. (C) The density plots of interaction energies are shown for the ITK_a and IT_a in dark red and dark blue (left); also, for ITK_a and IK in dark red and green, respectively (left).

## 2.4. Discussion

Integrin activation is central to a variety of cell functions, including cell-matrix adhesion, cell migration, and apoptosis. Kindlin and talin are both cytoplasmic proteins that directly interact with integrin tail and induce a high-affinity state of integrin for extracellular ligands [35]. Although talin can induce conformational changes in integrin, it has been shown that talin alone is not sufficient for the activation of integrin and kindlin also plays a key role in this process [49], [50]. While molecular mechanisms of talin-mediated integrin activation have been extensively studied, it is not yet clear how kindlin interferes with this process. Kindlin dysfunction has been associated with a number of human diseases, which are likely linked to deficiency in integrin activation; thus, knowing the molecular mechanism of kindlin-mediated integrin activation has potential impacts in therapeutic purposes. Here, we investigated the interplay between talin and kindlin in integrin activation using microsecond long molecular dynamics simulations (Figure 2.1).

Previous studies have shown that kindlin binding to integrin is not sufficient but is required for triggering integrin activation [25], [51], [80]. Moreover, Ma et al. showed that simultaneous transfection of kindlin2 with the head domain of talin enhances integrin activation and identified kindlin2 as a coactivator of talin [49]. However, the mechanisms of kindlin's involvement remain elusive, in particular it is still not known whether kindlin can induce conformational changes to integrin heterodimer. To address these questions and provide molecular details of the interaction among kindlin and talin with integrin, we developed all-atom microsecond-scale MD simulations of αIIbβ3 using an explicit lipid-water environment under three distinct scenarios: integrin in complex with talin1 (IT), kindlin2 (IK), and both talin1 and kindlin2 (ITK). We also performed a control simulation (I), in which only integrin was considered. This control simulation helps with better understanding of the effect of talin and kindlin interactions in integrin conformational changes (Figure 2.13A). Our IK simulation featuring integrin αIIbβ3 and kindlin2 showed that the main interactions that keep integrin in an inactive state, namely the IMC and OMC, remained stable over the course of 760 ns of the simulation when only kindlin is present (Figure 2.4B, 2.13B). This further confirmed that kindlin binding is insufficient for unclasping cytoplasm and transmembrane regions of αIIbβ3.

Interestingly, our simulations showed that kindlin2 binds to the integrin β3 tail more strongly in the absence of talin1, whereas talin1 binding to integrin is reinforced by kindlin2 (Figure 2.8). Talin1 interaction was particularly enhanced with the membrane

proximal (MP) region of integrin β3 (residues 720 to 736), while its interaction with the membrane proximal NPXY motif was gradually weakened over time. It should be noted that talin1 can still bind to integrin CT in IT and kindlin2 is not necessary for this interaction (Figure 2.8A, 2.8B). However, this interaction is mostly with the NPLY motif of integrin and the interaction with integrin MP region is very minimal (Figure 2.9D, 2.9E). Therefore, when kindlin2 is present, it indirectly pushes talin1 towards the membrane resulting in strong interaction with MP region of integrin as well, thus enhancing the talin-integrin interaction and a more effective disruption of the IMC in ITK compared to IT. This way, kindlin2 modifies the activation pathway by positioning talin1 more upward and closer to the membrane, resulting in stronger binding and a complete IMC disruption (Figure 2.13D).

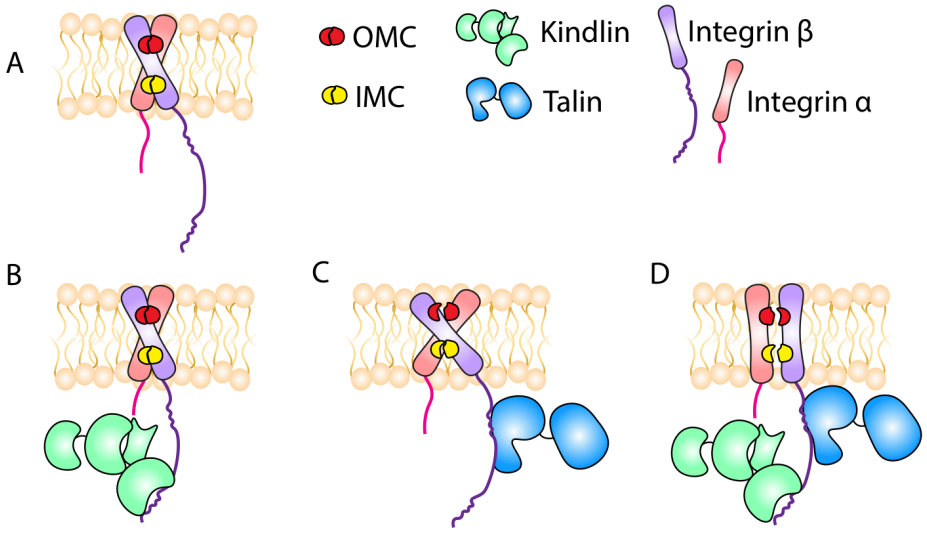


Figure 2.13: Schematic representation of the proposed kindlin-mediated integrin activation mechanism. (A) Integrin remains in a closed conformation when it is not interacting with talin or kindlin (with stable and strong interactions in IMC/OMC regions). (B) Kindlin alone is unable to disrupt the IMC or OMC interactions and therefore unable to induce conformational changes (i.e. angle changes between integrin α and β helices) in the transmembrane domain of integrin. (C) Talin binding to the integrin CT causes the complete disruption of OMC and destabilizes IMC interactions. Also, the angle between integrin α and β helices increases significantly upon talin binding. (D) Kindlin interaction with the membrane distal NPXY motif of integrin indirectly pushes talin towards the integrin membrane proximal region resulting in a stronger interaction between talin and the membrane proximal motif and a complete disruption of IMC, OMD and the parallelization of the transmembrane α and β helices.

Also, kindlin2 decreased the intradomain conformational changes of talin1, especially in F2 subdomain, which promoted both talin1-lipid and talin1-integrin β3 CT interactions (Figure 2.11A). Therefore, we suggest that the strength of kindlin2 binding to integrin does not necessarily correlate with activation, while stronger talin1 association can expedite the activation process. This further confirms the indirect role of kindlin2 as a cooperative partner for talin1 rather than a direct activator of integrin αIIbβ3. Although we did not observe a strong interaction between talin1 and membrane proximal region of β3 in IT simulations, it is quite conceivable that even without kindlin2's assistance, talin1 can eventually bind to the proximal region of integrin tail in a longer timescale.

On the other hand, the stronger binding of kindlin2 to integrin in the absence of talin1 observed in our simulations may have implications in talin-independent roles of kindlin in the formation and maturation of focal adhesions. Theodosiou et al. showed that subsequent to the cooperative activation of integrin by talin and kindlin, kindlin initiates a talin-independent signaling pathway at new adhesion sites by binding to other molecules such as paxillin to induce cell spreading [80]. Based on previous studies and our results, we propose that kindlin2 cooperates with talin1 to activate integrin by enhancing talin1's interactions with the CT of integrin. On the other hand, kindlin2 can bind more strongly to integrin in the absence of talin1 to perform talin1-independent signaling subsequent to integrin activation [80].

It is now widely accepted that the inner membrane clasp (IMC) and outer membrane clasp (OMC) between integrin subunits maintains the resting state of integrin and unclasping it triggers the inside-out signaling [25]. In the IMC, R995 of β-integrin forms two salt bridges with D723 and E726 on α-integrin, however, it has been shown that disrupting the R995-D723 interaction is most critical for integrin activation [25]. Our simulations indicated that talin1 disrupts R995-D723 interaction in both presence or absence of kindlin2, however, kindlin2 is also required for dissociating R995-E726 interaction within 1μs of simulation (Figure 2.4B).

Conversely, the OMC was destabilized in both cases (IT and ITK), causing significant conformational changes in the transmembrane region of integrin αIIbβ3 (Figure 2.2, 2.4, 2.13C, 2.13D). The destabilization of OMC is highly correlated with the dramatic angle change between αIIb and β3 (θ) in both IT and ITK (Figure 2.6 and Figure 2.7). We noticed that the angle change in ITK was in reverse direction relative to that in IT, i.e., decreasing angle in ITK and increasing angle in IT (Figure 2.2). Previous studies suggested that talin-

mediated integrin activation involved an increase in the αIIb-β3 crossing angle and subsequent separation of the transmembrane domains [26], [57]. However, recent studies showed that transmembrane domains of integrin subunits were close to each other in all conformational snapshots including active, inactive and intermediate states, contradicting the notion of chain separation as an indicator of integrin activation [27], [115]. Since the angle change in ITK led to disruption of the IMC and OMC interactions, we propose that the degree of angle change is more pivotal in integrin activation than the direction of such change. This is most likely because talin1 and kindlin2 eliminate the inhibitory effects of IMC and OMC, which allows for mechanical signals to be transmitted across the membrane, without complete separation of the transmembrane regions. This is also demonstrated by changes in the force distribution patterns of the transmembrane domains of integrin in both IT and ITK simulations (Figure 2.4C and 2.5). Furthermore, we showed previously that residue A711 in β3 helix is key for signal transmission across the transmembrane domain of integrin and an A711P mutation can disrupt integrin activation [98]. Our FDA analysis also indicated that A711 bears high forces in both IT and ITK but not in IK (Figure 2.4C), implying that signal transmission is activated upon IMC disruption. Overall, our study suggests that not only both talin1 and kindlin2 are essential for efficiently initiating the activation process, but also kindlin2 may modify the molecular mechanism of inside-out signaling at the integrin β3 tail, which eventually leads to the opening of the integrin ectodomain.

Although not studied in this work, it is important to note that kindlin may have several other roles in integrin activation and the formation of focal adhesions. For example, one possible role of kindlin in integrin activation may be preventing the association of cytoplasmic inhibitors of integrin activation such as filamin or α-actinin to the integrin tail. Also, kindlin may be involved in integrin clustering through dimerization [90]. Moreover, kindlin binding to actin can enhance cytoskeletal coupling to the membrane. Therefore, simultaneous binding of kindlin and talin to the integrin β increases the overall force applied to the integrin tail, which may facilitate focal adhesion formation and maturation.

While our results focus on the integrin β3, the CT of integrins are more than 60% similar to each other (Figure 2.14). This high level of similarities with the conserved active sites between integrins shows the potential of having the same activation mechanisms and suggests that activation of different integrin receptors may at least be initiated in a similar manner. However, further computational studies are needed to uncover the mechanism of kindlin-mediated integrin activation in other members of integrin subfamilies.

```
                723  726                    744         752     756
β3    KLLITIHDRKEFAKFEEERARAKWDTANNPLYKEATSTFT-NITYRGT-----------     762
β1    KLLMIIHDRREFAKFEKEKMNAKWDTGENPIYKSAVTTVV-NPKYEGK-----------     798
β2    KALIHLSDLREYRRFEKEKLKSQWNN-DNPLFKSATTTVM-NPKFAES-----------     769
β5    KLLVTIHDRREFAKFQSERSRARYEMASNPLYRKPISTHT……NKSYNGTVD---------     799
β6    KLLVSFHDRKEVAKFEAERSKAKWQTGTNPLYRGSTSTFK-NVTYKHREKQKVDLSTDC     788
β7    RLSVEIYDRREYSRFEKEQQQLNWKQDSNPLYKSAITTTI-NPRFQEADSPTL------     798
      :  : : * :*  :*: *: . .::.   **:::   :*   *  :
```

Figure 2.14: Multiple sequence alignment of integrin β. Sequences alignment of integrin β cytoplasmic tails with highlighted conserved regions: membrane proximal salt bridge residues (red), talin binding site (blue), TTV motif (purple), and kindlin binding site (green).

Taken together, our results shed light on the molecular mechanisms by which kindlin2 cooperates with talin1 in integrin αIIbβ3 activation. This is the first computational study, to the best of our knowledge, that models the interplay between kindlin2 with talin1 in promoting inside-out signaling through integrin binding.

# Chapter 3

# Integrin α-β Crossing Angle Change During Activation

The contents of this chapter have been partially published as:

Z. Haydari, H. Shams, Z. Jahed, and M. R. K. Mofrad, "Kindlin Assists Talin to Promote Integrin Activation," *Biophys. J.*, vol. 118, no. 8, pp. 1977–1991, Apr. 2020.

## 3.1. Introduction

Integrins are transmembrane proteins that mediate the signaling between the cytoplasm and extracellular matrix to promote cell adhesion and spreading. In order to trigger signaling, integrins must be activated from a low-affinity state to a high-affinity state for binding to extracellular ligands. Previous studies had shown that talin was both necessary and sufficient for integrin activation [15], [48], however, recent evidence suggests that talin cannot activate integrin without the help of kindlin family of proteins [49], [50]. Hence, kindlin is now believed to be required for integrin activation and serves as a co-activator of integrin with talin [51].

Despite the importance of kindlin in integrin activation, the lack of structural information for kindlin has limited progress towards understanding the molecular mechanisms of its role in integrin activation and its interplay with talin. All computational studies published to date have ignored the role of kindlin in their models due to the lack of kindlin's crystal structure. [26], [27], [59], [96], [97]. In 2017, the first molecular structure of kindlin was finally resolved and revealed the molecular details of kindlin's interactions with integrins [47].

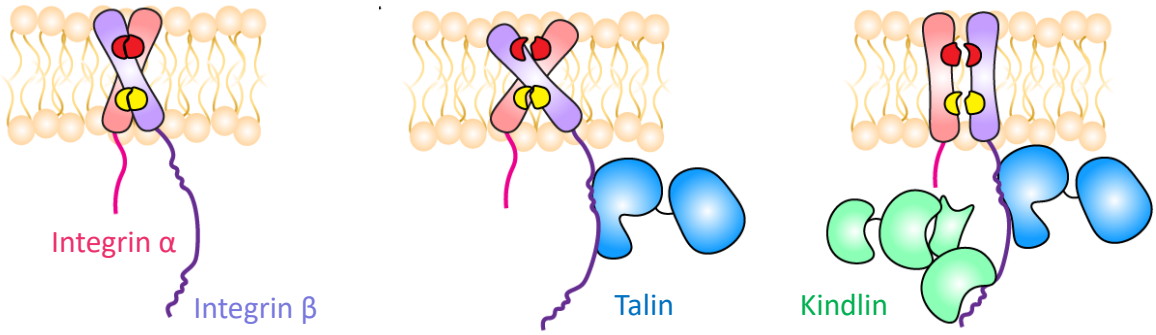


Figure 3.1: Schematic representations of the integrin activation mechanism by talin and/or kindlin interactions (proposed in Chapter 2). Integrin remains in a closed conformation when it is not interacting with cytoplasmic activators (left). Talin interaction with the membrane proximal NxxY motif of integrin β destabilizes its transmembrane interactions and increases α-β crossing angle (middle). Kindlin binding to the membrane distal NxxY motif of integrin pushes talin toward the integrin membrane proximal region of integrin and disrupts its transmembrane interactions. Simultaneous binding of talin and kindlin decreases the α-β crossing angle and causes the parallelization of transmembrane helices.

In the previous chapter, we discussed the importance of kindlin cooperation with talin for integrin activation. We observed that contrary to previous computational studies on integrin activation, the complete separation of IMC and OMC happens when the α-β crossing angle is decreased towards parallelization (Figure 3.1). This is observed when a more complete case of kindlin cooperation with talin is considered. This observation is different from the notion of crossing angle increase in the previous studies [27], [58]. In this chapter, we provide a more comprehensive analysis of this angle change. In particular, we show that through kindlin-talin cooperation the trend in decrease in the crossing angle is independent of the initial configuration of talin, kindlin, and integrin, further corroborating this intermediate step in the activation process.

## 3.2. Computational Procedures

### System setup

The crystal structure of TM/CT domains of integrin αIIbβ3 (PDB: 2KNC [103]), talin1 (PDB: 3IVF [83]), and kindlin2 FERM domain (PDB: 5XPY [47]) were taken from the Protein Data Bank. Two different models were built using VMD: integrin αIIbβ3 in complex with either talin1 (IT) and both talin1 and kindlin2 (ITK). First, the TM domains of integrin were embedded in a patch of POPC lipid bilayer with dimensions of 200×250 $Å^2$ using VMD. Also, the lipid chains overlapping with integrin were removed. Two different orientations of talin and kindlin with respect to integrin and membrane were tested for both models (IT, IT_o, ITK, and ITK_o).

The initial orientations of talin and kindlin molecules were not chosen randomly since the crystal structures of integrin bound to both talin and kindlin are available. Basically, we used the resolved structures of integrin αIIbβ3 dimer, talin, and kindlin in our models. Then, we incorporate the available structures of integrin-talin/kindlin complexes as templates for finding the best orientations of the molecules. The details of initial orientations are chosen based on experimentally reported data of the binding sites and lipid interactions [47], [83], [107], [116], [117]. Therefore, based on 3G9W [107] and 5XQ1 [47] complexes as structural templates for integrin, talin, and kindlin, we set up talin and kindlin orientations such that their integrin binding locations face the cytoplasmic regions of integrin. We also positioned talin close to its binding regions on the membrane and kindlin within a 15Å distance from the membrane. We positioned talin and kindlin close to their binding sites on integrin with a few water layers in between the molecules.

In the second orientation simulations (ITK_o and IT_o), we changed the initial orientations of talin and kindlin and repeated the simulations. Keeping in mind the general initial conditions as reported by experimental results, we increased the distance of talin and kindlin with respect to their NxxY binding location on integrin by 3 Å. We also changed the position of talin to become closer to integrin α subunit. We also increased the distance between kindlin F0 subdomain with membrane by 5 Å. Then, all systems were solvated using TIP3P explicit water model in NAMD [108] and water molecules inside the lipid membrane were removed. Additionally, all systems were neutralized and ionized with 150 mM of KCl. The total number of atoms reached 744,946 in ITK, 556,876 in IT, 745,559 in ITK_o, and 556,511 in IT_o.

**MD simulations**

We performed all-atom molecular dynamics (MD) simulations to investigate the conformational changes of integrin αIIbβ3 dimer upon simultaneous interaction with talin and kindlin. Two different orientations of talin and kindlin relative to integrin and membrane were tested (ITK, IT, ITK_o, and IT_o). Molecular dynamics simulations were carried out using NAMD and CHARMM36 force field [109]. Molecular visualization and analyses were performed using Visual Molecular Dynamics (VMD) package [110]. Periodic boundary conditions were used in all three dimensions and a 2 fs time step was used in all simulations. The Langevin piston Nose-Hoover pressure control algorithm, and the Langevin damping thermostat for temperature control were used [109]. Pressure was maintained at 1 bar and temperature at 310 K with a damping coefficient of 5/ps. Each trial was initially minimized for 100,000 timesteps using the conjugate gradient and line search algorithm to relax the structures and remove all bad contacts. Following the minimization process, each configuration was equilibrated for 25 ns or longer until equilibrium was reached. Fully equilibrated structures were then used in the final production simulations that ran for 1000 ns for ITK and IT, and 500 ns for ITK_o and IT_o.

**Normal mode analysis (NMA)**

To predict the large-scale functional motions of the integrin αIIbβ3 structure, we first performed a normal mode analysis (NMA). Elastic network modeling (ENM) using the Dynomics ENM 1.0 online tool was used to conduct the NMA analysis and produce visualizations of the data [118]. The crystal structure of transmembrane and cytoplasmic domains of integrin αIIbβ3 in complex with membrane was used as the input.

## 3.3. Results

### Changes in the α-β crossing angle is a favorable motion of the integrin αIIbβ3 dimer

To explore the structural dynamics of the integrin dimer, we first calculated the normal modes of transmembrane domains and cytoplasmic tails of integrin αIIbβ3 heterodimer (Figure 3.2). The low frequency nonrigid body NMA mode of the integrin αIIbβ3 dimer corresponds to outward and inward motion of the bottom part of the transmembrane region. These motions resulted in an increase or decrease in the crossing angle between the transmembrane domains of αIIb and β3 helices. Additionally, we performed dynamic cross correlation analysis between all residue pairs on the integrin dimer as obtained from the average of all modes in NMA (Figure 3.2A). Of particular interest was an anti-correlated motion between the transmembrane and helical regions of cytoplasmic domain of αIIb and β3 helices (black box in Figure 3.2 left). The NMA result showed that both increasing and decreasing in the αIIb-β3 crossing angle are low-frequency modes suggesting that they are possible or large scale motions of the integrin dimer. Moreover, αIIb and β3 helices of integrin dimer have higher fluctuations in their cytoplasmic regions as obtained by the two slowest NMA modes (Figure 3.2B).

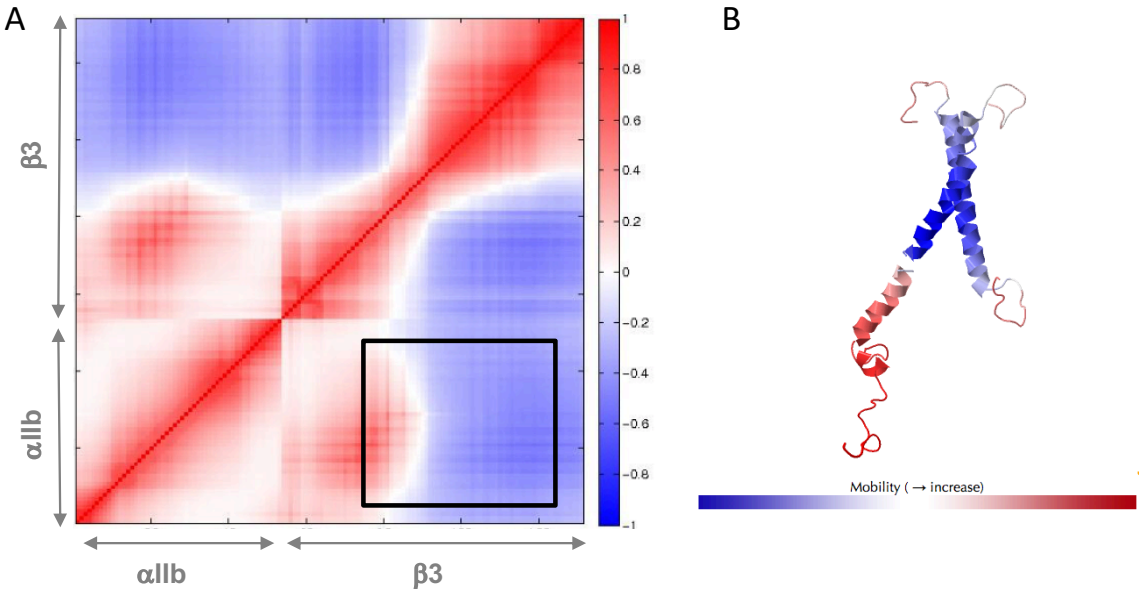


Figure 3.2: Normal mode analyses of integrin αIIbβ3 heterodimer. (A) Dynamic cross correlation heatmap of the transmembrane and cytoplasmic domains of integrin dimer averaged over all modes is shown. αIIb and β3 subdomains are indicated on the heat map. A black box is drawn to indicate

that the transmembrane and helical region of cytoplasmic domains of integrin αIIb and β3 helices are negatively correlated. (B) The integrin dimer structure is colored based on the size of the fluctuations driven by the slowest two modes.

### The α-β crossing angle changes during the activation process

To quantify the detailed conformational transition of integrin heterodimer in both configurations of talin and kindlin, we measured the α–β crossing angle and also the change in α and β angles with respect to z-axis (perpendicular to the membrane) as a function of time in all simulations (Figure 3.3). Two different scenarios considered in our simulations, namely integrin in complex with talin (IT) and integrin in complex with both talin and kindlin (ITK). Additional simulations were performed featuring a different initial orientation of talin and kindlin in both scenarios (see Computational Procedures for more details). These simulations are called IT_o and ITK_o from this point on. The angle of residues 967–979 in αIIb and residues 697– 709 in β3 were calculated with respect to each other and also for each one with respect to z-axis. As we showed in Chapter 2, the angle θ decreases throughout the ITK simulation and approaches zero after 400 ns. Interestingly, we observed the same behavior in the angle θ in ITK_o simulation (Figure 3.3A). The angle θ starts from 40° and approaches 17° in 500 ns in the second orientation of ITK. In the cases of talin binding without kindlin, our results showed an increase in angle θ in both orientations (IT and IT_o).

Next, we determined the conformational changes in α and β helices individually to understand the contribution of each in the changes of crossing angle. Specifically, we measured the angle between the transmembrane domain of α/β and z-axis, which is perpendicular to lipid bilayer ($\theta_a$ and $\theta_b$ in Figure 3.3B and C). The angle $\theta_a$ is not stable in IT and IT_o simulations and significantly increases after 400 and 500 ns, respectively. The angle $\theta_a$ exhibits less fluctuations in ITK and ITK_o simulations compared to the case of IT and IT_o simulations. On the other hand, the angle $\theta_b$ is almost stable in IT and IT_o simulations, while it significantly decreases in either of ITK and ITK_o simulations (i.e., 40° change in ITK and 20° change in ITK_o).

The results show that the observed decrease in α-β crossing angle in ITK and ITK_o is mainly due to the conformational changes in β helix ($\theta_b$ angle). This is clearly in contrast with the changes of α-β crossing angle in the cases of talin binding without kindlin (IT and IT_o), which depend on the conformational changes of α helix ($\theta_a$ angle).

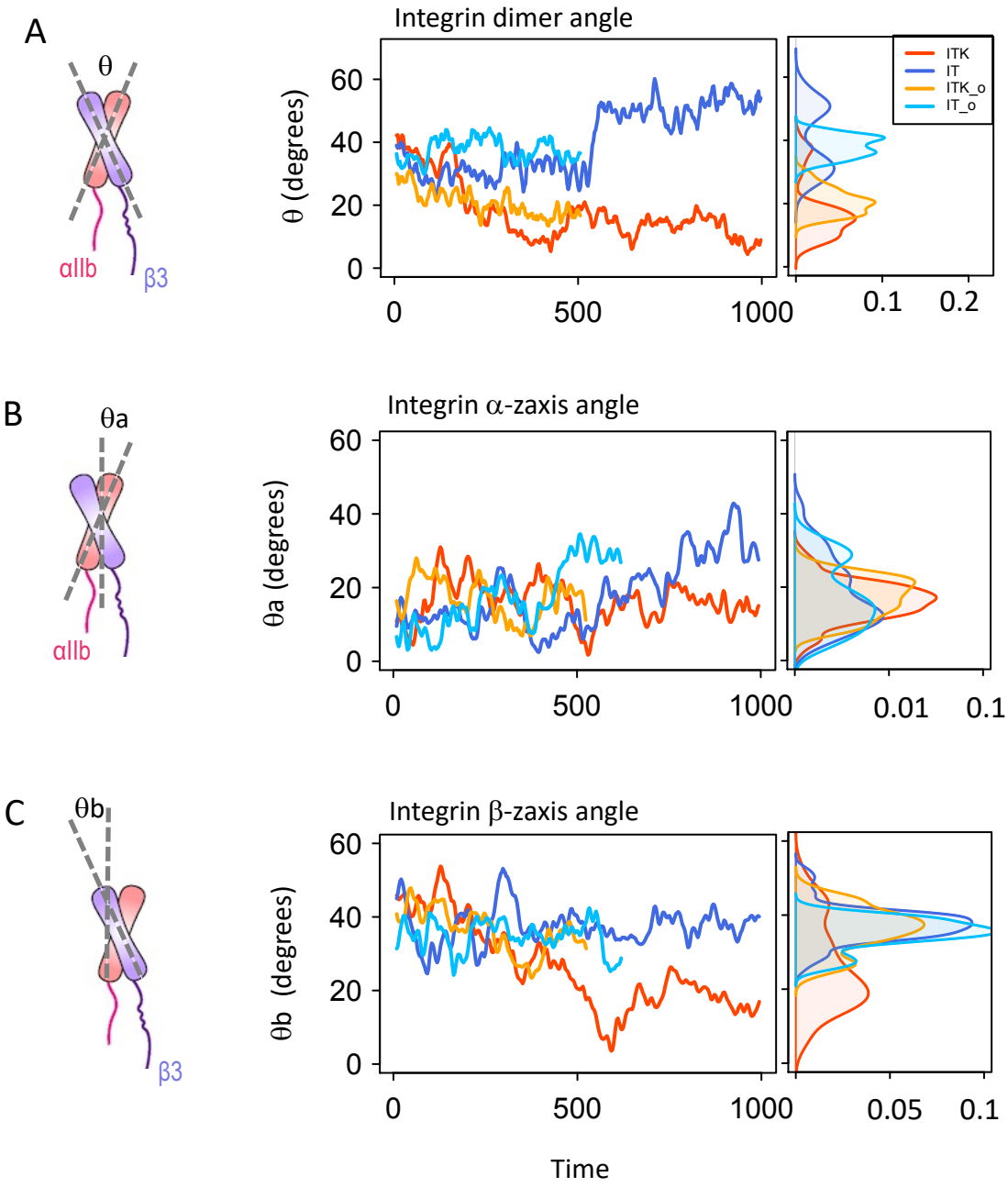


Figure 3.3: The conformational changes of integrin αIIbβ3 dimer during activation. (A) A schematic representation of the integrin dimer showing angle θ between the αIIb and β3 helices is given (left). The time and density plots of angle θ for the ITK, IT, ITK_o, and IT_o simulations are shown in red, blue, orange, and light blue, respectively. Two different orientations of talin and kindlin were used for both talin-only (IT and IT_o) and talin in complex with kindlin simulations (ITK and ITK_o). (B) A schematic representation of the integrin dimer showing the angle $\theta_a$ between the αIIb and z-axis (perpendicular to lipid bilayer) is shown (left). The time and density

plots of angle $\theta_a$ for the ITK, IT, ITK_o, and IT_o simulations are shown. (C) The same schematic representation and plots are shown for the angle $\theta_b$ between integrin β3 helix and z-axis.

## The changes in IMC and OMC interactions as a result of changes in the α-β crossing angle

To determine the consequences of α-β crossing angle change in the interaction energies between transmembrane helices of integrin dimer, we measured the nonbonded interaction energies between the IMC and OMC regions (Figure 3.4A and B). Our results showed that the interaction energies of IMC and OMC decrease upon simultaneous binding of talin and kindlin in both orientations (ITK and ITK_o). However, in the cases of talin binding without kindlin (IT and IT_o), the interactions are unstable.

Next, to understand whether changes in the α-β crossing angle are correlated with the interaction energies of IMC and OMC, we performed a cross correlation analysis. Based on the results, there is no correlation between the angle θ and IMC. This suggests that IMC dissociation is directly regulated by cytoplasmic interactions and not through angle change. Conversely, dynamics of OMC interactions were highly correlated with angle θ in both orientations considered in simulations of ITK, IT, ITK_o, and IT_o (Figure 3.4C bottom), implying the direct effect of α-β crossing angle in disruption of interactions in OMC region. This indicates that OMC dissociation is directly regulated by the change in integrin dimer angle. The reverse correlations of ITK and IT reflect opposite directions of angle change.

Our results indicate that the decrease in the α-β crossing angle of integrin dimer upon simultaneous binding of talin and kindlin causes the separation of integrin transmembrane helices at both IMC and OMC regions, thus initiating the activation process. Also, our results confirm that the destabilization of integrin dimer interactions is independent of the configuration of talin and kindlin.

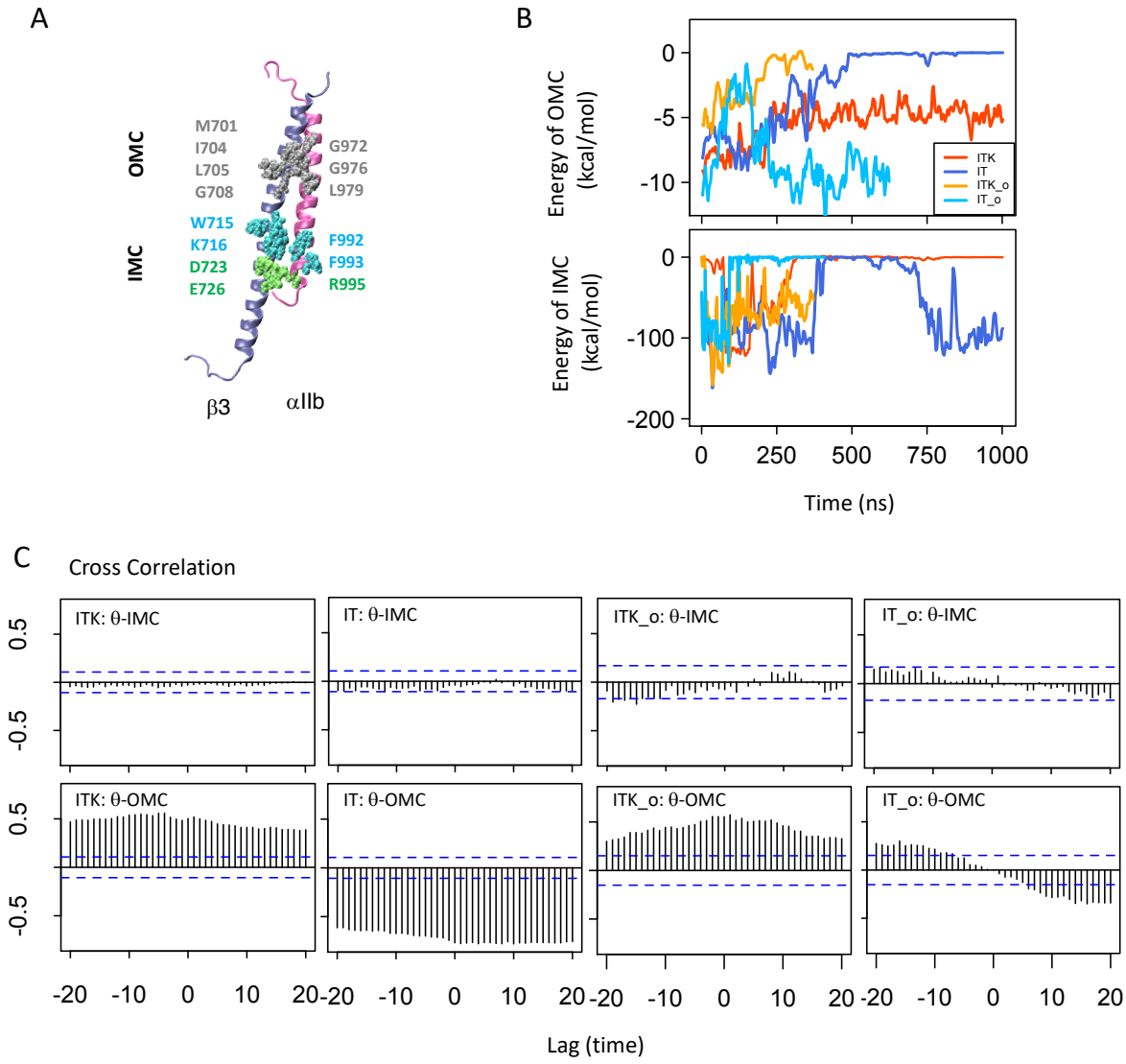


Figure 3.4: IMC and OMC interactions between αIIb and β3 helices. (A) Structure of the αIIb (mauve) β3 (iceblue) heterodimer. Interacting residues in the OMC region are shown in silver, in the IMC region in blue, and the αIIb R995 - β3 D723/D726 salt bridges in green. (B) The time and density plots of energy of interactions between OMC (top) and IMC (bottom) residues are shown for the ITK, IT, ITK_o, and IT_o simulations in red, blue, orange, and light blue, respectively. (C) Cross correlation of IMC and α-β crossing angle (top); and OMC and α-β crossing angle (bottom) are shown. The horizontal blue lines are the approximate 95% confidence interval. Cross correlation plot is shown for each of the four ITK, IT, ITK_o, and IT_o simulations. High correlations exist between angle θ and OMC in all simulations, while the IMC correlations are negligible.

**Interaction between integrin α tail and talin/kindlin does not correlate with the α-β crossing angle**

Integrin αIIb cytoplasmic tail contains only 15 residues. It has been shown that the interaction of integrin α tail with the β subunit contributes to maintaining the resting state of integrin dimer [59]. Binding of cytoplasmic proteins, such as talin and kindlin, to the integrin β tail promotes the dissociation between α and β cytoplasmic regions. Previous computational studies on talin-mediated integrin activation revealed the important interactions between α tail and talin F3 subdomain during the activation process. To examine the effect of α interaction with talin and/or kindlin in integrin dimer angle change, we analyzed the interactions between cytoplasmic tail of integrin αIIb and talin/kindlin in our simulations (Figure 3.5).

First, the αIIb-talin/kindlin interactions were determined by observing the last frames of the simulations (Figure 3.5A and C). Interestingly, we observed an interaction between αIIb and kindlin in ITK and between αIIb and talin in ITK_o. The nonbonded interaction energies between αIIb tail and talin/kindlin confirm these observations (Figure 3.5B). Specifically, we calculated the nonbonded interaction energy between residues 994 to 1008 of αIIb and all talin and kindlin residues. The interaction energy between αIIb and talin is zero throughout the ITK simulation. However, αIIb is able to bind talin from the beginning of ITK_o and maintain a strong interaction over the course of simulation. In the absence of kindlin, there is no observed interaction between talin and αIIb in IT, however, talin can strongly bind to αIIb in IT_o (Figure 3.5C and D).

The integrin αIIb interacts with different molecules in each of the two different orientations considered in ITK and ITK_o simulations. However, despite these differences, we observed the same behavior in the α-β crossing angle. Therefore, we conclude that the integrin dimer angle change is independent of αIIb-talin/kindlin interactions. Cross correlation between kindlin-αIIb interaction and angle θ show only a small correlation in ITK. The talin-αIIb interaction and angle θ also exhibit a small correlation in IT_o simulation (Figure 3.5E top). However, there is no correlation between talin-αIIb interaction and angle θ in IT and kindlin-αIIb interaction and angle θ in ITK_o (Figure 3.5E bottom).

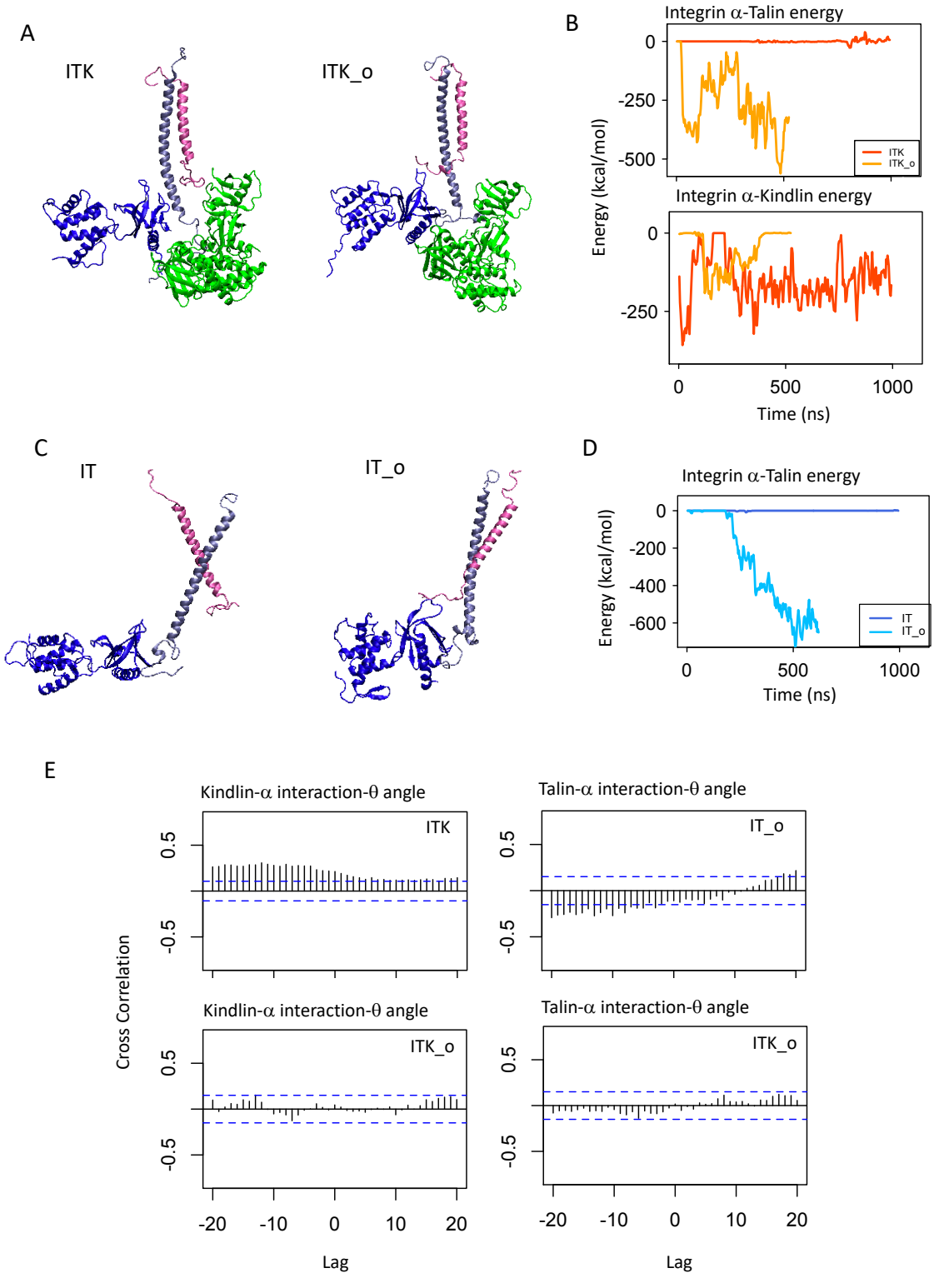
A
ITK
ITK_o
B
Integrin α-Talin energy
Integrin α-Kindlin energy
Energy (kcal/mol)
Time (ns)
ITK
ITK_o
C
IT
IT_o
D
Integrin α-Talin energy
Energy (kcal/mol)
Time (ns)
IT
IT_o
E
Kindlin-α interaction-θ angle
Talin-α interaction-θ angle
Cross Correlation
Lag
ITK
IT_o
ITK_o

Figure 3.5: Interaction between integrin αIIb and talin/kindlin. (A) simulation snapshots of ITK and ITK_o showing the interaction of αIIb with talin/kindlin are shown for the last frame of the simulations. (B) The time plots of energy of interactions between αIIb tail and talin (top) and kindlin (bottom) are shown for ITK and ITK_o simulations in red and orange, respectively. (C) Simulation snapshots of IT and IT_o showing the interaction of αIIb with talin are shown for the last frame of the simulations. (D) The time plot of energy of interaction between αIIb tail and talin is shown for IT and IT_o simulations in blue and light blue, respectively. (E) Cross correlation between binding energy of kindlin-integrin αIIb and angle θ in ITK simulation (top left) and talin-integrin αIIb binding energy and angle θ in IT_o simulation (top right) are shown. Also, cross correlation between kindlin-αIIb interaction/talin-αIIb interaction and angle θ are shown for ITK_o simulation (bottom).

### Interaction of talin and kindlin with the membrane does not correlate with the α-β crossing angle

Talin has an extended conformation and it has been observed that its F1, F2, and F3 subdomains are parallel to the membrane and interact with the membrane. Basically, it is known that K256, K272, K274, and R277 residues of talin1 bind to the membrane [27], [83]. Moreover, experimental observations discovered that kindlin binds to the membrane from its F0 (residues 70, 74, 76, 77, 81) and F1 (residues 144 to 163) subdomains [47]. To determine if membrane interactions has any effect on α-β crossing angle, we first measured the interaction of talin and kindlin with membrane. Our results show that in both configurations of talin and kindlin considered in ITK, ITK_o, IT, and IT_o simulations, talin subdomains are close to the membrane and are able to make strong interactions with the membrane (Figure 3.6A). However, as discussed in the "Computational Procedures" Section, kindlin subdomains are about 15 and 20 Å far from the membrane in the first and second configuration simulations, respectively. Moreover, interestingly enough, the simulations revealed that the F0 subdomain of kindlin moves up and interacts with the membrane after 500 ns in ITK and 100 ns in ITK_o simulation (Figure 3.6B).

The results of talin and kindlin interactions with the membrane match well with the experimental observations and confirm that talin/kindlin-membrane interactions do not depend on their initial orientations; i.e. kindlin has the flexibility to change its conformation during the simulation time and form interactions with the membrane in its both configurations (ITK and ITK_o).

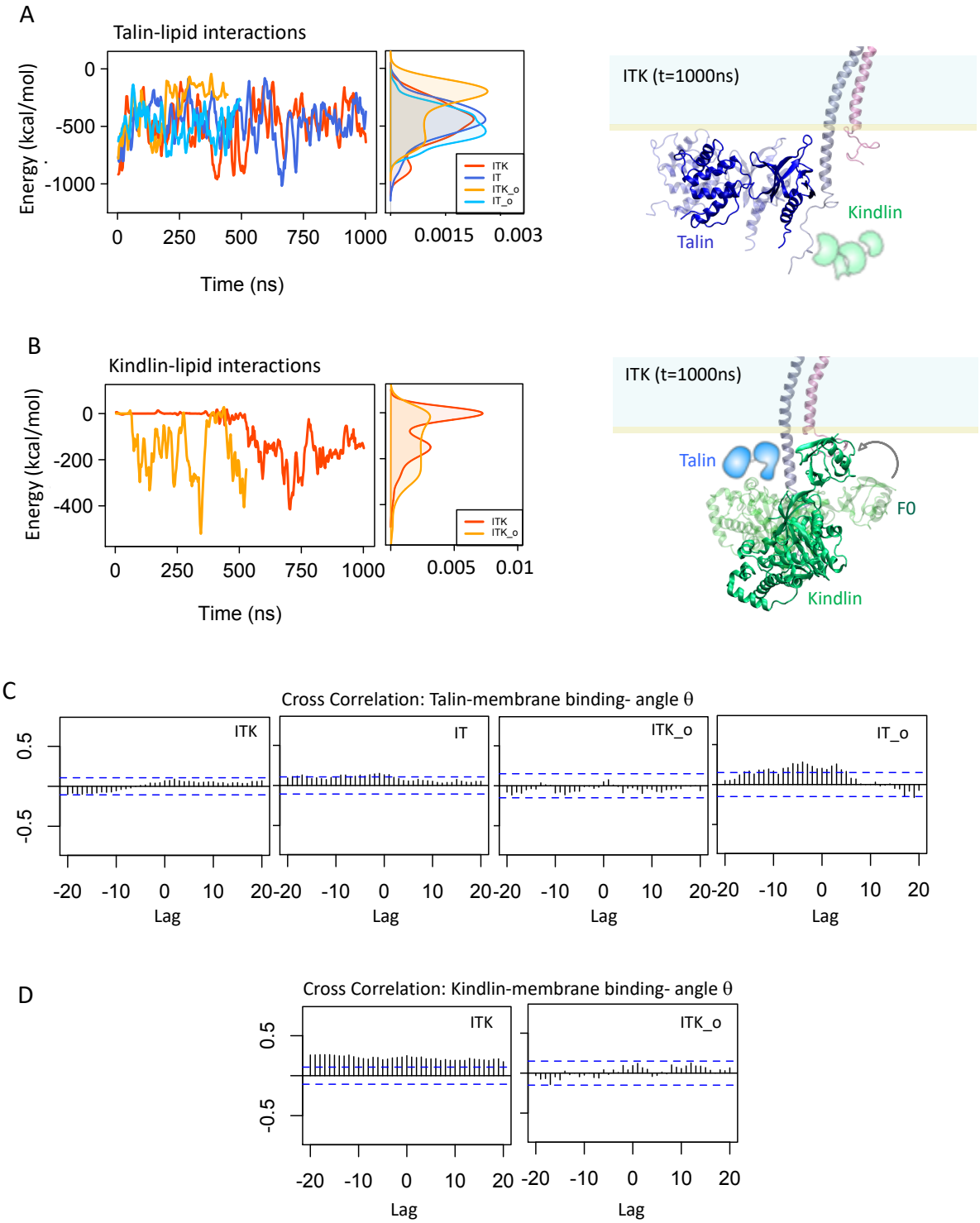


Figure 3.6: Interaction of talin and kindlin with the membrane during integrin activation. (A) The time and density plots of interaction energies between talin and membrane are shown for ITK, IT, ITK_o, and IT_o simulations (left). Cartoon representations of integrin αIIbβ3 and talin overlaid

with schematic of kindlin are shown for the last frame of the ITK simulation (1000 ns). The initial orientation of talin is shown transparent. (B) The time and density plots of interaction energies between kindlin and membrane are shown for ITK and ITK_o simulations (left). Cartoon representations of integrin αIIbβ3 and kindlin overlaid with schematic of talin are shown for the last frame of the ITK simulation (1000 ns). Also, the initial orientation of kindlin is shown transparent. (C) Cross correlation function between talin-membrane interaction energy and angle θ in ITK, IT, ITK_o, and IT_o simulations are shown. (D) Cross correlation between kindlin-membrane interaction energy and angle θ are shown for ITK and ITK_o simulations.

Then, to determine if there is any correlation between membrane interactions with the cytoplasmic proteins and the conformational changes of integrin dimer, the cross-correlation function were used. Cross correlation analyses of the talin/kindlin-membrane interaction energy and angle θ show no significant correlation between them in all simulation scenarios (Figure 3.6C and D).

**Interaction of talin and kindlin with the integrin β tail is correlated with the α-β crossing angle**

In order to find the effect of talin and kindlin interactions with the cytoplasmic tail of integrin on α-β crossing angle, we analyzed the talin/kindlin-β3 interactions and their correlations with angle θ. We first calculated the nonbonded interaction energies between the cytoplasmic tail of integrin β3 and talin or kindlin (Figure 3.7A and B). Specifically, we calculated the interaction between residues 720–762 of β3 and residues 569–680 of talin or residues 560–680 of kindlin. Our results show that talin binds more strongly to the cytoplasmic tail of β3 when kindlin is present. This observation is independent of the initial configuration of talin and kindlin (Figure 3.7A). The overlaid density plots of talin-integrin interactions show higher peak value in ITK_o compared with IT_o. Also, our results show a stable interaction between kindlin and β3 tail in both ITK and ITK_o simulations.

The cross correlation analyses of kindlin-β3 binding and angle θ reveal a high correlation between kindlin binding and α-β crossing angle (Figure 3.7C and D). This confirms the direct role of kindlin in integrin dimer angle change and activation. The forces from kindlin binding with the membrane distal NxxY motif of integrin β3 can allosterically propagate through the transmembrane domain and decrease α-β crossing angle, thus leading to the disruption of IMC and OMC and subsequently, initiation of integrin activation.

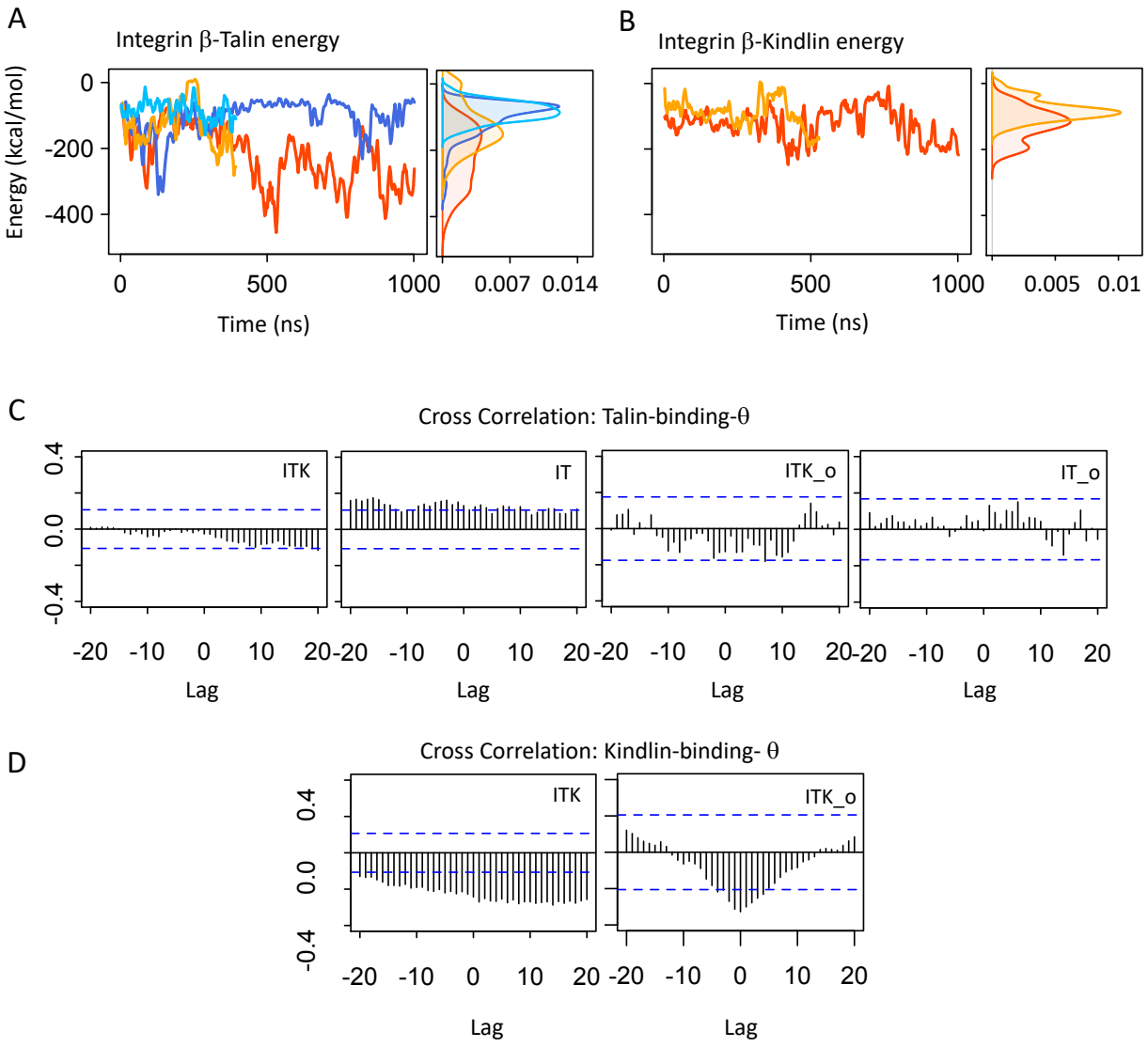


Figure 3.7: Interactions of talin and kindlin with integrin β3. (A) The time and density plots of interaction energies between integrin β3 CT and talin F3 subdomain are shown in ITK, IT, ITK_o, and IT_o simulations. (B) The time and density plots of interaction energies between integrin β3 CT and kindlin F3 subdomain are shown for ITK and ITK_o simulations. (C) Cross correlation function between binding energy of talin-integrin β3 and angle θ in all simulations are shown. (D) Cross correlation between binding energy of kindlin-integrin β3 and angle θ in ITK and ITK_o simulations are shown.

## 3.4. Discussion

Integrin activation is the first step in leukocyte-endothelial adhesion. It plays an important role in a variety of cell functions, including cell-matrix adhesion, cell migration, and apoptosis. Activation of integrin involves conformational changes of its dimer from a bent-closed state to an extended-open state. Among cytoplasmic proteins, talin and kindlin are known to change integrin conformation through their interactions with β subunit. These interactions initiate the activation process. Although molecular mechanisms of talin-mediated integrin activation have been studied, the role of kindlin in conformational changes of integrin was not known. To understand the contribution of kindlin in conformational changes of integrin dimer during the activation process, we developed all-atom microsecond-scale MD simulations of αIIbβ3 using an explicit lipid-water environment under two distinct scenarios: (i) integrin in complex with talin (IT) and (ii) integrin in complex with both talin and kindlin (ITK). We also performed additional simulations using a different orientation of talin and kindlin in both scenarios (IT_o and ITK_o) to show the effect of talin and kindlin initial configurations in integrin conformational changes.

Previous studies suggested that talin-mediated integrin activation involved an increase in the α-β crossing angle and subsequent separation of the transmembrane domains [27], [58]. However, when we considered kindlin binding simultaneously with talin in our simulations (ITK and ITK_o), we observed that the integrin dimer crossing angle was decreased. To study the reasons behind this opposite behavior in the conformational changes, we analyzed the effect of talin/kindlin interactions with lipid bilayer, integrin α tail, and integrin β tails on the α-β crossing angle (Figures 3.5-3.7).

It is well known that the IMC and OMC interactions between integrin subunits maintain the closed state, while unclasping them triggers the activation process. Our simulations indicated that simultaneous interactions of talin and kindlin with integrin can destabilize both IMC and OMC as a result of a dramatic decrease in integrin dimer crossing angle. Interestingly, this angle change is independent of the initial orientations of talin and kindlin (Figure 3.4). On the other hand, our control simulations (IT and IT_o) showed that in the cases of talin binding without kindlin cooperation, talin is not capable of complete destabilization of integrin dimer (Figure 3.4). This further highlights the direct role of kindlin in integrin activation. Basically, the binding forces from kindlin interaction with integrin β in both orientations of ITK scenarios (ITK and ITK_o) can allosterically

propagate through the transmembrane domain and decrease α-β crossing angle, thus leading to the destabilization of IMC and OMC and subsequently, initiation of integrin activation.

Also, our cross correlation analyses showed minimal or no correlation between α-β crossing angle and talin/kindlin-α tail interactions in both orientations of talin and kindlin (Figure 3.5). Previous studies had suggested that interaction of talin with integrin α tail initiates the activation process by breaking the R995-D723 salt bridge in IMC [58]. However, we didn't observe talin-α tail interaction in our simulations in which we considered the first orientations of talin and kindlin, i.e., ITK and IT. On the other hand, a complete disruption of IMC was observed in the ITK simulation. Therefore, we conjecture that the dissociation of α and β helices in the IMC region is not directly mediated through talin-α tail interaction.

Moreover, the decrease in the α-β crossing angle towards parallelization in both orientations of ITK simulations (ITK and ITK_o) may also have implications for the role of kindlin in integrin clustering and focal adhesion strengthening. Recent studies showed that kindlin recruitment in leukocyte adhesion is necessary for integrin micro-clustering [4]. The unexpected dimerization of kindlin, as revealed in the solved crystal structure, suggests a mechanism by which kindlin can initiate clustering of integrins [47]. The initiation of clustering could potentially be mediated either through dimerization of kindlin after binding to integrins or via simultaneous binding of two integrins to a kindlin dimer. While the recent experimental studies suggest that kindlin has a role in integrin clustering, the details of integrin clustering as mediated by kindlin still remain unknown. In particular, it is not clear what is the favorable crossing angle for integrin clustering. Further studies would be needed to reveal the optimum crossing angle that leads to integrin clustering.

Taken together, our findings reveal details of the conformational changes within integrin dimer during the activation process through simultaneous interaction of talin and kindlin. Using cross correlation analyses we proposed that the changes in the α-β crossing angle of integrin dimer directly mediated through kindlin-β binding and not α tail or membrane interactions (Figures 3.5-3.7). This is the first computational study, to the best of our knowledge, that examines the role of kindlin in the cascade of processes that leads to the conformational changes of integrin dimer.

# Chapter 4

# Molecular Mechanisms of STIM-Mediated Orai Channel Gating

The contents of this chapter have been submitted for publication as:

Z. Haydari, H. Shams, Y. Man, and M. R. K. Mofrad, "Molecular mechanisms of STIM-mediated Orai channel gating," *Biophys. J.*, submitted.

## 4.1. Introduction

The immune response is regulated by a series of molecular processes involved in leukocyte recruitment. Migration of circulating leukocytes to the site of infection is primarily mediated by adhesion molecules [62]. Circulating leukocytes first engage with the luminal surface of endothelial cells through integrin receptors forming nascent adhesions [119]. Integrins then assemble in two stages, micro- and macro-clustering, via a positive feedback mechanism [4], [5], [17], [120], which eventually leads to adhesion reinforcement and leukocyte arrest [62]. Dysregulation in leukocyte recruitment is linked to a number of immunological, muscular, and inflammatory disorders including atherosclerosis, LADI, and LADII [121], [122]. Understanding molecular mechanisms of leukocyte adhesion to endothelial cell is, therefore, crucial for developing novel therapeutic interventions.

Orai protein is the pore subunit of the calcium release activated channel (CRAC) that plays a central role in leukocyte adhesion and adhesion strengthening. Recent studies have shown that $Ca^{2+}$ flux through Orai protein is necessary for integrin macro-clustering and adhesion maturation [4], [61], [62]. Stromal interaction molecule (STIM) is a $Ca^{+2}$ sensor in the endoplasmic reticulum (ER) that activates the Orai channel in response to the lower intracellular calcium contents [123]. STIM proteins cluster upon depletion of ER calcium storage and reach the plasma membrane to physically bind and activate Orai channel (Figure 4.1A) [71], [120], [124]. The STIM family of ER calcium sensors include two members, i.e. STIM1 and STIM2. It has been shown that the CRAC-activation domain (CAD or SOAR domain, ~100 residues) of STIM1 is essential for activating Orai1, a member of the Orai family [63]–[65]. STIM1 strongly binds to the C-terminus of Orai1 (TM4-extension helices), but was shown to also interact with the N-terminus (TM1 helices) [125], [126]. Although the N-terminus binding site has been suggested to trigger Orai1 channel activity, the necessity of STIM1 association to this binding site for promoting Orai1 activation is still unknown [65], [69], [70]. A recent study has shown that a STIM1 dimer can independently bind and cross-link two Orai1 subunits, which is essential for Orai1 clustering and promoting further cooperative functionality [127].

The crystal structure of drosophila Orai (dOrai) features a hexameric structure, which is produced by repeating the three dimers around the pore axis (Figure 4.1B) [128]. Each monomer is composed of four transmembrane helices, TM1 to TM4, and a cytoplasmic extension of TM4 (TM4e). The TM4e of adjacent Orai subunits form a coiled-coil structure in the closed conformation of Orai. The pore of the Orai channel comprises of six TM1

helices where ion flux across the membrane is regulated through residue-residue contacts (Figure 4.1C). Orai pore can be divided into four regions: selectivity filter, hydrophobic region, basic region, and cytosolic region (Figure 4.1C).

Two models have been suggested for CRAC channel gating: in the first model, the gate is assumed to be at the extracellular side of the pore near residue V102 (Figure. 4.1C). This model is based on an experimental observation in which replacing V102 with polar residues resulted in an activation pathway independent of STIM1, suggesting that V102 most likely serves as a hydrophobic gate [129], [130]. The second model assumes that the channel gate is located at the cytoplasmic side near R91 (Figure. 4.1C) as the R91W mutation maintains the closed state of the channel [131], [132].

Here, we employed all-atomic MD simulations to study the allosteric regulation of Orai1 channel activation upon STIM1 binding (Figure 4.1A). The high sequence identity between drosophila and human Orai1 (70%) enabled us to effectively homology model the human protein in order to obtain more applicable outcomes. Our results provide mechanistic insights into STIM1-induced Orai1 activation and highlight key residues involved in this process. Based on our findings, we suggest that STIM1 binding to the C-terminus of Orai1 is sufficient for channel gating and at least one channel gate is located near residue S90 on TM1 helices.

## 4.2. Computational Procedures

### Model Preparation

*Homology modeling.* We used Phyre2 to create a homology model of the full-length structure of human Orai1 [133]. The crystal structure of drosophila Orai1 (PDB ID: 4HKR) [128], and the C-terminus region of human Orai1 (residue 272 to 292, PDB ID: 2MAK) were taken as templates [134]. Templates underwent structural refinement and the Phyre2 dimer output was taken for the next step (confidence level of 99%). Then, the model hexamerized using a python tool developed by Michael Palmer [135].

*Sequence and structural alignment.* Sequences of human Orai1 and drosophila Orai proteins were aligned using UniProt [136]. In order to properly orient STIM1 near Orai1, the structure of STIM1 CC1-CC2 homodimer in complex with two Orai1 C-terminal domains (PDB ID: 2MAK) was first aligned to the homology modeled human Orai1

structure using VMD [110]. Then, the structure of STIM1 CC1-CC2 homodimer in the apo state (PDB ID: 2MAJ) was aligned to the human Orai1 structure.

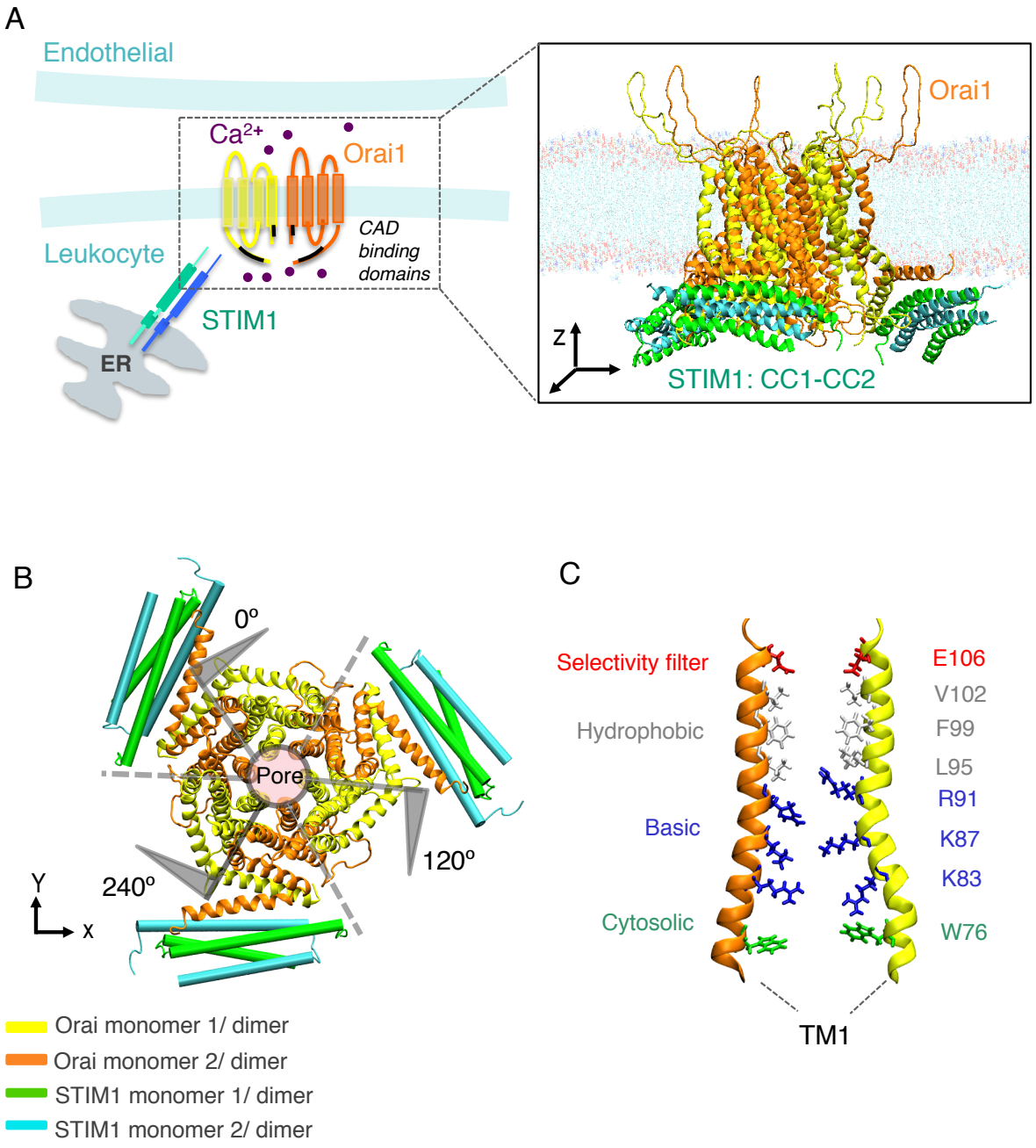


Figure 4.1: STIM1 interactions with Orai1 monomers mediate Orai1 channel gating. (A) A schematic model of Orai1 activation in the process of leukocyte recruitment is shown (left). For clarity, only one dimer of Orai1 is shown. The molecular model of Orai1-STIM1 complex consisting of Orai1 full hexamer structure (produced from repeating the dimer shown in *yellow* and

*orange*) embedded in the POPC membrane bound to three STIM1 dimers CC1-CC2 domains (*cyan* and *green*) depicted in the *Insert*. B) A top-down view of the hexameric Orai1 structure is shown. (C) A side view of TM1 residues lining the Orai1 pore colored based on functionality: selectivity filter (*red*), hydrophobic gate (*white*), basic gate (*blue*), and cytosolic region (*green*). For clarity, only two TM1 helices from spatially opposite subunits are represented.

**Molecular Dynamics Simulations**

We used all-atom MD simulations to investigate the conformational changes of Orai1 upon STIM1 binding. Molecular dynamics simulations were performed using NAMD with the CHARMM force field [109]. Molecular visualization and analysis were performed using Visual Molecular Dynamics (VMD) package and R [110]. The configuration of the system in the binding simulations included full-length structure of Orai1 embedded in the plasma membrane and three CC1-CC2 homodimers of STIM1; the position of STIM1 relative to Orai1 was determined by structural alignment. STIM1 was excluded from control simulations. A sufficiently large triclinic box (size: 19.2x19.5x15.9 nm3) was generated to ensure that molecules did not interact with their periodic image. The TIP3P water model was used for solvating the system and water molecules were removed from the hydrophobic region of the lipid membrane [108]. The number of atoms reached 643,303 and 635,509 for the binding and control simulations, respectively. Periodic boundary conditions were used in three dimensions and a 2 fs timestep was used in all simulations. The Langevin piston Nose-Hoover pressure control algorithm, and the Langevin damping thermostat for temperature control were used [109]. Pressure was maintained at 1 bar and temperature at 310 K with a damping coefficient of 5/ps. The system was initially minimized for 60,000 timesteps using conjugate gradient and line search algorithm to remove all bad contacts. Following the minimization process, each configuration was equilibrated for 5 ns or longer. Fully equilibrated structures were then used in the production simulations, which ran for 120 ns, and repeated two times to produce statistically significant results.

*Interaction energy calculations.* The total nonbonded energies, electrostatic, and van der Waals interactions were calculated using NAMD energy plugin in VMD where the cutoff for nonbonded interactions was set to 12 Å. A switching function was used for all calculations with a switching distance of 10 Å [109], [110]. The energies were calculated between each C-terminus of Orai1 dimer and STIM1 dimer independently. Each Orai1 dimer interacted distinctly with only one STIM1 dimer and these interaction energies were averaged. Only residues 265-290 of Orai1 C-terminus and residues 350-385 of STIM1 CC1-CC2 domain was used in the energy calculations, as the other parts did not interact

with each other.

*Residue Cross Correlation*. To examine how atomic fluctuations and displacements within the integrin heterodimer are correlated throughout our simulations, we performed pairwise residue cross correlation analysis using the cross-correlation function (''*dccm.xyz*'') in the Bio3D package [113]. The matrix of all pairwise cross correlations between residues was visualized using a dynamical cross correlation heatmap.

*RMSF.* The Bio3D R package was used for calculating root mean-square fluctuation (RMSF) [113]. The RMSF was averaged over the three identical Orai1 dimers that formed the Orai1 hexamer in each of the three simulation runs for both binding and control simulations. In total, six data sets were averaged in both binding and control simulations.

*Cross correlation function.* The cross-correlation function (CCF) in R was used to understand the relationship between two time series representing different features along the trajectories [113]. The first argument was treated as the predictor (cause) of the second argument. The lag period indicates when the effect of a change in one feature is reflected in the other feature.

*Pore volume:* To quantify how the conformational changes of Orai1 pore facilitate the ion flux across the channel, we measured the pore volume using the 3Vee server [137]. This server was used to calculate the accessible volume of Orai1 pore for different time steps of the binding and control simulations by automatically analyzing the internal volume from a protein structure [138].

*Number of water molecules:* The total number of water molecules in the pore region of Orai1 channel were calculated using an in-house tcl script, which calculates the number of water molecules inside a cylindrical structure. The Orai1 pore was divided into 28 different segments along the axial direction. VMD tcl code calculates the number of water molecules in each segment, which is a cylindrical slice with a constant diameter. The total number of water molecules is then found by summing over different segments.

## 4.3. Results

To explore the role of STIM1 in the conformational changes of Orai1 pore and channel gating, we developed all-atomic MD simulations of Orai1 hexamer in complex with three STIM1 dimers using an explicit lipid-water environment. Our control simulations featured the closed structure of Orai1 hexamer in the absence of STIM1. Here we first examine the structural dynamics within Orai1 and STIM1 dimers. Then, we look at the complex formation between Orai1-STIM1 binding regions. Next, we quantify the conformational changes of Orai1 pore by measuring the changes in TM1 helices and the capacity of the pore. Finally, we report the important interactions that potentially maintain the open structure of the Orai1 basic region.

**Dynamic cross correlation of Orai1-STIM1 domains**

To investigate whether and how the conformational changes within the Orai1 and STIM1 helices are correlated, we calculated the residue cross correlation between all residue pairs in the three Orai1 and Orai1-STIM1 dimers in both binding and control simulations (Figure 4.2A and B). In general, the level of residue correlations is higher in the binding simulation compared to the control simulation resulting in a relatively darker heatmap shown in Figure 4.2A. Binding forces from STIM1 interaction with the C-terminus of Orai1 propagate through the Orai1 channel and make conformational changes within different helices.

The dynamic cross correlation of Orai1-STIM1 dimers show the positive correlation between TM4e of adjacent monomers of Orai1 (black boxes in Figure 4.2A). However, this correlation was not observed between TM4e of Orai1 dimers in the control simulation, when STIM1 protein is not present (black boxes in Figure 4.2B). Also, the CC2 subdomain of STIM1 monomers are negatively correlated with the TM4e helices of Orai1 monomers (yellow boxes in Figure 4.2A). Note that CC2 domains of STIM1 dimers are bound to the Orai1 TM4e helices, causing their motions to be negatively correlated during Orai1 channel gating due to the coupling between these helices. The negative correlation means that the CC2 and TM4e helices move toward each other and therefore their motions are on the opposite direction. Additionally, a high positive correlation exists between TM3 and TM4 helices within each Orai1 monomer in the binding simulation.

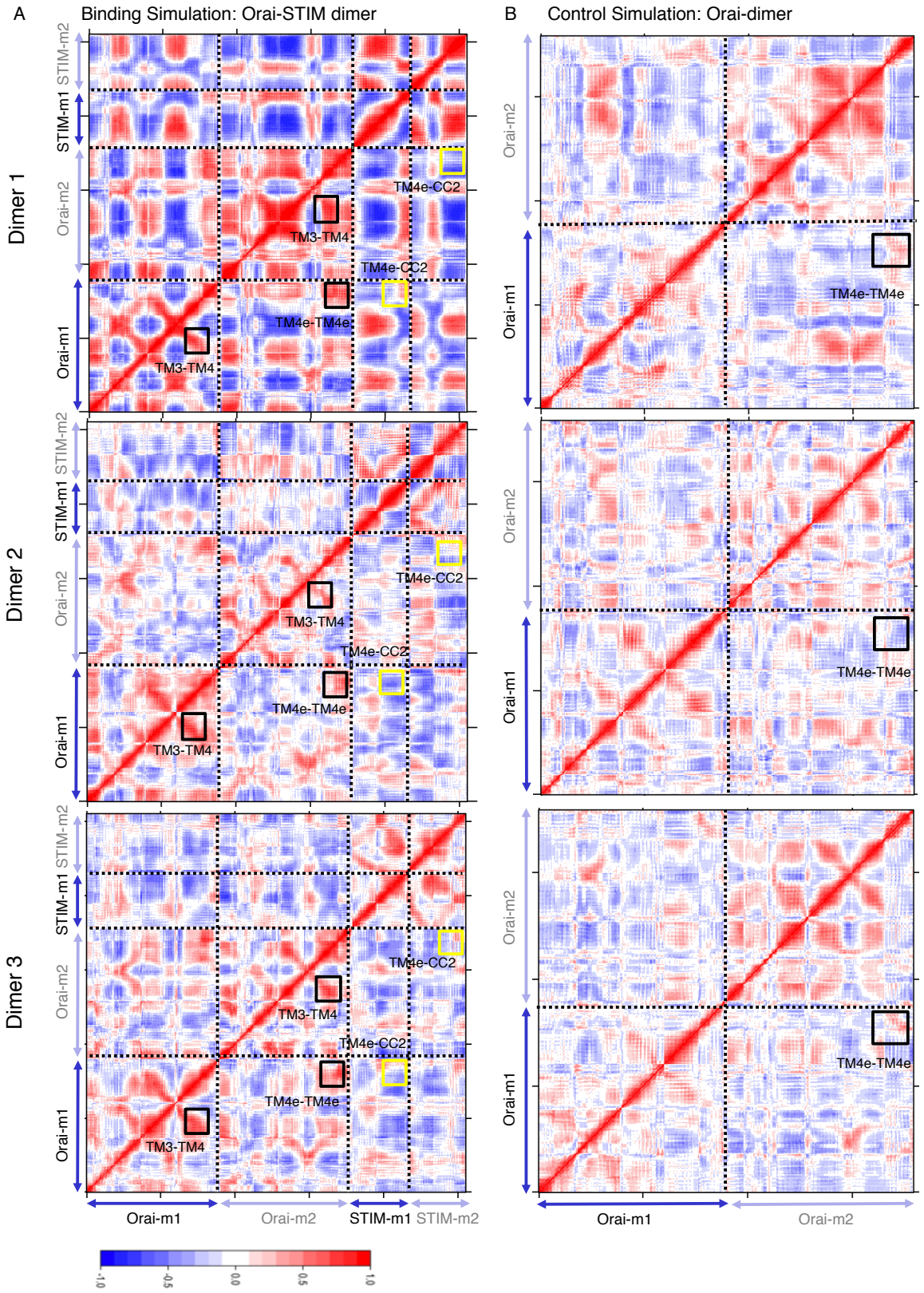
A
Binding Simulation: Orai-STIM dimer
B
Control Simulation: Orai-dimer
Dimer 1
Dimer 2
Dimer 3
STIM-m2
STIM-m1
Orai-m2
Orai-m1
TM4e-CC2
TM3-TM4
TM4e-TM4e
Orai-m1
Orai-m2
STIM-m1
STIM-m2
-1.0
-0.5
0.0
0.5
1.0

Figure 4.2: Dynamic cross correlation of Orai1 and Orai1-STIM1 dimers. (A) Residue cross-correlation heatmap of three Orai1-STIM1 dimers in the binding simulation are shown. Orai1 and STIM1 monomers are indicated on the heatmap; black and gray labels around the plot mark the monomer 1 and 2 of Orai1 and STIM1 dimers, respectively. Black boxes indicate regions that show positive correlation between TM4e of adjacent Orai1 monomers and TM3-TM4 helices within each monomer. Also, TM4e of Orai1 monomers are negatively correlated with CC2 domain of STIM1 monomers indicated by yellow boxes. (B) Dynamic cross-correlation heatmap of three Orai1 dimers of control simulation are shown. Black boxes are drawn to indicate that TM4e of adjacent monomers are not correlated in the absence of STIM1 protein. Also, the lighter heatmaps in control simulation compared to the binding simulation show less fluctuation and conformational changes within the Orai1 helices when STIM1 is not present.

## Complex formation between STIM1 and Orai1 proteins

To determine the strength of the Orai1-STIM1 interaction and downstream conformational transitions in both molecules, we measured the nonbonded interaction energy and the angle between the binding helices of Orai1 and STIM1 proteins (Figures 4.3 and 4.4). In the initial configuration of the system, the unbound conformational states of proteins were used and their binding sites were placed next to each other, while allowing at least one water layer to form between them. The interaction energy between the Orai1 C-terminus (residues 265-290) and the STIM1 CC2 domain (residues 350-385) increased to -1000 kcal/mol within 120 ns. This confirms the strong association and complex formation between TM4e and CC2 helices (Figure 4.3A and B).

The TM4e helices, within the cytoplasmic region of the Orai1 dimer, are associated by a hydrophobic interaction between residues L273 and L276 in the native state (Figure 4.3A). These hydrophobic interactions between C-terminus of Orai1 are known to maintain the closed state of the Orai1 protein and disruption of these interactions leads to channel activation [130]. Our simulation results showed an increase in the average distance between the center of mass of L273 and L276 residues in adjacent monomers upon STIM1 interaction (Figure 4.3C). As STIM1 approached the Orai1 C-terminus, the interaction between these residues was disrupted allowing further opening of the Orai1 C-terminus.

The angle between C-terminus helices of adjacent Orai1 subunits ($\beta$), as well as the angle between CC2 domains of STIM1 dimer ($\theta$), are clear measures of the conformational transition during Orai1-STIM1 complex formation (Figure 4.4 A and D). The $\beta$ angle decreased from 153° to 140° in the beginning of the binding simulation, whereas it increased to 170° in the control simulation (Figure 4.4C). Angle comparison with the

crystal structures of drosophila Orai [128], and human STIM1 in complex with C-terminal helices of Orai1 [134], indicated that in the absence of STIM1, Orai1 tends to be in the closed conformation. The $\theta$ angle in STIM1 also reduced from 180° to 160° resulting in the opening of STIM1 helices. The coiled-coil conformation of the Orai1 C-terminus in complex with the STIM1 CC1-CC2 domain was then formed. Since reduction in $\beta$ occurs upon STIM1 binding and involves L273-L276 disassociation, we refer to $\beta$ as the gating angle.

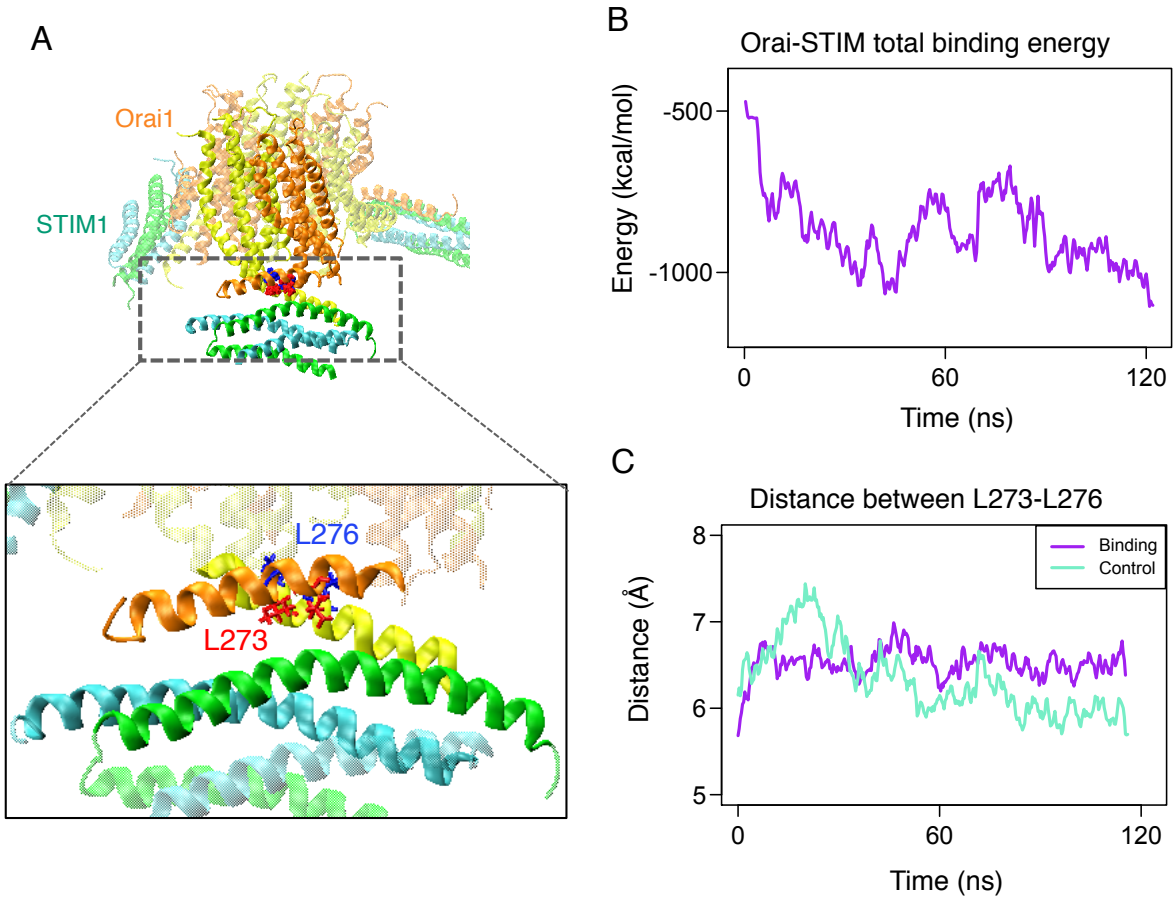


Figure 4.3. Interaction between Orai1 and STIM1. (A) The interaction between Orai1 hexamer (*yellow* and *orange*) and three STIM1 CC1-CC2 homodimers (*cyan* and *green*), all in their unbound states, were modeled. A hydrophobic interaction between residues L273 (*red*) and L276 (*blue*) in the C-terminus of Orai1 is necessary for the formation of the coiled-coil region. These residues are also involved in hydrophobic interaction with STIM1. (B) The total interaction energy between the Orai1 C-terminus (residues 265-290) and STIM1 (residues 350-385) is shown. (C) The time plot of distance between the center of mass of residues L273 of one Orai1 monomer and L276 in the adjacent monomer of Orai1 are shown for the binding and control simulations in purple and green, respectively.

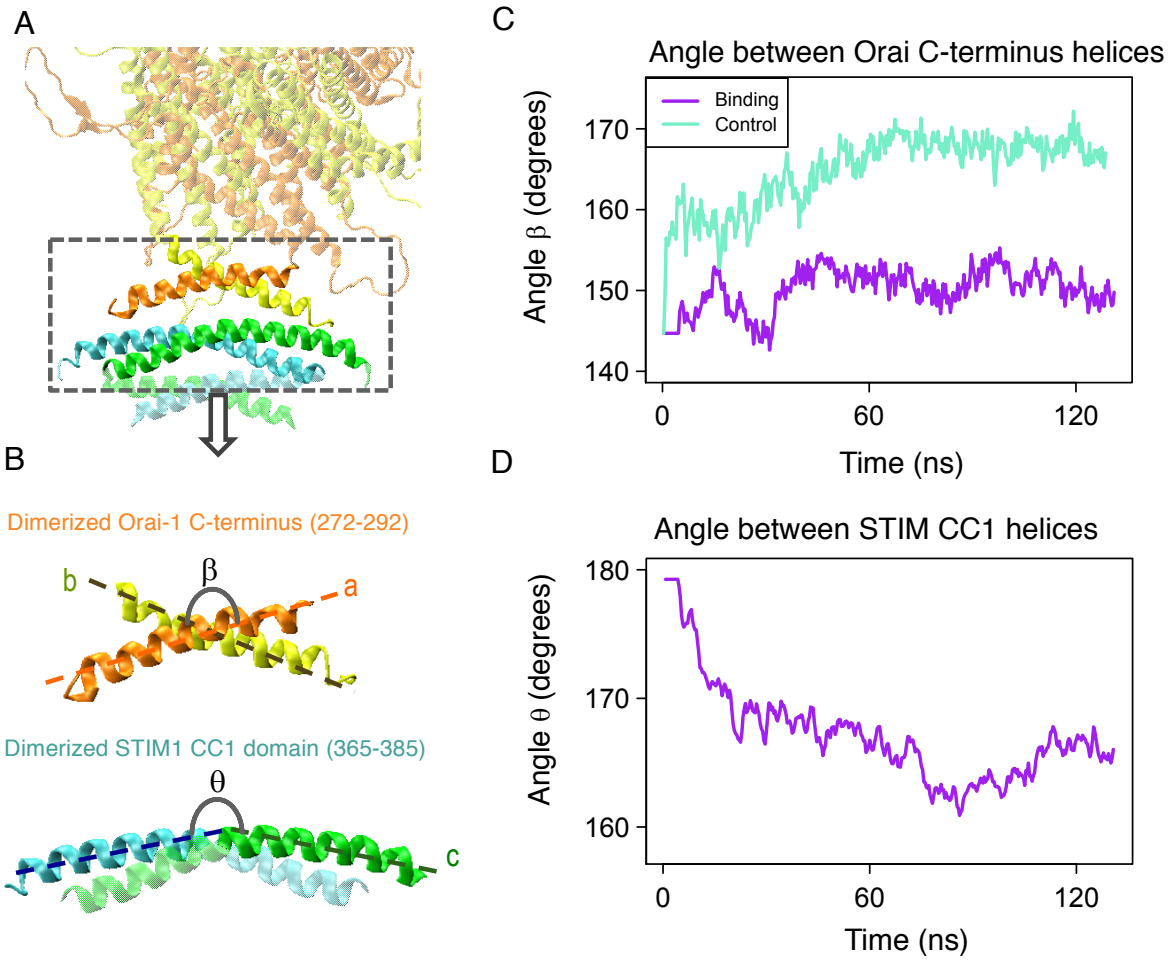


Figure 4.4. STIM1-induced conformational changes in the Orai1 C-terminus. A) A side view of the Orai1 C-terminus and STIM1 in one dimer of the Orai1 hexamer. B) The zoom-in view of the Orai1 C-terminus and STIM1 CC1-CC2 dimer showing $\beta$ and $\theta$ angles. C) The average $\beta$ angle changed from 153° to 140° in the binding simulations. Since there is no STIM1 molecule, the angle increased and reached around 170° in the control simulations indicating that the channel remains closed. D) The $\theta$ angle showed a significant conformational change, which led to the opening of STIM1 helices. The final angle of ~160° shows a parallel coiled-coil interaction of the Orai1 C-terminus with the STIM1 CC1-CC2 domain.

### The formation of kinks in the TM1 helices of Orai1

To show how the binding forces of STIM1 propagate through the Orai1 pore region leading to channel gating, we next analyzed the conformational changes in Orai1 pore helices. These conformational changes were determined by comparing the first and last frames of

our MD simulations, featuring an identical starting conformation of Orai1 for both binding and control simulations. It can be seen that there is a kink in TM1 helices of binding simulations at 120 ns. However, no significant change was observed in the conformation of TM1 helices in control simulation (Figure 4.5A). Our simulation results showed formation of a kink near residue S90 in the TM1 helix of each Orai1 monomer upon STIM1 interaction, whereas no noticeable kink was observed in the control simulation. The average kink angle (γ) is around 165° in the control simulation, whereas it changed from 165° to 150° in the binding simulations, which depicts a remarkable deformation centered at S90 (Figure 4.5B). Thereby, flexibility of basic pore residues, S89 through T92, allowed for widening of the pore in this part of the channel upon STIM1 binding showing that these residues along the pore operate as a channel gate.

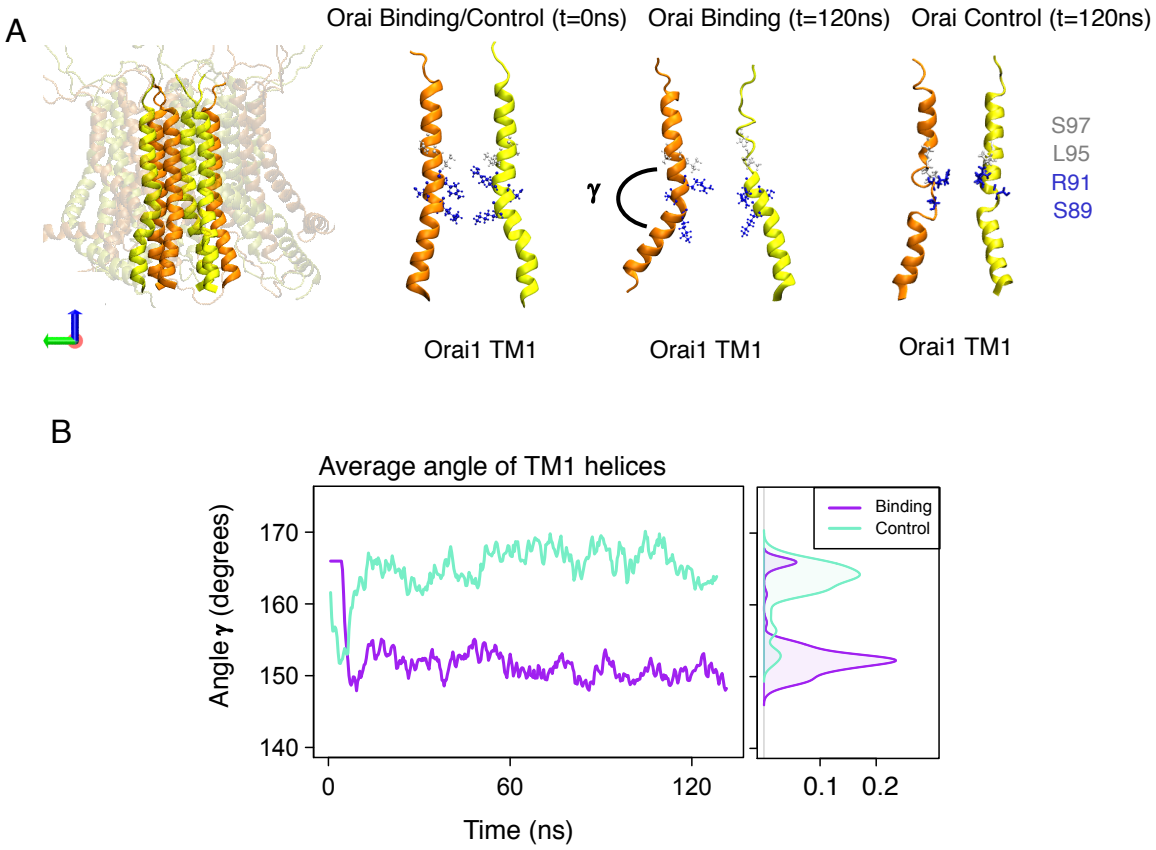


Figure 4.5: Formation of a kink in TM1 helices of Orai1 upon STIM1 binding. (A) Cartoon representations of the two opposing Orai1 monomers. Snapshots of the trajectories of these TM1 helices at 120 ns are shown for both binding and control simulations. Kinks centered around S90 were formed in TM1 helices after STIM1 binding. Important TM1 residues lining the Orai1 pore

were shown. For clarity, only two TM1 domains from two opposing subunits are represented. (B) The kink was quantified by the γ angle of the TM1 helices. The γ angle changes from 170° to 150° in the binding simulations. However, such a change was not observed in the control simulations, indicating that STIM1 binding induced this deformation.

### The change of the Orai1 pore capacity

STIM1 binding causes conformational changes in the pore region of the Orai1 channel. To confirm that these changes result in dilating the pore to facilitate ion influx through the channel, we measured the pore volume and the number of water molecules inside the pore in both binding and control simulations. The density plots of the average pore volume showed the effect of STIM1 association on widening the pore (Figure 4.6).

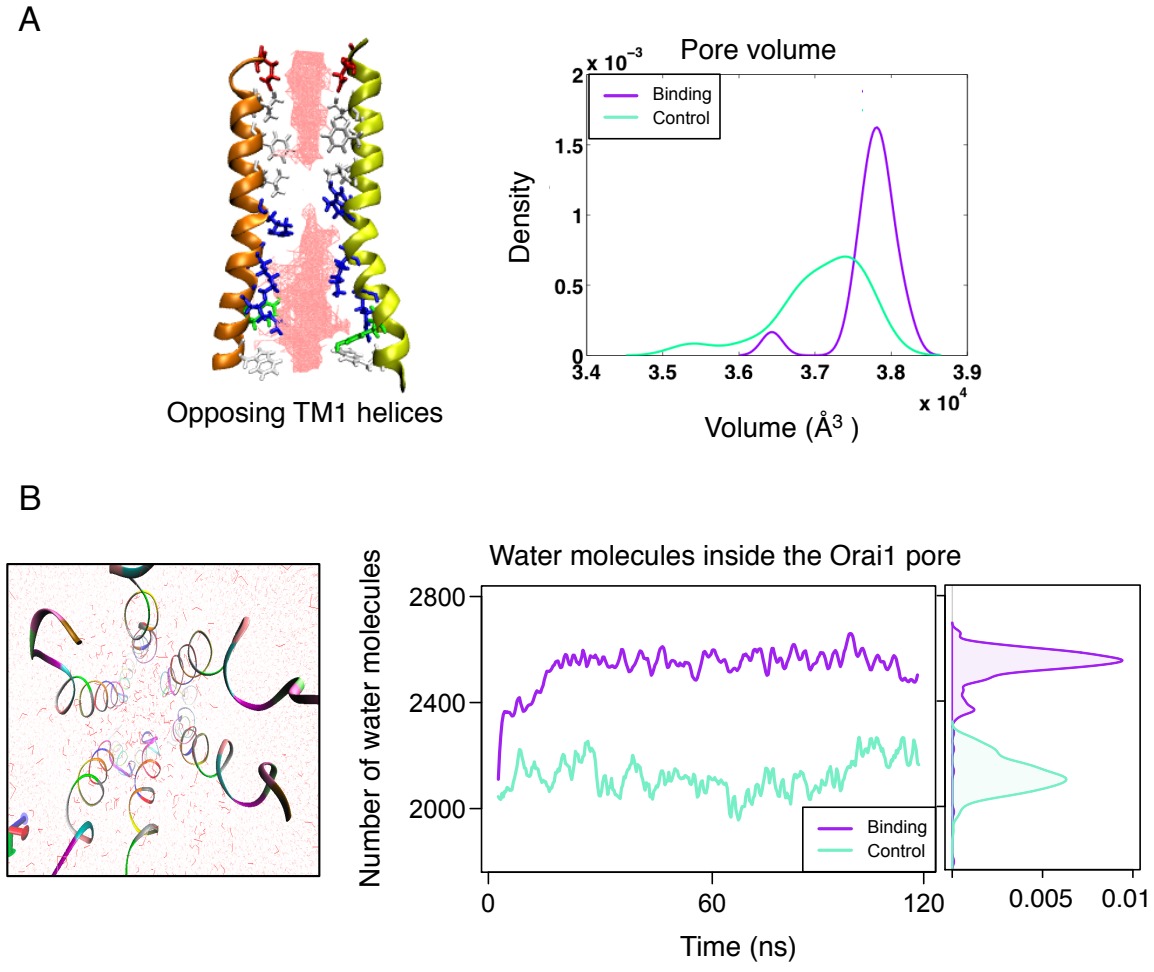


Figure 4.6: Orai1 pore capacity change. (A) Two opposing TM1 helices lining the Orai1 pore with key residues labeled. The solvent accessible pore volume, mapped between the TM1 helices, is

shown in pink (left). The density plots of the volume change of the Orai1 pore, in binding and control simulations are shown in purple and green, respectively (right). The shifted peak value of the pore volume in the binding simulation relative to control clearly indicates widening of the pore in response to STIM1 binding. (B) The time and density plots of the number of water molecules inside the Orai1 pore are shown for both binding and control simulations in purple and green, respectively.

Specifically, the average peak value of the volume in the control simulation was 37 $nm^3$, whereas the peak was shifted to 38 $nm^3$ in the binding simulations (Figure 4.6A), showing that the kink contributes to further opening of the pore and potentially regulates channel gating. Moreover, our results showed a significant increase in the number of water molecules inside the Orai1 pore during the first 30 ns of the binding simulations (Figure 4.6B). Then, the number of water molecules remained stable throughout the simulation. It is worth noting that the number of water molecules almost remained constant in the control simulation, further corroborating the role of STIM1 in dilating the Orai1 pore.

**RMSF Analyses**

To determine the changes in the dynamics of Orai1 helices upon STIM1 interaction, we calculated the root mean square fluctuation (RMSF) of Orai1 residues in STIM1-bound simulations and compared their values to the apo state. For the RMSF calculation, we split the hexamer into two groups of structurally similar monomers based on their orientation within the hexamer (Figure 4.7). The RMSF was then averaged over the identical monomers and standard deviation of each residue is indicative of the range of fluctuations. As shown in Figure 7, the RMSF-135 and RMSF-246 refers to chains P1, P3, P5 and P2, P4, P6, respectively.

The TM1 and TM4e helices within the pore had the highest RMSF compared to other neighboring helices in both apo and bound states. Such high mobility is likely to be critical for regulating channel gating and ion flux. The range of fluctuations of TM3 and TM4 helices in the apo state was markedly different between two sets of monomers, which suggests an intrinsic difference in the flexibility of monomers. Also, the higher standard deviation of most regions in the control simulation suggests a softer motion of the protein in the apo state, whereas STIM1 binding most likely locks Orai1 in the activated state.

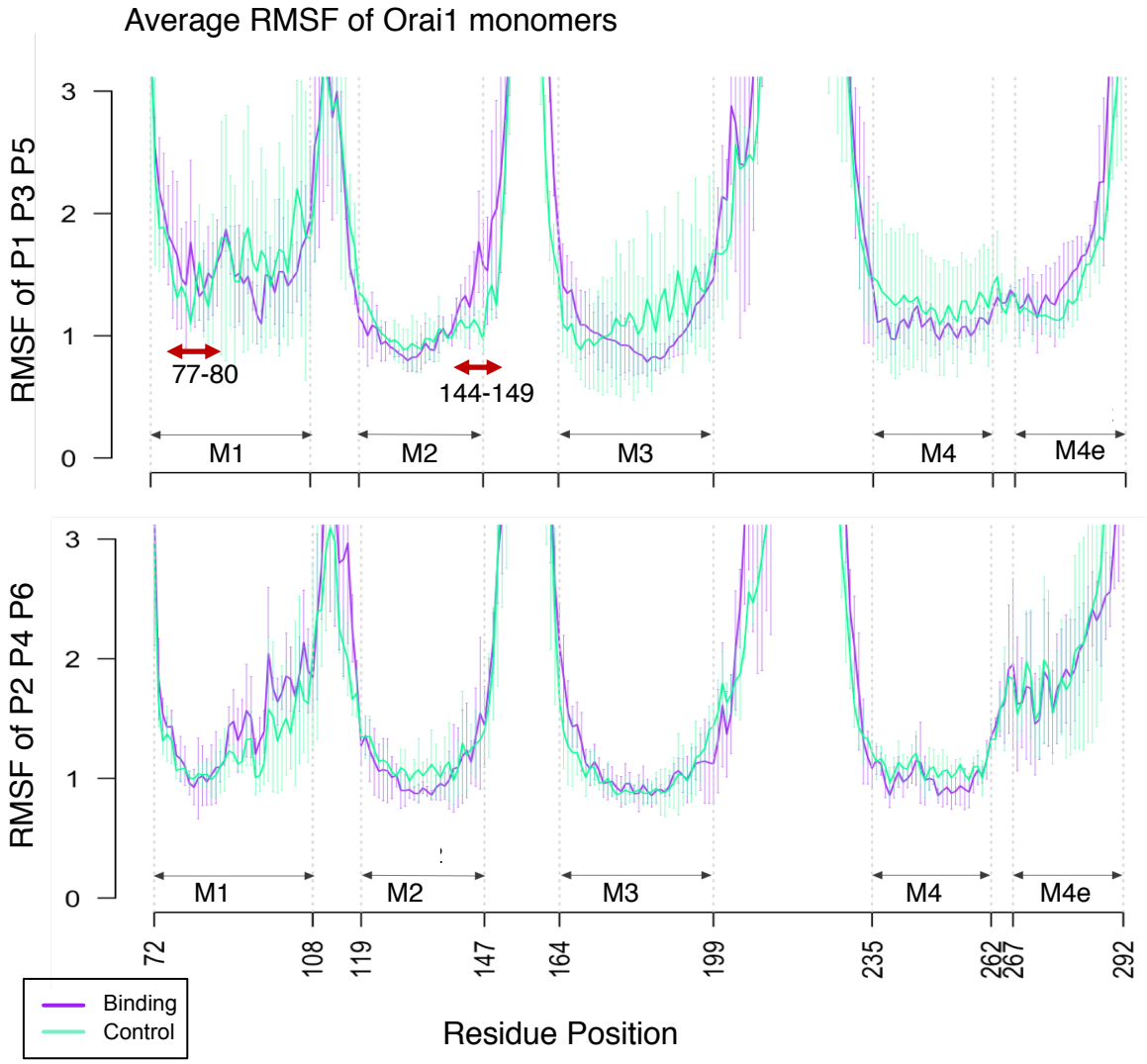


Figure 4.7. RMSF analyses of the Orai1 protein in the presence and absence of STIM1 simulations. The RMSF in the binding and control simulations for P1 P3 P5 monomers (*top*) and P2 P4 P6 monomers (*bottom*) separately. Important regions where the RMSF is higher in the bound state compared to the apo state are marked by red arrows. These regions consist of residues 77-80 in TM1 helices and residues 144-149 in TM2 helices of P1 P3 P5 monomers.

It is crucial to understand how forces are transmitted from the STIM1 binding site to the central pore leading to channel activation. Zhou et al. suggested that the 'Nexus' region at the junction of TM4 and its extension (residues 261-265) contributes to channel opening [139]. They proposed that a hydrophobic interaction between L261 on TM4, and either I174 or L175 on TM3 mechanically bridges the STIM1 binding site to the TM3 helix. Our

RMSF results indicate that the average RMSF of the Nexus region (261-265) remained unchanged after STIM1 association suggesting that Nexus most likely acts as an invariable, passive linkage between the channel pore and STIM1 binding site.

Moreover, we observed significant differences between the RMSF of two specific regions at residues 77-80 and 144-149 in P1 P3 P5 monomers. The RMSF-135 of TM1 and TM2 showed higher fluctuations in residues 77-80 and 144-149 in the bound state (Figure 4.7). This observation indicates that the conformational changes in these two regions as a result of STIM1 binding most likely contribute to transmitting binding forces from the STIM1 binding site to the channel pore. Details of interactions between key residues mediating force transmission are discussed in the next section.

**Formation of R78-E149 salt bridges maintain the Orai1 pore open conformation**

As discussed in the previous section, the RMSF results showed a higher fluctuation of residues 77-80 of TM1 and 144-149 of TM2 in binding simulation compared to the control simulation. In order to see the relative conformational changes of these helices, we calculated the angle between TM1 and TM2 in both apo and bound simulations (Figure 4.8B). The results showed significant increase in the TM1-TM2 angle from 128° to 140°, upon STIM1 interaction. However, the angle is almost stable throughout the control simulation. Then, our detailed analyses of these regions revealed the formation of salt bridges between residues R78 on TM1 and E149 on TM2 upon STIM1 interaction (Figure 4.8A). The total interaction energy between R78 and E149 residues confirm the strong binding between these residues (Figure 4.8C). Our results indicate that there is a -200 kcal/mole decrease in the total interaction energy between R78-E149 residues, while we observed no interaction between these residues in the control simulation.

Next, to understand whether the changes in the interaction energies between these residues were correlated with the kink angle ($\gamma$) of TM1 helices, we performed a cross correlation analysis. The cross correlation analysis showed a notable correlation between the interaction energy of R78-E149 and $\gamma$ angle (Figure 4.8D). This suggests that the STIM1-induced salt bridges between cytoplasmic regions of TM1 and TM2 helices following TM1 bending keeps the basic region of the Orai1 pore open.

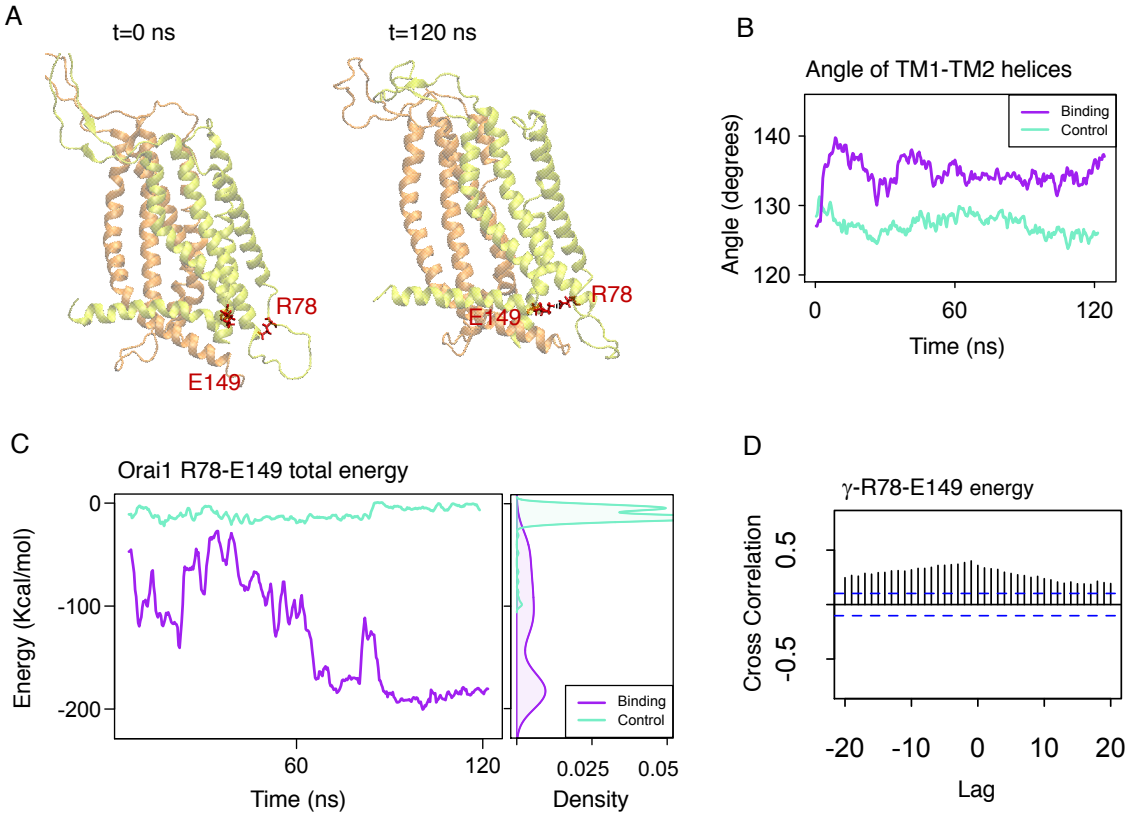


Figure 4.8: Formation of the R78-E149 salt bridges maintain the Orai1 pore in the open conformation. (A) VMD snapshots in cartoon representation of Orai1 dimer in binding simulation at t=0 and t=120 ns. (B) The time plot of the angle between TM1 and TM2 helices of Orai1 monomers are shown for both binding and control simulations. (C) The time and density plots of the total energy of interactions between R78 and E149 residues are shown for binding and control simulations in purple and green, respectively. (D) Cross correlation function between γ angle and R78-E149 interaction energy is shown.

## 4.4. Discussion

The CRAC channel regulates calcium influx through the ER $Ca^{2+}$ sensor, STIM1, and the CRAC channel subunit, Orai1. Recent studies have provided important structural and functional insights into the Orai1-STIM1 complex [71], [139]–[141], however, dynamic regulatory mechanisms of Orai1 activation through direct physical binding to STIM1 is still elusive. Palty et al. [142], and Zhang et al. [123] demonstrated that STIM1 binding to the N-terminus of Orai1 is necessary for channel activation and gating. Conversely, Zhou et al. showed that STIM1 binding to the C-terminus of Orai1 is both necessary and sufficient for Orai1 activation [142]–[144]. Our simulations indicated that STIM1

association with just the C-terminus of Orai1 can induce notable conformational changes in favor of channel opening (Figures 4.3-4.8). Also, diameter changes near selected residues of the pore, 2Å at E106 within the selectivity filter and 3Å at R91 inside the basic region, allows a single calcium ion to pass through the pore. It should be noted that our system did not include STIM1 interaction with the N-terminal domain of Orai1, because the exact binding site of STIM1 with the N-terminus of Orai1 is not known. Thereby, we cannot exclude the possibility of alternative activation mechanisms may exist and needs to further be studied.

We showed that STIM1 binding remotely changes the pore volume by inducing kinks within the basic region of TM1 helices and dilating the pore (Figure 4.6). Previous studies also discussed the importance of a basic residue, R91, for ion conductance as the R91W mutation results in a constitutively closed channel leading to lethal immune deficiency [132]. Our results suggest that the flexibility of the whole basic region permits channel opening in response to STIM1 binding (Figure 4.5). The selectivity filter and hydrophobic regions may also contribute to channel gating [65], [145] as the hydrophobic tie between L273-L276 is necessary for channel gating [68]. Our simulations suggest that STIM1 association can trigger channel gating by weakening the L273-L276 bond (Figure 4.3).

One of the important questions in Orai1 activation is how forces from STIM binding get transmitted to the pore and activate the channel. Crystal structure and mutational studies of Orai1 channel provide some insight about how STIM binding is allosterically propagated throughout the pore [73]. Zhou et al. suggested that the 'Nexus' region at the junction of TM4 and its extension (residues 261-265) contributes to channel opening [139]. However, our results showed no significant RMSF changes in the Nexus region after STIM1 association, suggesting that Nexus most likely acts as an invariable, passive linkage between the channel pore and STIM1 binding site.

Furthermore, our detailed residue-based analyses between TM1 and TM2 helices of Orai1 revealed an important interaction between residues R78 on TM1 and E149 on TM2 and formation of salt bridges between these residues upon STIM1 binding and TM1 bending (see Figure 4.8). We propose that the R78-E149 interaction is key for Orai1 activation and channel gating as it maintains the open conformation of Orai1 pore near the basic region.

In summary, our findings suggest that STIM1 association locks Orai1 into a new conformational state that is optimized for transmitting forces directly from the STIM1 binding site to the pore, which is essential for force-induced channel activation.

# Chapter 5

# Conclusions and Future Directions

Immune system response to inflammation involves a cascade of biological events, through which leukocyte recruitment happens. Leukocyte adhesion and firm adhesion to endothelial cell are key steps in this cascade. When there is a disruption in the arrest of rolling leukocytes, a number of human diseases may arise including atherosclerosis, LADI, and LADIII diseases [4], [121]. Therefore, it is important to understand the molecular mechanisms by which leukocytes adhere to endothelial cells and migrate towards the infection site. Integrin is one of the most important molecules in leukocyte recruitment since it is involved in different steps of this cascade, including adhesion, migration, and transmigration. In order to initiate leukocyte adhesion, integrins must get activated from a low-affinity state (bent conformation) to a high-affinity state (extended conformation) to bind to the endothelial ligand.

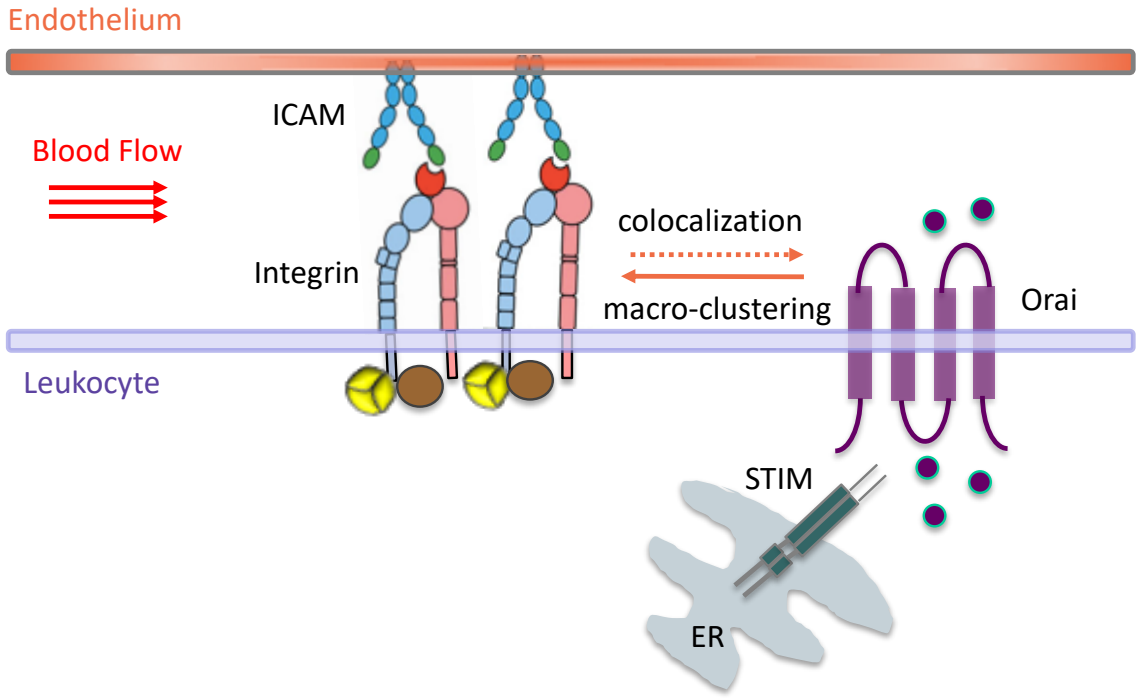


Figure 5.1: A schematic showing the steps of leukocyte adhesion and firm adhesion to endothelial wall. First, the shear force from blood flow is sensed by integrin-ICAM bonds. Then, integrin-ICAM bonds take up tensile forces, leading to the recruitment of kindlin to facilitate $Ca^{2+}$ flux. Although, the detailed mechanisms remain unknown, it has been suggested the increase in $Ca^{2+}$ flux is mediated by integrin-Orai colocalization. Finally, $Ca^{2+}$ flux through Orai channel enhances integrin clustering, which results in adhesion strengthening. In this process, STIM protein clusters and reaches the plasma membrane to directly bind and activate Orai protein.

Chemokine signaling initiates inside-out activation by inducing talin binding to the cytoplasmic tail of integrin and integrin-ICAM binding. Then, tensile forces acting on integrin-ICAM bonds recruit kindlin to the adhesion site. Kindlin recruitment to the site of adhesion plays an important role in integrin activation and micro-clustering. It has been shown that micro-clustering of integrins result in an increased inward $Ca^{2+}$ flux through integrin-Orai colocalization (Figure 5.1) [4], [5]. Then, $Ca^{2+}$ flux further enhances integrin clustering resulting in macro-clusters. This mechanism reinforces leukocyte attachment to the endothelial wall. To enable $Ca^{2+}$ influx, Orai channel pore needs to be activated to an open state through physical interaction with STIM protein.

Integrin activation and $Ca^{2+}$ signaling are two important processes in leukocyte adhesion. Therefore, understanding the molecular basis of kindlin-mediated integrin activation and STIM-mediated Orai activation might have potential important implications in designing new therapeutic interventions. In my dissertation, I studied these two important activation mechanisms using molecular dynamics simulations. My analyses unraveled the details of these protein activation processes as summarized in the following sections.

## 5.1. Kindlin-Mediated Integrin Activation

Integrins are transmembrane proteins that mediate the signaling between the cytoplasm and extracellular matrix to promote cell adhesion. In order to initiate signaling, integrins must be activated from a low-affinity state to a high-affinity state for binding to extracellular molecules. Previous works assumed that talin binding was both necessary and sufficient for integrin activation. However, recent findings contradict this notion and suggest that kindlin protein is also necessary in this process. We developed all-tom microsecond molecular dynamic models to study the effect of kindlin protein in talin-mediated integrin activation. We performed rigorous simulations to understand the effect of talin and kindlin individually and also simultaneously, when they cooperate with each other. We had three important observations:

(i) Kindlin cooperates with talin to facilitate integrin activation by enhancing talin interactions with the membrane proximal region of the integrin β3 resulting in a more effective disruption of the inner membrane clasp (dissociating the salt bridges between αIIb R995 and β3 E726) and outer membrane clasp.

(ii) Not only both talin and kindlin are essential for efficiently initiating the activation process, but also kindlin modifies the molecular mechanism of inside-out signaling by

decreasing the crossing angle between transmembrane helices of integrin αIIbβ3, which eventually results in parallelization of integrin dimer.

(iii) Our control simulation featuring integrin in complex with kindlin confirms the inability of kindlin to unclasp the cytoplasmic region of integrin αIIbβ3 and subsequent transmembrane conformational changes and separation.

In addition, we performed more comprehensive analyses on integrin α-β crossing angle to see the underlying reason behind reverse angle change in ITK (integrin in complex with both talin and kindlin) versus IT (integrin in complex with talin) simulations. Our analyses revealed that interaction of kindlin with integrin β subunits is highly correlated with the dramatic decrease in α-β crossing angle in integrin dimer. However, interestingly, there is no significant correlation between talin/kindlin interactions with integrin α tail/membrane and α-β crossing angle.

My work focused on the analyses of integrin αIIbβ3 can be replicated in future to study the activation mechanisms of other types of integrin. Integrin αIIbβ3 is the predominant type of integrin present in platelets, the full crystal structure of which is available. It is interesting to note that while the cytoplasmic tail of different integrin subtypes exhibits more than 60% similarity to each other, their activation mechanisms might be type-specific [98], [146]. Therefore, follow up computational studies, similar to what I presented in this dissertation, would need to reveal the differences in activation mechanisms for integrin subfamilies, such as integrin αLβ2.

Contemporary computational studies use dissociation of inner membrane clasp (IMC) and outer membrane clasp (OMC) as a measure of integrin activation. However, whether IMC and OMC disruption would result in conformational changes of integrin ectodomain, leading to integrin activation still remains elusive. Microsecond molecular dynamic simulations of the full structure of integrin dimer, including its extracellular domains, with talin and/or kindlin FERM domains would be needed to discover the sequence of events from talin and kindlin binding to integrin activation, which can possibly reveal intermediate steps in this process.

After integrin changes its conformation to intermediate state (extended close), it senses the shear force from blood flow. High-affinity integrin-ligand bond formation and uptake of tensile force are necessary to catalyze downstream events required for leukocyte adhesion strengthening [5], [62]. Tensile forces facilitate physical association of kindlin with the

cytoplasmic domain of integrin. This step is necessary for local calcium flux and subsequent adhesion strengthening. Therefore, as a follow up research, the effect of tensile forces on extracellular part of integrin can be investigated. Steered molecular dynamics simulations of integrin dimer in complex with kindlin can be used for this purpose. The results of these simulations can be analyzed to find out the consequences of this external force on binding interaction between integrin and kindlin. Force distribution analyses of these results would reveal the changes in the internal forces within integrin dimer helices.

## 5.2. STIM-mediated Orai Activation

Orai is the pore subunit of CRAC channel and its activation by STIM binding is required for $Ca^{2+}$ influx through the cell. Precise regulation of Orai activity is critical for human health. Discovering the allosteric conformational changes necessary to transmit the signal from STIM binding site to the Orai pore has important therapeutic targets and is an interesting focus for research.

We used all-atom molecular dynamic simulations of the dimeric binding model of STIM, based on the NMR structure of STIM CC1-CC2 domains, in complex with Orai hexamer to study the role of STIM in Orai gating. Our results showed that STIM interactions with only the C-terminus of Orai contribute to channel gating by inducing a kink near residue S90, resulting in the widening of basic region of the pore. Our results support the second gating model proposed by Hou et. al [147]. Also, we proposed that the formation of R78-E149 salt bridges upon STIM binding and kink formation would potentially maintain the Orai open conformation. Moreover, our simulation results revealed some important residue pairs between TM helices, their association or dissociation of which potentially contribute to the transmission of force from STIM binding site to the Orai pore. For example, the interaction between I144 and I172 residues is disrupted over time, while G118-V197 interaction is formed after STIM binding.

There are very few solved crystal structures of Orai and STIM in different states. Moreover, no crystallographic data is available for the complex structure of these proteins, except for the NMR structure used in our model. Mapping the complex crystallographic structure of Orai and STIM proteins would greatly enhance our understanding of the structural interactions of these proteins and is highly demanded. Such information would enable future computational studies to discover the sequence of events from STIM binding to Orai gating.

Moreover, experimental evidence suggests that endoplasmic reticulum is constantly under tensile force [148]. Therefore, another area of follow up research that would need more investigation is whether the forces from endoplasmic reticulum on the STIM protein can impact Orai activation. Steered molecular dynamic simulation would help study the influence of forces in Orai gating.

Recent studies show that clustered high-affinity integrins mediate Orai channel calcium influx at the site of adhesion by colocalizing with Orai channel [21]. However, the molecular details of interactions between integrin/kindlin and Orai proteins are yet not known. One way to study these interactions is to perform experiments to find the complex crystal structure of integrin/kindlin-Orai that can reveal the binding locations between these proteins. Given the complexity of these experiments, computational modeling can be used to shed light to these interactions. For example, molecular docking analyses of integrin/kindlin and Orai can be used to find out possible complex structures between Orai-integrin and Orai-kindlin. Then, molecular dynamic simulations of these complex structures with or without STIM can be performed to monitor the effect of integrin/kindlin interactions on Orai channel gating and calcium flux. These computational models can go hand in hand with experimental studies to uncover the mechanisms of integrin/kindlin-Orai interactions and Orai channel gating.

# References:


[1] T. G. Kapp, F. Rechenmacher, T. R. Sobahi, and H. Kessler, "Integrin modulators: a patent review," *Expert Opin. Ther. Pat.*, vol. 23, no. 10, pp. 1273–1295, Oct. 2013.

[2] "Autoimmune Statistics | AARDA." [Online]. Available: http://www.aarda.org/autoimmune-information/autoimmune-statistics/. [Accessed: 18-Feb-2015].

[3] I. Mitroulis, V. I. Alexaki, I. Kourtzelis, A. Ziogas, G. Hajishengallis, and T. Chavakis, "Leukocyte integrins: role in leukocyte recruitment and as therapeutic targets in inflammatory disease.," *Pharmacol. Ther.*, vol. 147, pp. 123–135, Mar. 2015.

[4] N. Dixit, M.-H. Kim, J. Rossaint, I. Yamayoshi, A. Zarbock, and S. I. Simon, "Leukocyte function antigen-1, kindlin-3, and calcium flux orchestrate neutrophil recruitment during inflammation.," *J. Immunol.*, vol. 189, no. 12, pp. 5954–64, Dec. 2012.

[5] N. Dixit, I. Yamayoshi, A. Nazarian, and S. I. Simon, "Migrational guidance of neutrophils is mechanotransduced via high-affinity LFA-1 and calcium flux.," *J. Immunol.*, vol. 187, no. 1, pp. 472–81, Jul. 2011.

[6] R. Alon, D. A. Hammer, and T. A. Springer, "Lifetime of the P-selectin-carbohydrate bond and its response to tensile force in hydrodynamic flow," *Nature*, vol. 374, no. 6522, pp. 539–542, Apr. 1995.

[7] A. Zarbock, K. Ley, R. P. McEver, and A. Hidalgo, "Leukocyte ligands for endothelial selectins: specialized glycoconjugates that mediate rolling and signaling under flow.," *Blood*, vol. 118, no. 26, pp. 6743–51, Dec. 2011.

[8] M. Leick, V. Azcutia, G. Newton, and F. W. Luscinskas, "Leukocyte recruitment in inflammation: basic concepts and new mechanistic insights based on new models and microscopic imaging technologies," *Cell Tissue Res.*, vol. 355, no. 3, pp. 647–656, Mar. 2014.

[9] J. M. Schenkel and D. Masopust, "Tissue-resident memory T cells.," *Immunity*, vol. 41, no. 6, pp. 886–97, Dec. 2014.

[10] M. Phillipson, B. Heit, P. Colarusso, L. Liu, C. M. Ballantyne, and P. Kubes, "Intraluminal crawling of neutrophils to emigration sites: a molecularly distinct process from adhesion in the recruitment cascade," *J. Exp. Med.*, vol. 203, no. 12, pp. 2569–2575, Nov. 2006.

[11] K. Ley, C. Laudanna, M. I. Cybulsky, and S. Nourshargh, "Getting to the site of inflammation: the leukocyte adhesion cascade updated," *Nat. Rev. Immunol.*, vol. 7, no. 9, pp. 678–689, Sep. 2007.

[12] M. Moser *et al.*, “Kindlin-3 is required for β2 integrin–mediated leukocyte adhesion to endothelial cells,” *Nat. Med.*, vol. 15, no. 3, pp. 300–305, Mar. 2009.

[13] N. J. Anthis and I. D. Campbell, “The tail of integrin activation.,” *Trends Biochem. Sci.*, vol. 36, no. 4, pp. 191–8, Apr. 2011.

[14] C. Feng *et al.*, “Kindlin-3 mediates integrin αLβ2 outside-in signaling, and it interacts with scaffold protein receptor for activated-C kinase 1 (RACK1).,” *J. Biol. Chem.*, vol. 287, no. 14, pp. 10714–26, Mar. 2012.

[15] S. J. Shattil, C. Kim, and M. H. Ginsberg, “The final steps of integrin activation: the end game,” *Nat. Rev. Mol. Cell Biol.*, vol. 11, no. 4, pp. 288–300, Apr. 2010.

[16] S. J. Shattil and P. J. Newman, “Integrins: dynamic scaffolds for adhesion and signaling in platelets,” *Blood*, vol. 104, no. 6, pp. 1606–1615, Sep. 2004.

[17] A. Vararattanavech, X. Lin, J. Torres, and S.-M. Tan, “Disruption of the integrin alphaLbeta2 transmembrane domain interface by beta2 Thr-686 mutation activates alphaLbeta2 and promotes micro-clustering of the alphaL subunits.,” *J. Biol. Chem.*, vol. 284, no. 5, pp. 3239–49, Jan. 2009.

[18] B.-H. Luo, C. V. Carman, J. Takagi, and T. A. Springer, “Disrupting integrin transmembrane domain heterodimerization increases ligand binding affinity, not valency or clustering,” *Proc. Natl. Acad. Sci.*, vol. 102, no. 10, pp. 3679–3684, Mar. 2005.

[19] A. Cambi *et al.*, “Organization of the Integrin LFA-1 in Nanoclusters Regulates Its Activity,” *Mol. Biol. Cell*, vol. 17, no. 10, pp. 4270–4281, Oct. 2006.

[20] E. Evans, K. Kinoshita, S. Simon, and A. Leung, “Long-lived, high-strength states of ICAM-1 bonds to beta2 integrin, I: lifetimes of bonds to recombinant alphaLbeta2 under force.,” *Biophys. J.*, vol. 98, no. 8, pp. 1458–66, Apr. 2010.

[21] N. Dixit, M.-H. Kim, J. Rossaint, I. Yamayoshi, A. Zarbock, and S. I. Simon, “Leukocyte Function Antigen-1, Kindlin-3, and Calcium Flux Orchestrate Neutrophil Recruitment during Inflammation,” *J. Immunol.*, vol. 189, no. 12, pp. 5954–5964, 2012.

[22] C. V Carman and T. A. Springer, “Integrin avidity regulation: are changes in affinity and conformation underemphasized?,” *Curr. Opin. Cell Biol.*, vol. 15, no. 5, pp. 547–556, Oct. 2003.

[23] M. Kim, C. V Carman, W. Yang, A. Salas, and T. A. Springer, “The primacy of affinity over clustering in regulation of adhesiveness of the integrin {alpha}L{beta}2.,” *J. Cell Biol.*, vol. 167, no. 6, pp. 1241–53, Dec. 2004.

[24] L. Kurtz, L. Kao, D. Newman, I. Kurtz, and Q. Zhu, “Integrin αIIbβ3 inside-out activation: An in situ conformational analysis reveals a new mechanism,” *J. Biol. Chem.*, vol. 287, no. 27, pp. 23255–23625, 2012.

[25] K. Bledzka, J. Qin, and E. F. Plow, “Integrin αIIbβ3,” *Platelets*, pp. 227–241,

2019.

[26] M. Mehrbod, S. Trisno, and M. R. K. Mofrad, “On the activation of integrin αIIbβ3: outside-in and inside-out pathways.,” *Biophys. J.*, vol. 105, no. 6, pp. 1304–15, Sep. 2013.

[27] D. Provasi, A. Negri, B. S. Coller, and M. Filizola, “Talin-driven inside-out activation mechanism of platelet αIIbβ3 integrin probed by multimicrosecond, all-atom molecular dynamics simulations,” *Proteins Struct. Funct. Bioinforma.*, vol. 82, no. 12, pp. 3231–3240, 2014.

[28] S. J. Shattil, C. Kim, and M. H. Ginsberg, “The final steps of integrin activation: the end game,” *Nat. Rev. Mol. Cell Biol.*, vol. 11, no. 4, pp. 288–300, Apr. 2010.

[29] Z. Jahed, Z. Haydari, A. Rathish, and M. R. K. Mofrad, “Kindlin Is Mechanosensitive: Force-Induced Conformational Switch Mediates Cross-Talk among Integrins,” *Biophys. J.*, vol. 116, no. 6, pp. 1011–1024, Mar. 2019.

[30] Z. Jahed, H. Shams, M. Mehrbod, and M. R. K. Mofrad, “Mechanotransduction pathways linking the extracellular matrix to the nucleus.,” *Int. Rev. Cell Mol. Biol.*, vol. 310, pp. 171–220, Jan. 2014.

[31] W. Wan *et al.*, “Synergistic Effect of Matrix Stiffness and Inflammatory Factors on Osteogenic Differentiation of MSC,” *Biophys. J.*, vol. 117, no. 1, pp. 129–142, Jul. 2019.

[32] B. Nieswandt, D. Varga-Szabo, and M. Elvers, “Integrins in platelet activation.,” *J. Thromb. Haemost.*, vol. 7 Suppl 1, pp. 206–9, Jul. 2009.

[33] F. Ye, C. Kim, and M. H. Ginsberg, “Reconstruction of integrin activation,” *Blood*, vol. 119, no. 1, pp. 26–33, 2012.

[34] Z. Sun, M. Costell, and R. Fässler, “Integrin activation by talin, kindlin and mechanical forces,” *Nat. Cell Biol.*, vol. 21, no. 1, pp. 25–31, 2019.

[35] B.-H. Luo, C. V Carman, and T. A. Springer, “Structural basis of integrin regulation and signaling.,” *Annu. Rev. Immunol.*, vol. 25, pp. 619–47, 2007.

[36] J.-P. Xiong, T. Stehle, S. L. Goodman, and M. A. Arnaout, “New insights into the structural basis of integrin activation,” *Blood*, vol. 102, no. 4, pp. 1155–1159, Apr. 2003.

[37] J. Liu, Z. Wang, A. M. M. Thinn, Y.-Q. Ma, and J. Zhu, “The dual structural roles of the membrane distal region of the  -integrin cytoplasmic tail during integrin inside-out activation,” *J. Cell Sci.*, vol. 128, no. 9, pp. 1718–1731, 2015.

[38] J. Guo *et al.*, “Intramembrane ionic protein–lipid interaction regulates integrin structure and function,” *PLoS Biol.*, vol. 16, no. 11, pp. 1–28, 2018.

[39] F. Ye, A. K. Snider, and M. H. Ginsberg, “Talin and kindlin: The one-two punch in integrin activation,” *Front. Med. China*, vol. 8, no. 1, pp. 6–16, 2014.

[40] C. Cluzel, F. Saltel, J. Lussi, F. Paulhe, B. A. Imhof, and B. Wehrle-Haller, "The mechanisms and dynamics of αvβ3 integrin clustering in living cells," *J. Cell Biol.*, vol. 171, no. 2, pp. 383–392, Oct. 2005.

[41] R. Li, C. R. Babu, J. D. Lear, A. J. Wand, J. S. Bennett, and W. F. DeGrado, "Oligomerization of the integrin IIb 3: Roles of the transmembrane and cytoplasmic domains," *Proc. Natl. Acad. Sci.*, vol. 98, no. 22, pp. 12462–12467, Oct. 2001.

[42] R. Li *et al.*, "Activation of Integrin alphaIIbbeta3 by Modulation of Transmembrane Helix Associations," *Science (80-. ).*, vol. 300, no. 5620, pp. 795–798, May 2003.

[43] Y. Jamali, T. Jamali, and M. R. K. Mofrad, "An agent based model of integrin clustering: Exploring the role of ligand clustering, integrin homo-oligomerization, integrin–ligand affinity, membrane crowdedness and ligand mobility," *J. Comput. Phys.*, vol. 244, pp. 264–278, Jul. 2013.

[44] W. Wang, J. Zhu, T. A. Springer, and B.-H. Luo, "Tests of Integrin Transmembrane Domain Homo-oligomerization during Integrin Ligand Binding and Signaling," *J. Biol. Chem.*, vol. 286, no. 3, pp. 1860–1867, Jan. 2011.

[45] R. Li *et al.*, "Dimerization of the Transmembrane Domain of Integrin $\alpha_{IIb}$ Subunit in Cell Membranes," *J. Biol. Chem.*, vol. 279, no. 25, pp. 26666–26673, Jun. 2004.

[46] T. A. Bunch, "Integrin αIIbβ3 Activation in Chinese Hamster Ovary Cells and Platelets Increases Clustering Rather than Affinity," *J. Biol. Chem.*, vol. 285, no. 3, pp. 1841–1849, Jan. 2010.

[47] H. Li *et al.*, "Structural basis of kindlin-mediated integrin recognition and activation.," *Proc. Natl. Acad. Sci. U. S. A.*, vol. 114, no. 35, pp. 9349–9354, Jul. 2017.

[48] F. Ye *et al.*, "Recreation of the terminal events in physiological integrin activation.," *J. Cell Biol.*, vol. 188, no. 1, pp. 157–73, Jan. 2010.

[49] Y.-Q. Ma, J. Qin, C. Wu, and E. F. Plow, "Kindlin-2 (Mig-2): a co-activator of beta3 integrins.," *J. Cell Biol.*, vol. 181, no. 3, pp. 439–46, May 2008.

[50] E. F. Plow, J. Qin, and T. Byzova, "Kindling the flame of integrin activation and function with kindlins.," *Curr. Opin. Hematol.*, vol. 16, no. 5, pp. 323–8, Sep. 2009.

[51] E. F. Plow and J. Qin, "The Kindlin Family of Adapter Proteins," *Circ. Res.*, vol. 124, no. 2, pp. 202–204, Jan. 2019.

[52] K. Bledzka *et al.*, "Spatial coordination of kindlin-2 with talin head domain in interaction with integrin β cytoplasmic tails," *J. Biol. Chem.*, vol. 287, no. 29, pp. 24585–24594, 2012.

[53] A. C. Kalli, I. D. Campbell, and M. S. P. Sansom, "Conformational Changes in

Talin on Binding to Anionic Phospholipid Membranes Facilitate Signaling by Integrin Transmembrane Helices," *PLoS Comput. Biol.*, vol. 9, no. 10, 2013.

[54] T. L. Lau, C. Kim, M. H. Ginsberg, and T. S. Ulmer, "The structure of the integrin αiIbB3 transmembrane complex explains integrin transmembrane signalling," *EMBO J.*, vol. 28, no. 9, pp. 1351–1361, 2009.

[55] D. A. Calderwood, I. D. Campbell, and D. R. Critchley, "Talins and kindlins: Partners in integrin-mediated adhesion," *Nat. Rev. Mol. Cell Biol.*, vol. 14, no. 8, pp. 503–517, 2013.

[56] M. H. Ginsberg, "BMB-47-655.pdf," vol. 47, no. November, pp. 655–659, 2014.

[57] C. Kim, F. Ye, X. Hu, and M. H. Ginsberg, "Talin activates integrins by altering the topology of the β transmembrane domain," *J. Cell Biol.*, vol. 197, no. 5, pp. 605–611, 2012.

[58] M. Mehrbod, S. Trisno, and M. R. K. Mofrad, "On the activation of integrin αiIbβ3: Outside-in and inside-out pathways," *Biophys. J.*, vol. 105, no. 6, pp. 1304–1315, 2013.

[59] A. C. Kalli, I. D. Campbell, and M. S. P. Sansom, "Multiscale simulations suggest a mechanism for integrin inside-out activation," *Proc. Natl. Acad. Sci.*, vol. 108, no. 29, pp. 11890–11895, 2011.

[60] S. Kappel, A. Borgström, P. Stokłosa, K. Dörr, and C. Peinelt, "Store-operated calcium entry in disease: Beyond STIM/Orai expression levels.," *Semin. Cell Dev. Biol.*, vol. 94, pp. 66–73, 2019.

[61] K. Kinoshita, A. Leung, S. Simon, and E. Evans, "Long-lived, high-strength states of ICAM-1 bonds to beta2 integrin, II: lifetimes of LFA-1 bonds under force in leukocyte signaling.," *Biophys. J.*, vol. 98, no. 8, pp. 1467–75, Apr. 2010.

[62] S. I. Simon and C. E. Green, "Molecular Mechanics and Dynamics of Leukocyte Recruitment During Inflammation," *Annu. Rev. Biomed. Eng.*, vol. 7, no. 1, pp. 151–185, Aug. 2005.

[63] T. Kawasaki, I. Lange, and S. Feske, "A minimal regulatory domain in the C terminus of STIM1 binds to and activates ORAI1 CRAC channels," *Biochem. Biophys. Res. Commun.*, vol. 385, no. 1, pp. 49–54, Jul. 2009.

[64] I. Frischauf *et al.*, "Molecular determinants of the coupling between STIM1 and Orai channels: differential activation of Orai1-3 channels by a STIM1 coiled-coil mutant.," *J. Biol. Chem.*, vol. 284, no. 32, pp. 21696–706, Aug. 2009.

[65] E. D. Covington, M. M. Wu, and R. S. Lewis, "Essential role for the CRAC activation domain in store-dependent oligomerization of STIM1.," *Mol. Biol. Cell*, vol. 21, no. 11, pp. 1897–907, Jun. 2010.

[66] M. Prakriya and R. S. Lewis, "Store-Operated Calcium Channels," *Physiol. Rev.*, vol. 95, no. 4, pp. 1383–1436, Oct. 2015.

[67] R. Qiu and R. S. Lewis, “Structural features of STIM and Orai underlying store-operated calcium entry.,” *Curr. Opin. Cell Biol.*, vol. 57, pp. 90–98, 2019.

[68] R. M. Nwokonko, X. Cai, N. A. Loktionova, Y. Wang, Y. Zhou, and D. L. Gill, “The STIM-Orai Pathway: Conformational Coupling Between STIM and Orai in the Activation of Store-Operated Ca2+ Entry,” in *Advances in experimental medicine and biology*, vol. 993, 2017, pp. 83–98.

[69] C. Y. Park *et al.*, “STIM1 Clusters and Activates CRAC Channels via Direct Binding of a Cytosolic Domain to Orai1,” *Cell*, vol. 136, no. 5, pp. 876–890, Mar. 2009.

[70] M. K. Korzeniowski, I. M. Manjarrés, P. Varnai, and T. Balla, “Activation of STIM1-Orai1 involves an intramolecular switching mechanism.,” *Sci. Signal.*, vol. 3, no. 148, p. ra82, Nov. 2010.

[71] P. B. Stathopulos *et al.*, “STIM1/Orai1 coiled-coil interplay in the regulation of store-operated calcium entry.,” *Nat. Commun.*, vol. 4, p. 2963, Jan. 2013.

[72] M. Yen and R. S. Lewis, “Numbers count: How STIM and Orai stoichiometry affect store-operated calcium entry.,” *Cell Calcium*, vol. 79, pp. 35–43, 2019.

[73] M. Sallinger, S. Berlansky, and I. Frischauf, “Orai channels: key players in Ca2+ homeostasis,” *Curr. Opin. Physiol.*, Jun. 2020.

[74] B. A. McNally, A. Somasundaram, M. Yamashita, and M. Prakriya, “Gated regulation of CRAC channel ion selectivity by STIM1.,” *Nature*, vol. 482, no. 7384, pp. 241–5, Jan. 2012.

[75] M. Yamashita, P. S.-W. Yeung, C. E. Ing, B. A. McNally, R. Pomès, and M. Prakriya, “STIM1 activates CRAC channels through rotation of the pore helix to open a hydrophobic gate.,” *Nat. Commun.*, vol. 8, p. 14512, Feb. 2017.

[76] X. Hou, S. R. Burstein, and S. B. Long, “Structures reveal opening of the store-operated calcium channel Orai.,” *Elife*, vol. 7, 2018.

[77] I. Frischauf *et al.*, “Transmembrane helix connectivity in Orai1 controls two gates for calcium-dependent transcription.,” *Sci. Signal.*, vol. 10, no. 507, Nov. 2017.

[78] J. D. Humphries, M. R. Chastney, J. A. Askari, and M. J. Humphries, “Signal transduction via integrin adhesion complexes,” *Curr. Opin. Cell Biol.*, vol. 56, pp. 14–21, 2019.

[79] M. Kim, C. V Carman, and T. A. Springer, “Bidirectional Transmembrane Signaling by Cytoplasmic Domain Separation in Integrins,” *Science (80-. ).*, vol. 301, no. 5640, pp. 1720–1725, Sep. 2003.

[80] M. Theodosiou *et al.*, “Kindlin-2 cooperates with talin to activate integrins and induces cell spreading by directly binding paxillin,” *Elife*, vol. 5, pp. 1–24, 2016.

[81] P. Kammerer, J. Aretz, and R. Fässler, “Lucky kindlin: A cloverleaf at the integrin tail.,” *Proc. Natl. Acad. Sci. U. S. A.*, vol. 114, no. 35, pp. 9234–9236, Aug. 2017.

[82] M. Moser, B. Nieswandt, S. Ussar, M. Pozgajova, and R. Fässler, “Kindlin-3 is essential for integrin activation and platelet aggregation,” *Nat. Med.*, vol. 14, no. 3, pp. 325–330, 2008.

[83] P. R. Elliott *et al.*, “The Structure of the Talin Head Reveals a Novel Extended Conformation of the FERM Domain,” *Structure*, vol. 18, no. 10, pp. 1289–1299, Oct. 2010.

[84] M. Yao *et al.*, “The mechanical response of talin,” *Nat. Commun.*, vol. 7, no. May, pp. 1–11, 2016.

[85] S. E. Lee, R. D. Kamm, and M. R. K. Mofrad, “Force-induced activation of Talin and its possible role in focal adhesion mechanotransduction,” *J. Biomech.*, vol. 40, no. 9, pp. 2096–2106, 2007.

[86] J. Yan, M. Yao, B. T. Goult, and M. P. Sheetz, “Talin Dependent Mechanosensitivity of Cell Focal Adhesions,” *Cell. Mol. Bioeng.*, vol. 8, no. 1, pp. 151–159, 2015.

[87] A. W. M. Haining, M. Von Essen, S. J. Attwood, V. P. Hytönen, and A. Del Río Hernández, “All Subdomains of the Talin Rod Are Mechanically Vulnerable and May Contribute to Cellular Mechanosensing,” *ACS Nano*, vol. 10, no. 7, pp. 6648–6658, 2016.

[88] K. Baumann, “Mechanotransduction: Kindlin’ the fate of mesenchymal stem cells,” *Nat. Rev. Mol. Cell Biol.*, p. 2018, 2018.

[89] L. Guo *et al.*, “Kindlin-2 regulates mesenchymal stem cell differentiation through control of YAP1 / TAZ,” *J. Cell Biol.*, vol. 217, no. 4, pp. 1–21, 2018.

[90] H. Li *et al.*, “Structural basis of kindlin-mediated integrin recognition and activation,” *Proc. Natl. Acad. Sci.*, vol. 114, no. 35, pp. 9349–9354, 2017.

[91] K. Manibog, H. Li, S. Rakshit, and S. Sivasankar, “Resolving the molecular mechanism of cadherin catch bond formation,” *Nat. Commun.*, vol. 5, pp. 1–11, 2014.

[92] T. Evgeni, V. Sokurenko, Viola , Vogel, Wendy, “Catch bond mechanism of force-enhanced adhesion: counter- intuitive, elusive but … widespread?,” *J. Sex. Med.*, vol. 6, no. 4, pp. 247–253, 2009.

[93] J. Stricker, Y. Aratyn-Schaus, P. W. Oakes, and M. L. Gardel, “Spatiotemporal constraints on the force-dependent growth of focal adhesions,” *Biophys. J.*, vol. 100, no. 12, pp. 2883–2893, 2011.

[94] P. W. Oakes and M. L. Gardel, “Stressing the limits of focal adhesion mechanosensitivity,” *Curr. Opin. Cell Biol.*, vol. 30, no. 1, pp. 68–73, 2014.

[95] S. R. Coyer *et al.*, “Nanopatterning reveals an ECM area threshold for focal adhesion assembly and force transmission that is regulated by integrin activation and cytoskeleton tension,” *J. Cell Sci.*, vol. 125, no. 21, pp. 5110–5123, 2012.

[96] T. C. Bidone *et al.*, “Coarse-Grained Simulation of Full-Length Integrin Activation,” *Biophys. J.*, vol. 116, no. 6, pp. 1000–1010, 2019.

[97] A. C. Kalli, K. L. Wegener, B. T. Goult, N. J. Anthis, I. D. Campbell, and M. S. P. Sansom, “The Structure of the Talin/Integrin Complex at a Lipid Bilayer: An NMR and MD Simulation Study,” *Structure*, vol. 18, no. 10, pp. 1280–1288, 2010.

[98] H. Shams and M. R. K. Mofrad, “α-Actinin Induces a Kink in the Transmembrane Domain of β3-Integrin and Impairs Activation via Talin,” *Biophys. J.*, vol. 113, no. 4, pp. 948–956, 2017.

[99] J. Golji and M. R. K. Mofrad, “The interaction of vinculin with actin.,” *PLoS Comput. Biol.*, vol. 9, no. 4, p. e1002995, Apr. 2013.

[100] J. Golji, J. Lam, and M. R. K. Mofrad, “Vinculin activation is necessary for complete talin binding.,” *Biophys. J.*, vol. 100, no. 2, pp. 332–40, Jan. 2011.

[101] S. E. Lee, S. Chunsrivirot, R. D. Kamm, and M. R. K. Mofrad, “Molecular dynamics study of talin-vinculin binding,” *Biophys. J.*, vol. 95, no. 4, pp. 2027–2036, 2008.

[102] Z. Haydari, H. Shams, Z. Jahed, and M. R. K. Mofrad, “Kindlin Assists Talin to Promote Integrin Activation,” *Biophys. J.*, vol. 118, no. 8, pp. 1977–1991, Apr. 2020.

[103] A. M. Weljie, P. M. Hwang, H. J. Vogel, S. Misra, E. F. Plow, and J. Qin, “Solution structures of the cytoplasmic tail complex from platelet integrin alpha IIb- and beta 3-subunits.,” *Proc. Natl. Acad. Sci. U. S. A.*, vol. 99, no. 9, pp. 5878–83, Apr. 2002.

[104] D. A. Calderwood *et al.*, “The phosphotyrosine binding-like domain of talin activates integrins,” *J. Biol. Chem.*, vol. 277, no. 24, pp. 21749–21758, 2002.

[105] M. Moes *et al.*, “The integrin binding site 2 (IBS2) in the talin rod domain is essential for linking integrin β subunits to the cytoskeleton,” *J. Biol. Chem.*, vol. 282, no. 23, pp. 17280–17288, 2007.

[106] H. Li *et al.*, “Structural basis of kindlin-mediated integrin recognition and activation.,” *Proc. Natl. Acad. Sci. U. S. A.*, vol. 114, no. 35, pp. 9349–9354, Aug. 2017.

[107] N. J. Anthis *et al.*, “The structure of an integrin / talin complex reveals the basis of inside-out signal transduction,” *EMBO J.*, vol. 28, no. 22, pp. 3623–3632, 2009.

[108] W. L. Jorgensen, J. Chandrasekhar, J. D. Madura, R. W. Impey, and M. L. Klein, “Comparison of simple potential functions for simulating liquid water,” *J. Chem. Phys.*, vol. 79, no. 2, pp. 926–935, Jul. 1983.

[109] J. C. Phillips *et al.*, “Scalable molecular dynamics with NAMD.,” *J. Comput. Chem.*, vol. 26, no. 16, pp. 1781–802, Dec. 2005.

[110] W. Humphrey, A. Dalke, and K. Schulten, “VMD: visual molecular dynamics.,” *J.*

*Mol. Graph.*, vol. 14, no. 1, pp. 33–8, 27–8, Feb. 1996.

[111] H. Bengtsson *et al.*, "Package 'matrixStats' Title Functions that Apply to Rows and Columns of Matrices (and to Vectors)," 2018.

[112] "Package 'gplots' Title Various R Programming Tools for Plotting Data," 2019.

[113] B. J. Grant, A. P. C. Rodrigues, K. M. ElSawy, J. A. McCammon, and L. S. D. Caves, "Bio3d: an R package for the comparative analysis of protein structures," *Bioinformatics*, vol. 22, no. 21, pp. 2695–2696, Nov. 2006.

[114] B. I. Costescu and F. Gräter, "Time-resolved force distribution analysis," *BMC Biophys.*, vol. 6, no. 1, p. 5, Dec. 2013.

[115] E. T. Eng, B. J. Smagghe, T. Walz, and T. A. Springer, "Intact alphaIIbbeta3 integrin is extended after activation as measured by solution X-ray scattering and electron microscopy.," *J. Biol. Chem.*, vol. 286, no. 40, pp. 35218–26, Oct. 2011.

[116] K. L. Wegener *et al.*, "Structural basis of integrin activation by talin.," *Cell*, vol. 128, no. 1, pp. 171–82, Jan. 2007.

[117] D. R. Critchley and A. R. Gingras, "Talin at a glance.," *J. Cell Sci.*, vol. 121, no. Pt 9, pp. 1345–7, May 2008.

[118] H. Li, Y.-Y. Chang, J. Y. Lee, I. Bahar, and L.-W. Yang, "DynOmics: dynamics of structural proteome and beyond," *Nucleic Acids Res.*, vol. 45, no. W1, pp. W374–W380, Jul. 2017.

[119] I. Mitroulis, V. I. Alexaki, I. Kourtzelis, A. Ziogas, G. Hajishengallis, and T. Chavakis, "Leukocyte integrins: Role in leukocyte recruitment and as therapeutic targets in inflammatory disease," *Pharmacol. Ther.*, vol. 147, pp. 123–135, Mar. 2015.

[120] W. Bergmeier, C. Weidinger, I. Zee, and S. Feske, "Emerging roles of store-operated $Ca^{2+}$ entry through STIM and ORAI proteins in immunity, hemostasis and cancer.," *Channels (Austin).*, vol. 7, no. 5, pp. 379–91, Jan. .

[121] S. Schmidt, M. Moser, and M. Sperandio, "The molecular basis of leukocyte recruitment and its deficiencies," *Mol. Immunol.*, vol. 55, no. 1, pp. 49–58, Aug. 2013.

[122] M. I. Cybulsky, D. Won, and M. Haidari, "Leukocyte recruitment to atherosclerotic lesions.," *Can. J. Cardiol.*, vol. 20 Suppl B, p. 24B–28B, Aug. 2004.

[123] S. L. Zhang *et al.*, "STIM1 is a Ca2+ sensor that activates CRAC channels and migrates from the Ca2+ store to the plasma membrane," *Nature*, vol. 437, no. 7060, pp. 902–905, Oct. 2005.

[124] P. B. . S. R. . F. M. . Z. L. . G.-S. G. M. . M. M. . R. C. . I. M. Stathopulos, "STIM1/Orai1 coiled-coil interplay in the regulation of store-operated calcium entry.," *Nat Commun*, vol. 4, p. 2963, 2013.

[125] R. M. Nwokonko, X. Cai, N. A. Loktionova, Y. Wang, Y. Zhou, and D. L. Gill, "The STIM-Orai Pathway: Conformational Coupling Between STIM and Orai in the Activation of Store-Operated Ca2+ Entry," Springer, Cham, 2017, pp. 83–98.

[126] K. M. Kim *et al.*, "Distinct gating mechanism of SOC channel involving STIM-Orai coupling and an intramolecular interaction of Orai in Caenorhabditis elegans."

[127] Y. Zhou *et al.*, "Cross-linking of Orai1 channels by STIM proteins.," *Proc. Natl. Acad. Sci. U. S. A.*, vol. 115, no. 15, pp. E3398–E3407, Apr. 2018.

[128] X. Hou, L. Pedi, M. M. Diver, and S. B. Long, "Crystal structure of the calcium release-activated calcium channel Orai.," *Science*, vol. 338, no. 6112, pp. 1308–13, Dec. 2012.

[129] B. A. McNally, A. Somasundaram, M. Yamashita, and M. Prakriya, "Gated regulation of CRAC channel ion selectivity by STIM1," *Nature*, vol. 482, no. 7384, pp. 241–245, Feb. 2012.

[130] Z. Haydari, H. Shams, and M. R. K. Mofrad, "Molecular Mechanisms of STIM1-Mediated Orai-1 Channel Activation," *Biophys. J.*, vol. 110, no. 3, p. 265a, Feb. 2016.

[131] S. Feske *et al.*, "A mutation in Orai1 causes immune deficiency by abrogating CRAC channel function," *Nature*, vol. 441, no. 7090, pp. 179–185, May 2006.

[132] M. Muik *et al.*, "Dynamic coupling of the putative coiled-coil domain of ORAI1 with STIM1 mediates ORAI1 channel activation.," *J. Biol. Chem.*, vol. 283, no. 12, pp. 8014–22, Mar. 2008.

[133] L. A. Kelley and M. J. E. Sternberg, "Protein structure prediction on the Web: a case study using the Phyre server.," *Nat. Protoc.*, vol. 4, no. 3, pp. 363–71, Jan. 2009.

[134] P. B. Stathopulos *et al.*, "ARTICLE STIM1/Orai1 coiled-coil interplay in the regulation of store-operated calcium entry," 2013.

[135] "No Title." [Online]. Available: http://watcut.uwaterloo.ca/tools/makemultimer/.

[136] M. Magrane and U. UniProt Consortium, "UniProt Knowledgebase: a hub of integrated protein data.," *Database (Oxford).*, vol. 2011, p. bar009, 2011.

[137] "No Title." [Online]. Available: http://3vee.molmovdb.org.

[138] N. R. Voss and M. Gerstein, "3V: cavity, channel and cleft volume calculator and extractor.," *Nucleic Acids Res.*, vol. 38, no. Web Server issue, pp. W555-62, Jul. 2010.

[139] Y. Zhou, X. Cai, R. M. Nwokonko, N. A. Loktionova, Y. Wang, and D. L. Gill, "The STIM-Orai coupling interface and gating of the Orai1 channel," *Cell Calcium*, vol. 63, pp. 8–13, May 2017.

[140] A. Vashisht, M. Trebak, and R. K. Motiani, “STIM and Orai proteins as novel targets for cancer therapy. A Review in the Theme: Cell and Molecular Processes in Cancer Metastasis,” *Am. J. Physiol. Physiol.*, vol. 309, no. 7, pp. C457–C469, Oct. 2015.

[141] L. Tirado-Lee, M. Yamashita, and M. Prakriya, “Conformational Changes in the Orai1 C-Terminus Evoked by STIM1 Binding,” *PLoS One*, vol. 10, no. 6, p. e0128622, Jun. 2015.

[142] R. Palty and E. Y. Isacoff, “Cooperative Binding of Stromal Interaction Molecule 1 (STIM1) to the N and C Termini of Calcium Release-activated Calcium Modulator 1 (Orai1).,” *J. Biol. Chem.*, vol. 291, no. 1, pp. 334–41, Jan. 2016.

[143] R. Palty, C. Stanley, and E. Y. Isacoff, “Critical role for Orai1 C-terminal domain and TM4 in CRAC channel gating,” *Cell Res.*, vol. 25, no. 8, pp. 963–980, Aug. 2015.

[144] R. Palty, Z. Fu, and E. Y. Isacoff, “Sequential Steps of CRAC Channel Activation,” *Cell Rep.*, vol. 19, no. 9, pp. 1929–1939, May 2017.

[145] A. Amcheslavsky *et al.*, “Molecular Biophysics of Orai Store-Operated Ca(2+) Channels.,” *Biophys. J.*, vol. 108, no. 2, pp. 237–246, Jan. 2015.

[146] N. Miyazaki, K. Iwasaki, and J. Takagi, “A systematic survey of conformational states in β1 and β4 integrins using negative-stain electron microscopy,” *J. Cell Sci.*, vol. 131, no. 10, p. jcs216754, 2018.

[147] X. Hou, S. R. Burstein, and S. B. Long, “Structures reveal opening of the store-operated calcium channel Orai,” *Elife*, vol. 7, pp. 1–28, 2018.

[148] A. Upadhyaya and M. P. Sheetz, “Tension in tubulovesicular networks of Golgi and endoplasmic reticulum membranes.,” *Biophys. J.*, vol. 86, no. 5, pp. 2923–8, May 2004.